2012

Modeling, Simulation and Experimental Verification of an Electric Bicycle with Regenerative Braking

Maulik Kalolia
Cleveland State University

MODELING, SIMULATION AND EXPERIMENTAL VERIFICATION OF AN ELECTRIC BICYCLE WITH REGENERATIVE BRAKING

MAULIK KALOLIA

Bachelor of Science in Mechatronics Engineering

Sardar Patel University

Vallabh Vidhyanagar, India June, 2007

submitted in partial fulfillment of requirements for the degree

MASTERS OF SCIENCE IN MECHANICAL ENGINEERING

at the

CLEVELAND STATE UNIVERSITY

December, 2012

This thesis has been approved
for the department of MECHANICAL ENGINEERING
and the College of Graduate Studies by:

Thesis Chairperson, Hanz Richter, Ph.D.

Department & Date

Daniel Simon, Ph.D.

Department & Date

Ana Stankovic, Ph.D.

Department & Date

ACKNOWLEDGMENTS

I would like to thank my advisor Dr. Hanz Richter, who provided essential support and assistance throughout my graduate career, and also for his guidance which immensely contributed towards the completion of this thesis. This thesis would not have been realized without his support. I would also like to thank Daniel Simon and Ana Stankovic for being in my thesis committee. Thanks are also due to my family and friends who have encouraged, supported and inspired me.

MODELING, SIMULATION AND EXPERIMENTAL VERIFICATION OF AN ELECTRIC BICYCLE WITH REGENERATIVE BRAKING

MAULIK KALOLIA

ABSTRACT

Electric bicycles are widely available in user markets. However their use as a daily commuting vehicle is limited due to the need for frequent recharging. This thesis focuses on the mathematical modeling of electrical bicycle with regenerative breaking. Basic bond graphs methods are discussed here to develop state space models for mechatronic systems. A bond graph based mathematical model of an electric bicycle with regeneration is developed in this thesis. Mathematical models are tested in simulation, generating different road scenarios. Parameters required for the simulation are calculated using an experimental setup. The thesis shows the capability of bond graphs to assist in calculations for regenerative charging. The main focus of this thesis is to evaluate simulation models against a prototype. Simulation results and road testing of the prototype indicate the regenerative braking is not only feasible, but an advantage to implement in an electric bicycle. It is shown that the distance between battery recharge is improved by as much as 10% depending on riding conditions.

TABLE OF CONTENTS

LIST OF FIGURES

CHAPTER I

INTRODUCTION

This chapter gives brief idea about the requirements and motivation for this thesis. It also talks about literature and technology review and their current limitations. The practical benefits of implementing this research are discussed here. Overall thesis organization is also presented.

1.1 Motivation

In the last decades personal electrical vehicles (PEV) like electric bicycles have emerged as a new category of transportation. Bicycling is regarded as an active mode of transportation and a part of daily commuting vehicle in some of the world's urban areas. The United States has also seen an increase in the number of miles traveled in bicycles with the purpose of commuting [3]. Conferences and seminars are arranged by governmental and community organizations to increase community awareness and to increase bicycle use in daily life. "Bike to work week" is observed by Ohio Department of Transportation (ODOT) to encourage people to use a bicycle as a daily commuting vehicle. Shared bike lanes are created with main road for commuters (Figure 1.1) to promote bicycling. Figure 1.2 shows the different bike routes in Cleveland area.

Even with these initiatives, bicycles are not a widespread mode of commuting in the

Figure 1.1: Shared Bicycle Lanes

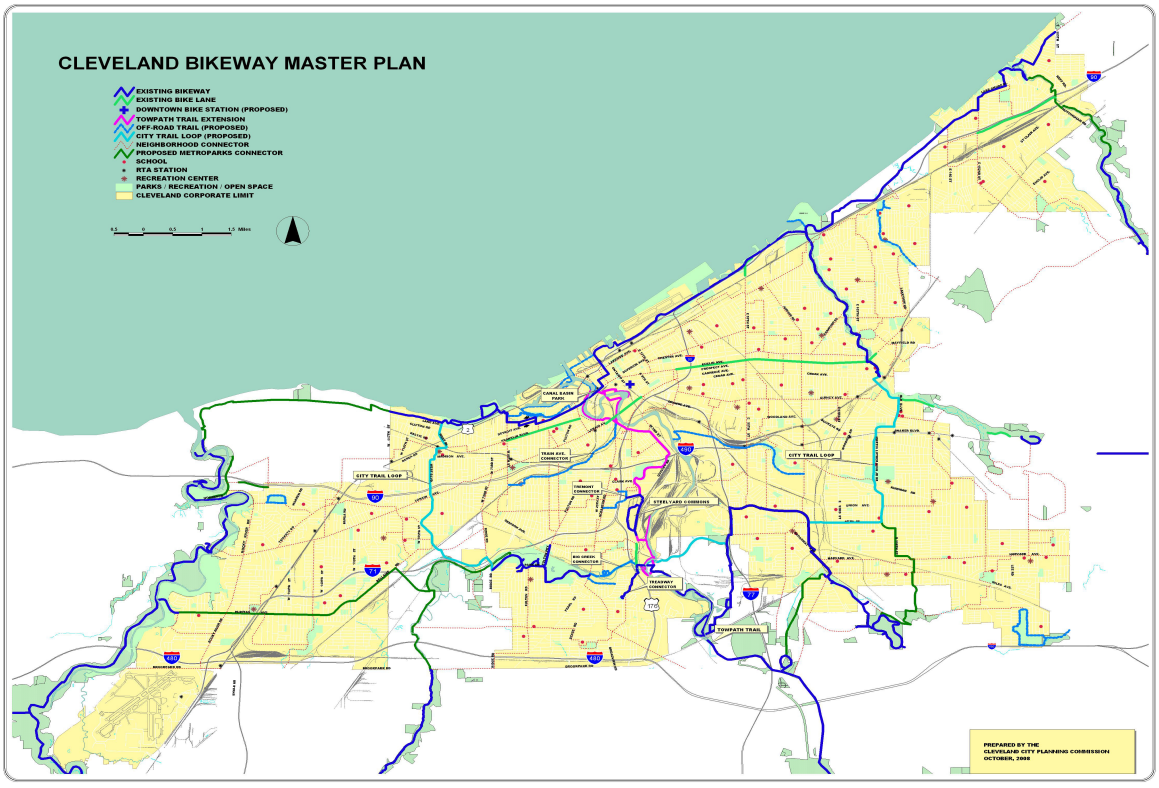

Figure 1.2: Bicycle Path Map in Cleveland [15]

US. Two main obstacles preventing a more generalized reliance on bicycles are evident: i. commuters are not willing to spend much more time to reach their destination, and ii., few commuters are fit enough to sustain a ride of several miles, potentially facing hills and adverse wind. These reasons provide our motivation to optimize the design of pedal-assist (hybrid) bicycles, which can reduce the impact of both obstacles. Weather is another impediment in areas like Cleveland, but seeking an increase in bicycle ridership during fair-weather seasons seems reasonable.

The fitness factor works two ways: a commuter may immediately rule out bicycling as a commuting alternative on lack of fitness grounds, and vice versa, if the commuter decided to undertake riding, his/her fitness and overall health level would improve. The electric bicycle, due to its speed and pedal assistance features, has the potential to become a viable alternative which can save time and effort.

Existing electric bicycles, however, are very limited in *range* (the distance traveled in one battery charge), representing a problem for commuting from suburban areas, typically 10 to 15 miles from downtown. This limitation of electric bicycles needs to be addressed through applied engineering research.

The purpose of this research is to optimize the design of hybrid bicycles for commuting in urban areas by increasing their range using energy regeneration, continuously-variable transmission (CVT) technology and advanced pedal assistance algorithms. An improvement of the range in existing bicycle is sought by including energy regeneration system. This design is guided by mathematical modeling and simulation of the electric bicycle, laboratory tests and test rides.

Test ride of this prototype was conducted between Shaker Heights and the Cleveland downtown, a distance of 9 miles. This ride gave encouraging results, as the time required to cover the distance was barely larger than the time spent driving a car. The ride took near 30 min., but saved on pollution, time and money associated with parking and helped maintain rider health. It was found that the range of our prototype is about 10 miles, a figure too low

to be practical.

A significant amount of energy is wasted in braking operations. This motivate us to implement energy regeneration to capture part of this energy and redirect it to the battery, extending the range. Fit riders may also purposely set the bicycle to charge mode and charge the batteries with pedal power.

1.2 Literature Review

Some literature and technology review was done for this thesis research. Studies and analysis on electrical bicycles models, parts and its effect in community and environment have been conducted by different researchers and community organizations. Different work flows have been proposed for increasing the range of electric bicycles. A statistical study on increasing demand for electric bicycle in China was done by Zhen Dun [5]. According to the study the total amount for bicycles in china is 400 million, this shows that electric bicycles have large demand there. Dun proposed the used of permanent magnet DC motor, and rechargeable batteries. A basic physical model for vehicle motion parameters was conducted by Karl Ulrich [19]. He also presented a cost based analysis of different personal electric vehicles and the distance they can travel. Hwang [9] tested an electric bicycle powered by a proton exchange membrane fuel cell. The fuel-cell system was composed of a 300-W fuel-cell stack, metal hydride canisters, air pumps, solenoid valves, cooling fans, pressure and temperature sensors, and a microcontroller. They used the fuel cell system to drive the bicycle's electric motor. Fallbrook Technologies has designed a CVT for bicycles, *NuVinci*, which has infinitely-variable gear ratios. Daymak has developed brushless geared motors for electric bikes with Lithium batteries, which can convert standard bicycles in to electric vehicle.

Studies regarding the feasibility of energy regeneration in electric bicycles are not available in the open literature. Manufacturers of e-bike kits do not offer models with energy regeneration. This thesis is different from others in terms of its customization to urban

commuting and various rider profiles. As part of graduate studies at Cleveland State University, some preliminary work had been done on an electric bicycle prototype. A simple mathematical model was developed that did not include regeneration. Some parameters were measured in the laboratory. The complete model predicted remaining battery charge according to distance traveled.

1.3 Objective

The main objective of this thesis is to use mechatronics engineering to demonstrate energy regeneration in hybrid electric bicycles, aiming the design at an improvement in range. The improvement can be evaluated in a feasibility study consisting in various test rides using established bike lanes. The variables to be monitored include range, overall rider effort and average speed. These results can be made public and used to promote e-bike commuting.

This research work is based on analysis of the electric bicycle by mathematical modeling using bond graph techniques. Preparation of bond graph model for bike components and the overall system was the preliminary task. The bond graph technique allows a precise and detailed study of electromechanical energy transformation. Using a complete model of the bicycle it is straightforward to calculate how much energy will be used in different travel conditions. Other affecting factors like wind speed, slope angle and rolling resistance can be simulated and will affect range predictions.

Another objective is to study the effect of adding a CVT element in electric bicycle. Its use represents a trade off: the continuous range of gear ratios gives the flexibility to make adjustments for different riding conditions, but the overall bicycle weight increases. A cost-benefit analysis of CVT in comparison to manual gear shifting or fixed gear designs can be conducted.

Using this regenerative prototype setup the efficiency associated with the capturing braking energy through regenerative braking can be evaluated. The high efficiency of hybrid

automobiles is due in large part to such regeneration. In bicycles, lower masses and speeds may produce lesser benefits, but an engineering study is in order.

1.4 Composition of Thesis

This thesis is organized as follows. The fundamentals of vehicle motion, dynamics, electric components like motor, batteries are described in Chapter 2. Theory and design methods of bond graphs are explained in Chapter 3. Detailed modeling and parameter calculations for the electric bicycle is shown in Chapter 4.

An evaluation of the mathematical model of the electric bicycle in different test scenarios is done using Matlab/Simulink in Chapter 5. Finally Physical design of the prototype and work flow for battery recharging circuit is developed in Chapter 6.

CHAPTER II

FUNDAMENTALS AND MECHANICS OF ELECTRIC VEHICLES

This chapter gives brief overview of components and working principles of electric bicycle. Basic forces acting on the moving vehicles and their effects on are discussed here using physics equations and theory. The functions and characteristics of each component for electric bicycle are described and equations to calculate their parameters are given. This chapter will help reader to get familiar with electric vehicles (EVS) technology and its working principles.

2.1 Vehicle Movement

Different forces act on the vehicle and their directions describe the behavior of the vehicle. According to Newton‘s second law, the algebraic sum of all this forces will give the linear velocity V of the vehicle as below.

$$\Sigma F_t - \Sigma F_r = M\frac{dV}{dt} \tag{2.1}$$

$$\frac{dV}{dt} = \frac{\Sigma F_t - \Sigma F_r}{M} \tag{2.2}$$

Here, the tractive force (F_t) is applied on a vehicle to drive in forward direction. When the vehicle is in motion, resistive forces (F_r) are acting in the opposite direction and try to stop

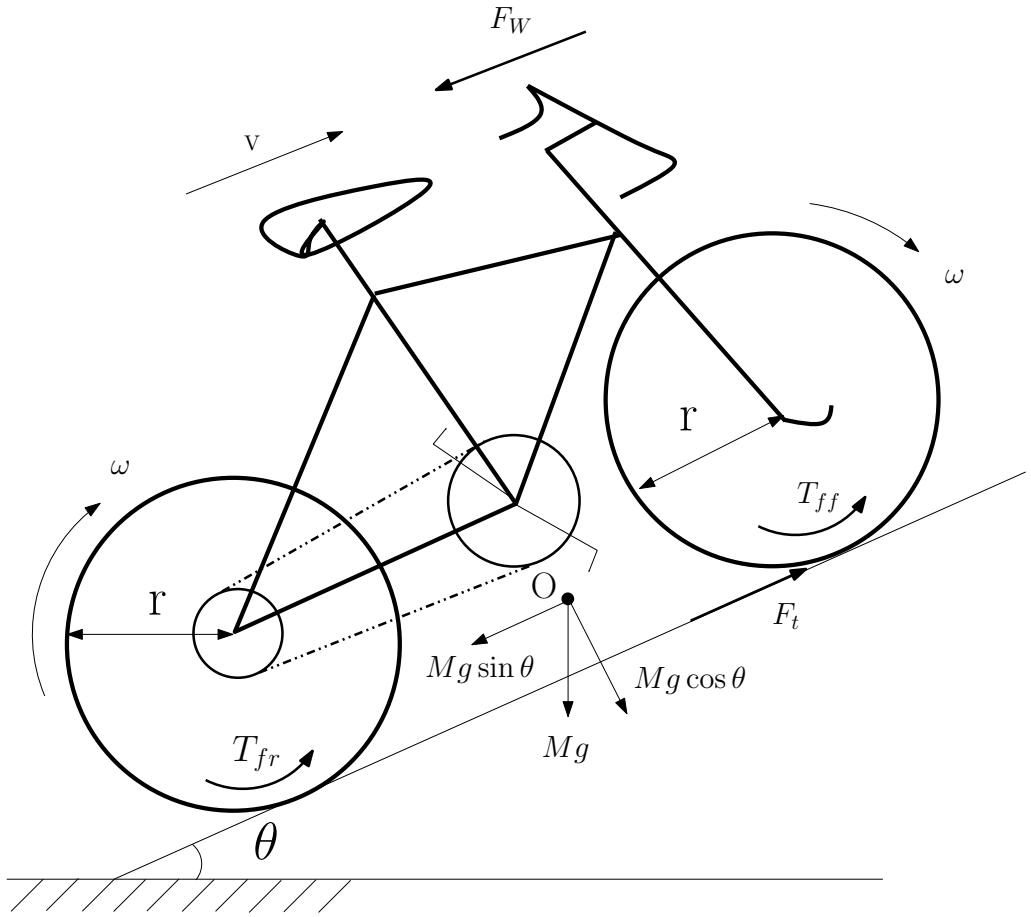

Figure 2.1: Forces Acting on a Bicycle Moving Uphill

the vehicle movement. In an electric bicycle, the driving force is applied by the motor or by paddling. Resistive forces are generated due to rolling resistance, aerodynamic drag and uphill grade resistance. V is the linear velocity of the vehicle and M is combined mass of vehicle and rider.

Figure 2.1 shows all different forces applied on bicycle when driving on an inclined surface. These forces are described in the following sections.

2.2 Vehicle Resistance

When bicycle is running on an inclined surface with angle θ, rolling resistance (F_r), aerodynamic drag(F_w), tire friction torques T_{rf} and T_{rr}, and grade resistance are applied on the

Table 2.1: Rolling Resistance Coefficients [6]

Conditions	**Rolling Resistance Coefficient**
Car tires on a concrete or asphalt road	0.013
Car tires on a rolled gravel road	0.02
Tar road	0.025
Unpaved road	0.05
Field	$0.1 - 0.35$
Truck tire on a concrete or asphalt road	$0.006 - 0.01$
Wheel on iron rail	$0.001 - 0.002$

bicycle.

2.2.1 Rolling Resistance

The rolling resistance is produced by tire deformation at the contact surface of the road. When wheel is stationary all forces due to weight of the bicycle and the rider are equally distributed on the road surface. Rolling resistance can be calculated using following formula.

$$F_r = Mgf_r \tag{2.3}$$

where M is the total mass of the bicycle, f_r is the rolling resistance constant and θ is the road angle. f_r is depends on tire structure, tire temperature, tire pressure, thread geometry, road roughness and road material. Rolling resistance values for different road conditions are shown in table 2.1

Figure 2.2 shows a rolling resistance chart of bicycle wheels developed by Jobst Brandt [13] for different road surfaces conditions.

2.2.2 Aerodynamic Drag

A vehicle traveling at a particular speed in air encounters resistance due to wind. Aerodynamic drag is depends on shape drag and skin factor. Air resistance increases with the square of velocity.

The aerodynamic drag force can be expressed as :

$$F_w = \frac{1}{\rho} A_f C_D (V - V_w)^2 \tag{2.4}$$

where, ρ is air density, A_f is vehicle front area, C_D is the aerodynamic drag coefficient, V is vehicle speed and V_W is wind speed.

2.2.3 Grade Resistance

When vehicle is on slope surface its weight produces a component in downward direction which helps or opposes forward motion. Grade resistance is positive in climbing and negative

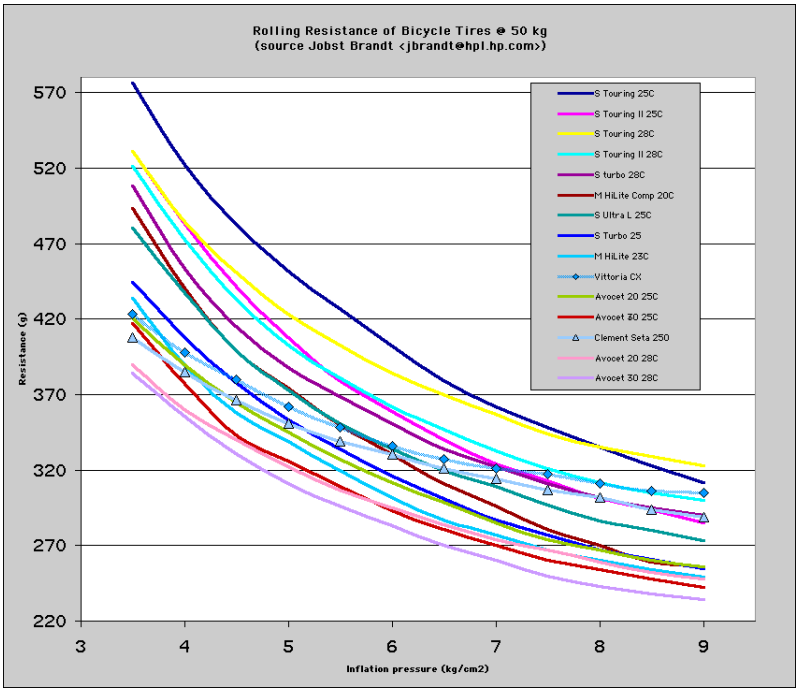

Figure 2.2: Rolling Resistance Chart

Figure 2.3: Hub Mounted DC motor

in descending. The grade resistance for a bicycle with slope angle θ can be expressed as

$$F_g = Mg \sin \theta \tag{2.5}$$

2.3 Vehicle Dynamics

When the bicycle is in motion in a longitudinal direction, the major external forces acting on it are, the front and rear tires rolling resistance F_{fr} and F_{rr}, aerodynamic drag force F_W, grade force F_g, Using all these force and their directions dynamic equation for the bicycle motion in longitudinal direction is expressed by

$$M\frac{dV}{dt} = (F_{tf} + F_{tr}) - (F_{rf} + F_w + F_g) \tag{2.6}$$

2.4 Power System

Electric power systems are the main driving force of electric bicycles. They consist of electric motors, power converters and electronic controllers.

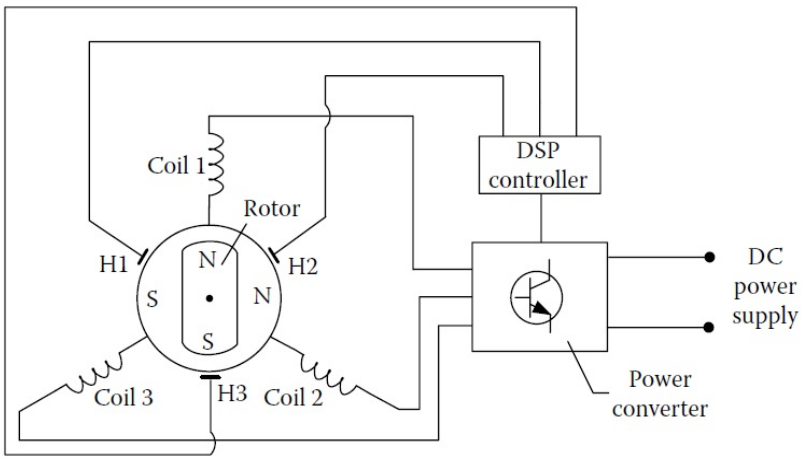

Figure 2.4: BLDC Drive System [6]

The electric motor converts the electrical energy into mechanical energy to drives the bicycle. Motor can also use as a generator to recharge the battery using regenerative braking. Two different kinds of electric motors are used in EVs and HEVs, commutator motors (DC) and commutator less (BLDC) motor. In DC motor commutation is done through sliding brush and they have simple controller, even for high speed applications. In brushless dc motors (BLDC) commutation is done electronically, it requires power converters.

Electric vehicles require frequent start and stop in urban driving, high torque and low speed hill climbing, low torque and high speed in cruising and wide range of speed profiles. These parameters effects the choice of motors for EVs

Motor torque is proportional to the current. In brush motor high level of current produces resistive losses in the brushes and it needs more cooling. DC motor also requires high maintenance. Due to this limitations DC motors are efficient in low torque and high speed applications. Brushless motors can produce high torque at low speed also. BLDC motors are used more in electric vehicles and it requires less maintenance

Figure 2.4 shows the BLDC motor drive system with BLDC motor and digital signal processor (DSP) based controller and power converter. Position of machine rotor is sensed by position sensors H1, H2, H3. This position information is feed to the controller. Controller

will supply gating signals to power converter. By turning on and turning off proper stator pole winding, the torque and speed of the machine are controlled.

2.5 Power Transmission System

Gears are the simple mechanical power transmission machine used to gain a mechanical advantage of rider or motor power in bicycles through increasing the torque or reducing the speed.

In some bicycles only one fixed gear ratio is available for power transmission. May bicycles have multiple gears and thus multiple gear ratios are available. Gear shifting mechanism gives selection of proper gear ratio based on riding condition and comforts. Different gear ratios can be used in cycling downhill, flat road, and uphill conditions.

The gear ratio depends on the ratio of the number of teeth on the chain ring to the number of teeth on the rear sprocket (cog).

$$GR = \frac{r_1}{r_2} \tag{2.7}$$

$$\text{wheel speed} = GR * \text{pedal speed} \tag{2.8}$$

To travel at same speed with lower gear ratio requires the rider to pedal at a faster speed but with less force. High gear ratio requires lower pedal speed but more input force.

Continuously Variable Transmission

Normal electric vehicles have regular gear transmission system in which only fixed numbers of gear ratios are available for different.

A *Continuously Variable Transmission (CVT)* is a transmission that can change steplessly through an infinite number of effective gear ratios between maximum and minimum values.

The flexibility of a CVT allows the driving shaft to maintain a constant angular velocity over a range of output velocities. CVT allows the engine to run at its most efficient (RPM)

(a) (b)

Figure 2.5: Gear trains (a) Manual Gears, (b) Continuous Variable Transmission (CVT) [10]

for a range of vehicle speeds and increases the fuel economy compare to other transmission systems. It can also be used to build kinetic energy recovery system during regenerative braking. CVT has been available for decades. It is used in newer hybrid cars, such as the Toyota Prius, Highlander and Camry, the Nissan Altima, and newer-model Ford Escape Hybrid SUVs. In bicycles CVTs are also available like $NuVinci$ from Fallbrook Technologies Inc as shown in figure 2.5.

Figure 2.6(a) shows a simplified cross section of the $NuVinci$ Continuously Variable Planetary (CVP) transmission. A bank of balls (planets) is placed in a circular array around a central idler and in contact with separate input and output discs (or traction rings). Power comes through the input disc and is transmitted to the balls, then to the output disc via traction at the rolling contact interface between the balls and discs.

Figure 2.6(b) presents the system kinematics, where r_i is the contact radius of the input contact, and r_o is the contact radius at the output contact. The tilt angle of the ball axis defines the gear ratio. It changes the ratio of r_i to r_o and thus changes the gear ratio [2]. This mechanism gives the ability to sweep the transmission through the entire range smoothly, while in motion or stopped.

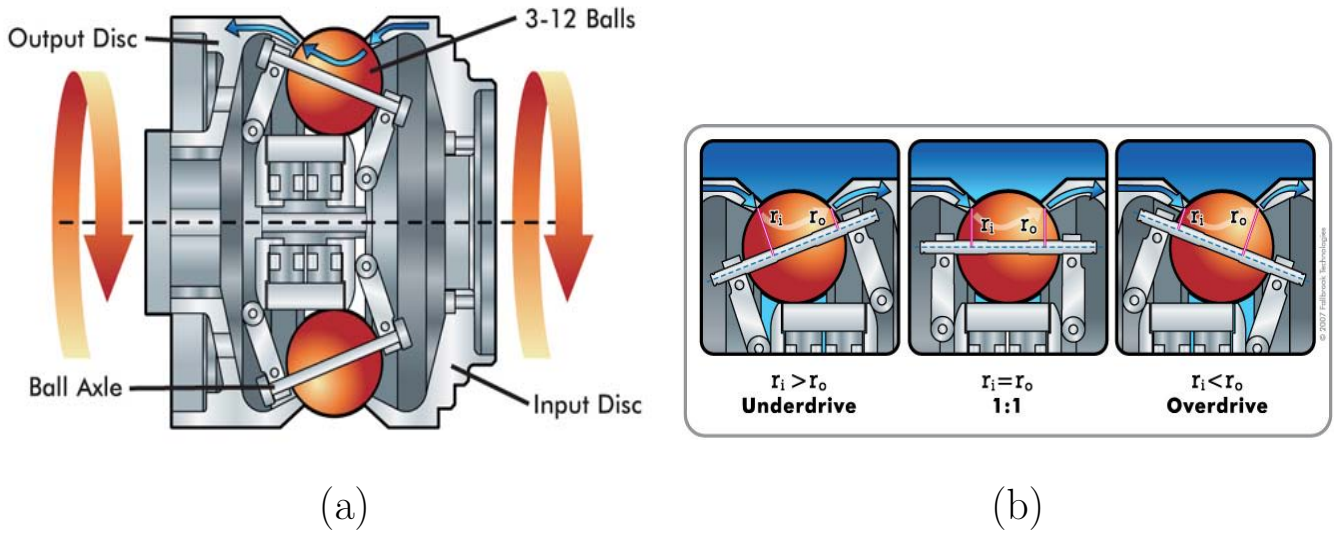

(a) (b)

Figure 2.6: (a)*NuVinci* CVP Geometric Configuration, (b)*NuVinci* Ratio Control

2.6 Energy Sources

Electric vehicles require a portable source of electrical energy, to be converted to mechanical energy in the electric motor for propulsion. Electric energy is typically obtained through the conversion of chemical energy stored in devices such as batteries and fuel cells. The efficiency of portable energy sources presents one of the biggest obstacles for the commercialization of EVs.

Since the beginning of research and development of EVs batteries have been the most popular choice of energy source. Various batteries are compared in terms of descriptors, such as specific energy, specific power, operating life, recharging rate etc. There are two basic types of batteries are available in the market. The non rechargeable battery, converts chemical energy into electrical energy. The electromechanical reactions in these batteries are non reversible and they are made for a single use. The Second type of battery is rechargeable batteries in which electromechanical reactions are reversible. In EVs rechargeable batteries are used in both ways, a main source of energy and a energy storage device.

2.6.1 Battery Principles

The batteries are made of unit cells containing the chemical energy that is convertible to electric energy. One or more of these electrolytic cells are connected in series to form one battery. The grouped cells are enclosed in a casing to form a battery module. A battery pack is a collection of individual battery modules connected in a series and parallel combination to deliver the desired voltage and energy to the power electronic drive system.

The energy stored in a battery is the difference in free energy between chemical components in the charged and discharged states. This available chemical energy in a cell is converted into electrical energy only on demand, using the basic components of a unit cell, which are the positive and negative electrodes, the separators, and the electrolytes as shown in figure. During battery operation, chemical reactions at each of the electrodes cause electrons to flow from one electrode to another. The flow of electrons in the cell is sustainable only if electrons generated in the chemical reaction are able to flow through an external electrical circuit that connects the two electrodes. The connection points between the electrodes and the external circuit are called the battery terminals.

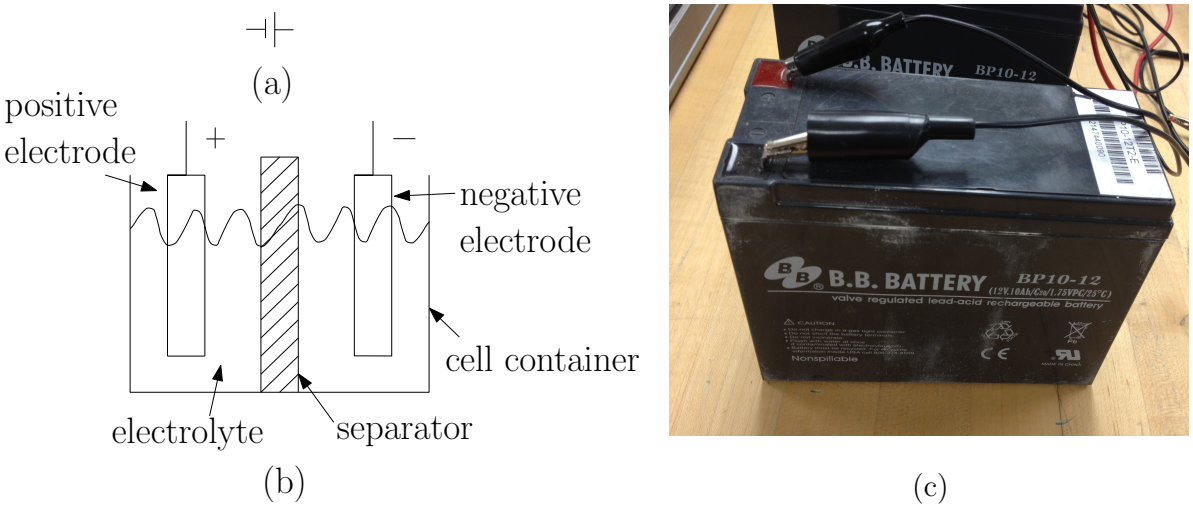

Figure 2.7: Components of Battery Cell (a) Cell Circuit Symbol (b) Cell Cross Section (c) 12 V,A-h Lead-Acid Battery

Table 2.2: Specific Energy of Batteries [8]

Battery	**Specific Energy (Wh/kg)**	
	Theoretical	**Practical**
Lead-acid	108	50
Nickel-cadmium		$20 - 30$
Nickel-zinc		90
Nickel-iron		60
Zinc-chlorine		90
Silver-zinc	500	100
Sodium-sulfur	770	$150 - 300$
Aluminium-air		300

The major types of rechargeable batteries considered for EV and HEV applications are:

- Lead-acid (Pb-acid)
- Nickel-cadmium (NiCd)
- Nickel-metal-hydride (NiMH)
- Lithium-ion (Li-ion)
- Lithium-polymer (Li-poly)
- Sodium-sulfur (NaS)
- Zinc-air (Zn-Air)

Theoretical and practical specific energies of several batteries are given in Table 2.2 for comparison.

From all different kind of batteries the lead-acid type of battery has the longest development history of all battery technology, particularly for their need and heavy use in industrial

EVs, such as for golf carts in sports, passenger cars in airports, and forklifts in storage facilities and supermarkets. The continued existence of the lead-acid batteries is due to following:

- Relatively low cost
- Easy availability of raw materials (lead, sulfur)
- Ease of manufacture
- Favorable electromechanical characteristics

The electric bicycle prototype developed in this thesis used Lead-acid type rechargeable batteries. Four $10A$, 12 $A-h/C_{20}$ rating lead-acid batteries are connected in series to get 48V terminal voltage.

2.6.2 Parameters

Battery Capacity

The amount of free charge generated by the active material at the negative electrode and consumed by the positive electrode is called the *battery capacity*. The capacity is measured in A-h (1 A-h=3600 C, or Coulomb, where 1 C is the charge transferred in 1 s by 1 A current in the MKS unit of charge) [8].

Discharge Rate

The*discharge rate* is the current at which a battery is discharged. The rate is expressed as Q/h rate, where Q is rated battery capacity and h is discharge time in hours. For a battery that has a capacity of Q_T A-h and that is discharged over Δt, the discharge rate is $Q_T/\Delta t$.

For example, a battery labeled as 100 A-h at $\frac{C}{5}$ rate has a 100A-h capacity at 5-h discharge rate (discharge current $= \frac{100}{5} = 20$ A)

State of Charge / Discharge

The state of charge (SOC) is the present capacity of the battery. It is the amount of capacity that remains after discharge from a top-of-charge condition. It is also defined as ratio of remaining capacity to full charged capacity. Fully charged battery has 100% SOC and a fully discharged battery has an SOC of 0%

The change in SOC in a time interval, dt, with discharging or charging current i may be expressed as

$$\Delta SOC = \frac{idt}{Q(i)} \tag{2.9}$$

where $Q(i)$ is the ampere-hour capacity of battery at current rate i. For discharging i is positive and for charging i is negative. Thus SOC of the battery can be expressed as

$$SOC = SOC_0 - \int \frac{idt}{Q(i)} \tag{2.10}$$

where SOC_0 is the initial value of SOC.

Battery energy

The energy of a battery is measured in terms of capacity and discharge voltage. To calculate energy, the capacity of the battery must be expressed in Coulombs In general, the theoretical stored energy is:

$$E_t = V_{bat} Q_T \tag{2.11}$$

where V_{bat} is the nominal no load terminal voltage, and Q_T is the theoretical capacity in C.

The *specific energy* of a battery is given by the unit for specific energy is Wh/kg.
A measurement of 1 A-h is equivalent to 3600 C, while 1 V refers to 1 J (J for joule) of work required to move 1 C charge from the negative to positive electrode. Therefore, the stored electrical potential energy in a 12 V, 100 A-h battery is $(12)(3.6x105)J = 4.32MJ$.

Table 2.2 shows the theoretical and practical values specific energy for different kinds of electrical batteries.

Battery power

Battery power characteristics are illustrated in Figure 2.8. The instantaneous battery terminal power is

$$p(t) = V_t i \tag{2.12}$$

where V_t is the battery terminal voltage and i is discharge current.

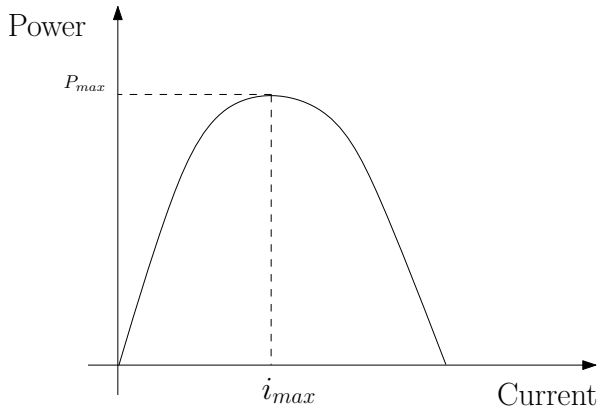

Figure 2.8: Battery Power Characteristics

Maximum power output is needed from the battery in fast discharge conditions, which occur when the electric motor is heavily loaded. Acceleration on a slope is such a condition, when the motor draws a lot of current to deliver maximum power required for traction. The maximum power of the battery can be found using following formula [8]:

$$P_{max} = \frac{E_v^2}{4R_t} \tag{2.13}$$

where E_v is the battery terminal voltage and R_t is internal resistance.

Rated continuous power is the maximum power that the battery can deliver over prolonged discharge intervals without damage to the battery. The rated *instantaneous power* is the maximum power that the battery can deliver over a short discharge interval without damage to the battery

CHAPTER III

BOND GRAPH METHOD

This chapter introduces the bond graph theory principles and its elements. This chapter helps the reader understand bond graph principles and their use in dynamic modeling of mechatronics system. All details of basic elements used in bond graphs are discussed here. Methods and rules to derive system equation and assign causality in bond graph are also presented.

3.1 Introduction

A bond graph is a graphical representation of a physical dynamic system. It captures the energy structure of physical system and provides insight into of system behavior. Moreover, the notations of causality provides a tool not only for formulation of system equations, but also for intuition based discussion of system behavior.

Bond graphs were invented by Prof.Henry Paynter in 1959. He gave the revolutionary idea of portraying systems in terms of power bonds, connecting the elements of the physical system to junction structures which were manifestation of the constraints [12]. The term "Bond Graph" comes from the fact that many of these graphs look like the bonds in chemistry. Later on, bond graph theory has been further developed by many researchers like Karnopp, Rosenberg, Thoma, Breedveld, etc. who have worked on extending this modeling

Domain	**Effort**,$e(t)$	**Flow**,$f(t)$
Mechanical translation	Force component,$F(t)$	Velocity component,$V(t)$
Mechanical rotation	Torque component,$\tau(t)$	Angular velocity component,$\omega(t)$
Hydraulic	Pressure,$P(t)$	Volume flow rate,$Q(t)$
Electric	Voltage,$e(t)$	Current,$i(t)$

Table 3.1: Power variable for different systems

technique to power hydraulics, mechatronics, general thermodynamic systems and recently to electronics and non-energetic systems like economics and queuing theory [1].

Using the language of bond graphs we can construct models of electrical, magnetic, mechanical, hydraulic, pneumatic, thermal, and other systems with only a small set of ideal elements. A complete physical system can be represented by the symbols and lines by identifying the power flow path in the system. Bond graph represents power interaction between different systems which is different from the bock diagram representation in which interaction between the systems are described by signals. Standard mathematical techniques allow the bond graph models to be translated into differential equations or computer simulation schemes [7] [14].

3.2 Power Variables of Bond Graphs

The fundamental idea of a bond graph is that power is transmitted between connected components by a combination of "effort" and "flow". Power can be used as a generalized co-ordinate to model the coupled systems residing in several energy domains. For example, in electric domains effort variable $e(t)$ is voltage and flow variable $f(t)$ is current, in mechanical domain effort variable $e(t)$ is force and flow variable $f(t)$ is velocity. Table1 3.1 shows the effort and flow variables in different physical domains.

In bond graph system, power flowing in to or out of a system can be represented by the product of effort and flow variables.

$$P(t) = e(t)f(t) \tag{3.1}$$

In dynamic system the effort , flow and power variables are change with the respect to time. So if we take the time integral if this two variable flow and effort we can get two new *energy variables*. These variables are called as *momentum* $p(t)$ and *displacement* $q(t)$

The momentum is defined as the time integral of an effort. That is,

$$p(t) = \int^t e(t)dt \tag{3.2}$$

The displacement is defined as the time integral of an flow. That is,

$$q(t) = \int^t f(t)dt \tag{3.3}$$

The energy E(t), passing in to or out if port is described as a integral of power, P(t). Thus

$$E(t) = \int^t P(t)dt = \int^t e(t)f(t)dt \tag{3.4}$$

3.3 Bond Graph Standard Elements and Causality Assignment

Bond graphs define a basic set of multiport elements that can be used to model subsystems in detail. These elements function as components of subsystem and system models and are, in many cases, idealized mathematical models of real components, such as resistors, capacitors, masses, springs, and pipes. In other cases, however, the basic elements are used to model physical effects.

In bond graphs, the inputs and the outputs are characterized by the *causal stroke*. The causal stroke indicates the direction in which the effort signal is directed. Causality establishes the cause and effect relationships between the factors of power. Here, in this section some causality assignment and rules are explained for basic bond graph elements

3.3.1 Basic 1-Port Elements

1- Port elements are expressed by a single port and each port contains single pair of effort and flow variables. Ports are classified as passive and active elements. The passive ports are idealizing elements because they contain no source of power. The inertia or inductor, compliance or capacitor, and resistor or dash pot are classified as passive elements.

R-Element

The *1-port resistor* is an element in which the *effort and flow variables at the single port are related by a static function*. Simple electrical resistors, mechanical dampers or dash pots, porous plugs in fluid lines, and other analogous passive elements are R type elements. R type elements dissipate energy. The bond graph symbol for the resistive element is shown in figure 3.1.

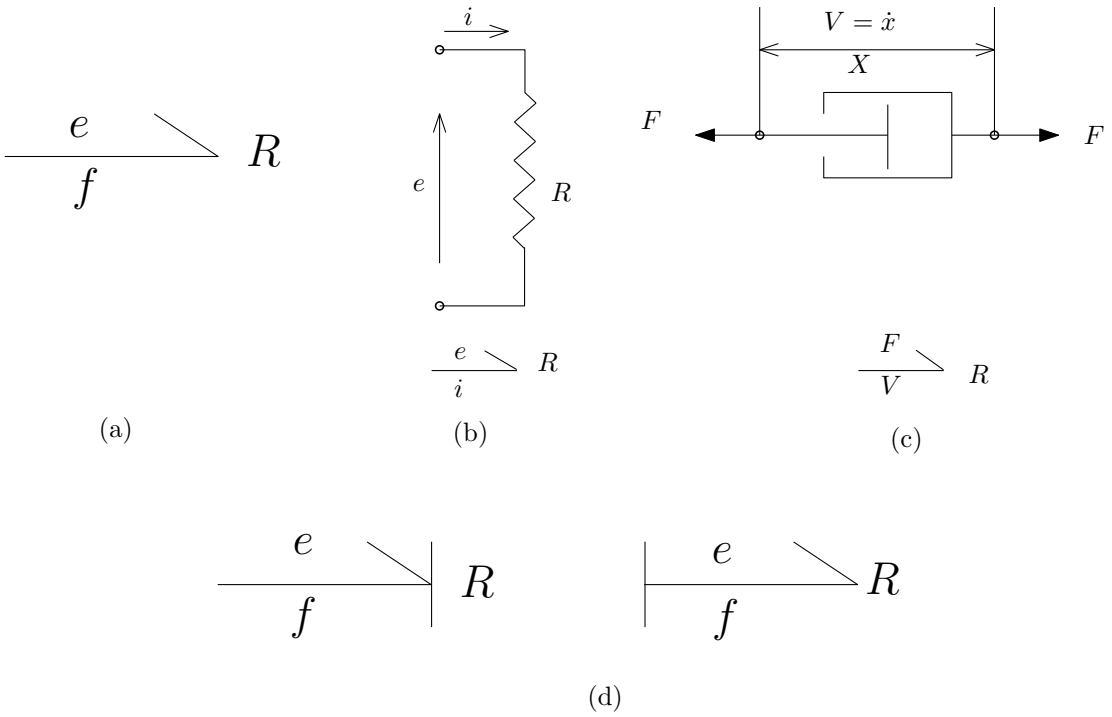

Figure 3.1: 1-port resistor (a) Bond-graph symbol; (b) Electrical Resistor, (c) Mechanical Damper; (d) Causality Assignment

The half arrow pointing towards R means that the power i.e., product of F and V (or $e * f$) is positive and flowing into R, where e, represents *effort* or *force*, and f, represents *flow* or velocity. The constitutive relationship between e, f and R is given as

$$e = Rf, \tag{3.5}$$

$$\text{Power} = ef = Rf^2, \tag{3.6}$$

1-port resistor is normally indifferent to the causality imposed upon it. From equation 3.5 we can say that *flow* and *effort* at this point are algebraically related and thus they have any one of two possible causal structures. We can apply a voltage and get a flow instantly, or apply a flow and get a voltage instantly, thus a resistor can be at either end of a causal bond(figure 3.1(d)). The two possibilities may be represented in equation form as follows:

$$e = Rf; f = \frac{e}{R} \tag{3.7}$$

C-Element

Consider a 1-port device in which a static constitutive relation exists between an *effort* and a *displacement*. Such a device stores and gives up energy without loss.

In bond graph terminology, an element that relates effort to the generalized displacement (or time integral of flow) is called a one port capacitor. In the physical terms, a capacitor is an idealization of devices like springs, torsion bars, electrical capacitors, gravity tanks, and accumulators, etc. The bond graphic symbol, defining constitutive relation for a C-element is shown in figure 3.2.

In a spring, the deformation (x) and the effort (F) at any moment is given by following equation. Here k is the stiffness of the spring and V is the velocity (*flow*).

$$F = kx, \tag{3.8}$$

$$F = k \int V dt \tag{3.9}$$

$$V = K^{-1} \frac{d}{dt} F, \tag{3.10}$$

In a capacitor, the charge accumulated on the plates (q) or voltage (e) is given by following equations, where i is the current.

$$e = \frac{q}{C}, \tag{3.11}$$

$$e = C^{-1} \int i dt, \tag{3.12}$$

$$i = C \frac{d}{dt} e, \tag{3.13}$$

In C elements when f is the input to the C, e is given by a static function of the time integral of f(equations 3.9 and 3.12) but when e is the input, f is the time derivative of a static function of e (equations 3.10 and 3.13). The implications of this two types of causality, are called integral causality(figure 3.2(d)) and derivative causality (figure 3.2(e)).

I-Elements

A third energy-storing 1-port arises if the momentum p is related by a static constitutive law to the flow f. Such an element is called *inertia* in bond graph terminology. The bond graph symbol for an inertia, the constitutive relation, and several physical examples are shown in Figure 3.3.

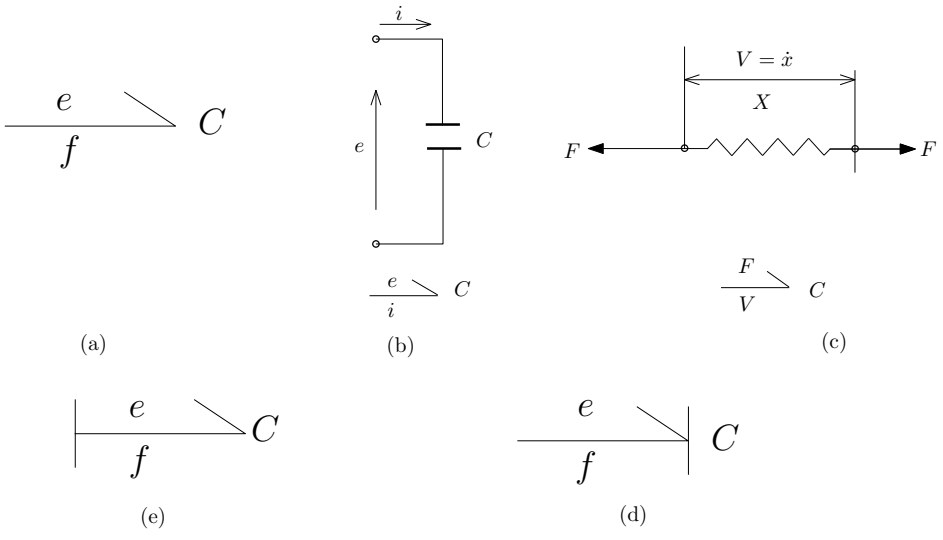

Figure 3.2: 1-Port Capacitor (a) Bond-Graph Symbol; (b) Electrical Capacitor ; (c) Mechanical Spring; (d) Integral Causality Assignment; (e) Derivative Causality Assignment

The inertia is used to model inductance effects (L) in electrical systems, and mass (M) or inertia effects (J) in mechanical or fluid systems.

Here, effort is the cause and velocity (and hence momentum) is the consequence. In mechanical system if force F (*effort* e) is applied on a body having mass M and if velocity due to this force is V then

$$F = ma, a = \dot{V} \tag{3.14}$$

$$F = m\dot{V}, \tag{3.15}$$

$$V = m^{-1} \int F dt \tag{3.16}$$

Similarly in electrical inductor

$$i = L^{-1} \int e dt \tag{3.17}$$

In I type storage elements the flow (f) is proportional to the time integral of the effort. Therefore, an I element receives *effort* (cause) and generates *flow* (effect). In this case,

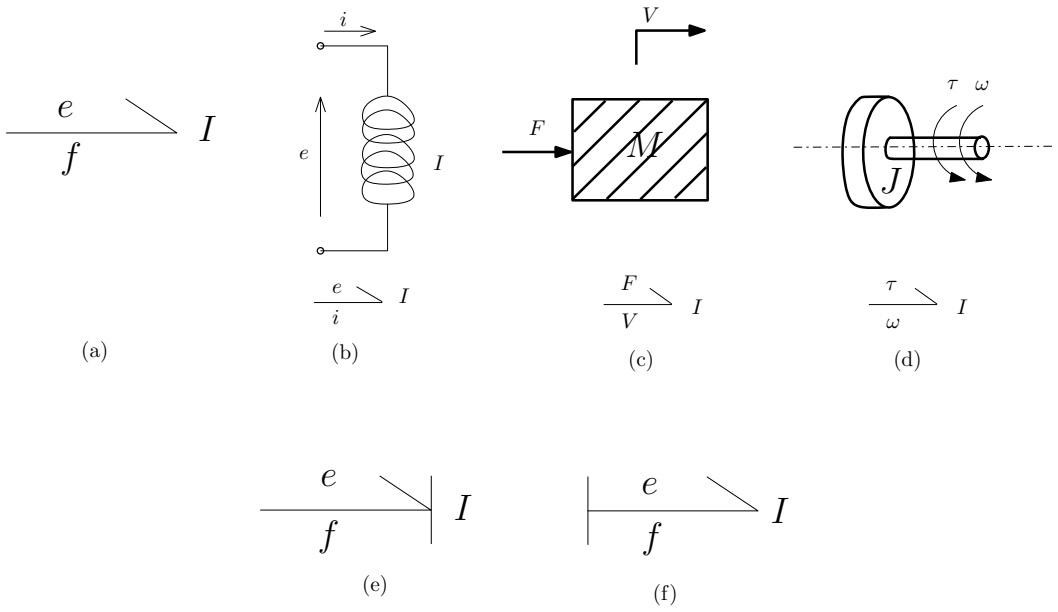

Figure 3.3: 1-Port Inductor (a) Bond-graph Symbol; (b) Electrical Inductor; (c) Mechanical Mass ; (d)rotation inertia; (e) Integral Causality assignment; (f) Derivative Causality Assignment

integral causality exists when e is the input to the inertia (equation 3.15 and 3.16, and derivative causality exists when f is the input (equation 3.17).

Effort and Flow Sources

Source elements supply power to a system. The effort source and the flow source, the 1-port sources, are idealized versions of voltage supplies, pressure sources, vibration shakers, constant-flow systems, and the like. In each case, an effort or flow is either maintained reasonably constant, independent of the power supplied or absorbed by the source, or constrained to be some particular function of time

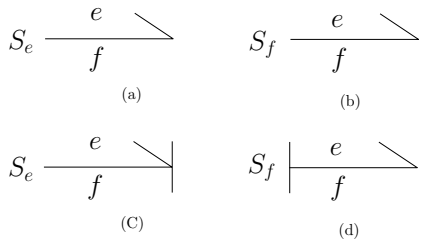

Figure 3.4: (a) Bond Graph Symbol of Source of Energy; (b) Bond Graph Symbol of Source of Flow, (c) Causality Assignment in Source of Energy Elements; (d) Causality Assignment For Source of Flow Elements

Sources impose either an effort or a flow on a system, but not both. Thus, if we use the symbols S_e and S_f for the abstract effort and flow sources, the only permissible causalities for these elements are shown in figure 3.4.

Here, if 1- port energy storage elements (C *and* Itype) have integral causality, they are independent. So in our causal assignments we make every effort to assign integral causality to each energy storage element. During causality assignment we will see that this is not always possible.

If an energy storage element is forced to accept derivative causality, then that element is not independent, and its energy variable(p or q) is algebraically related to the other energy variables in the system. The energy storage element in derivative causality still stores energy,

but its contribution to the system energy can be calculated algebraically from knowledge of the other energy variables, and, if the energy variable of the derivative element should happen to enter the equation formulation, it can be eliminated from the final state equations.

3.3.2 Basic 2-Port Elements

There are only two basic kinds of 2-port systems, *Transformer* and *Gyrator*. This two port systems are ideal in the specific sense power is conserved. It means that

$$e_1(t)f_1(t) = e_2(t)f_2(t), \tag{3.18}$$

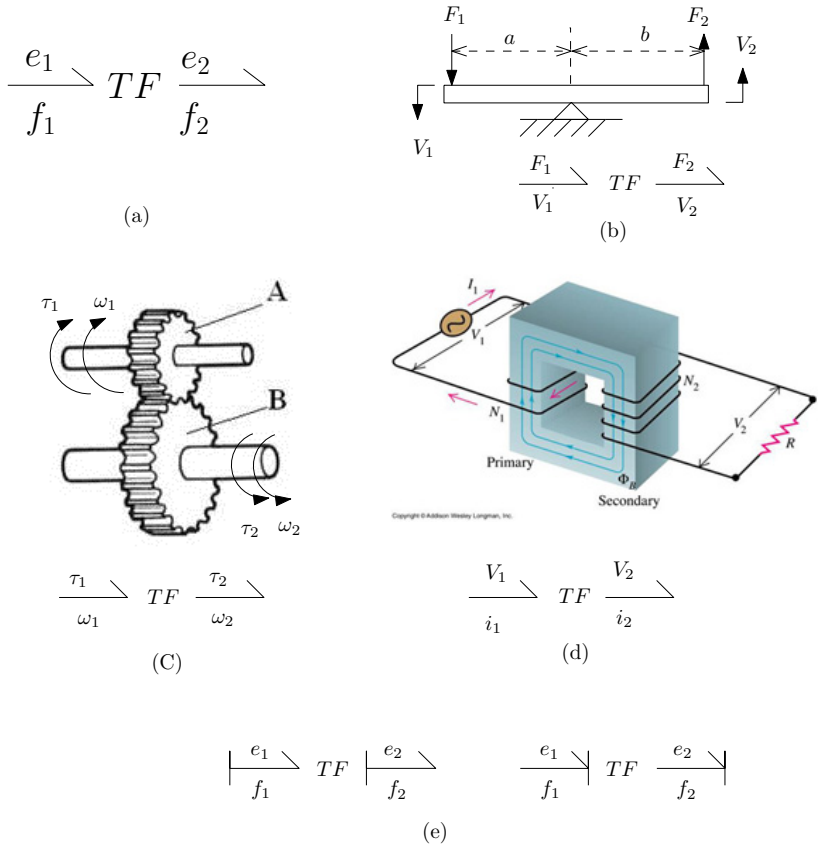

Figure 3.5: 2-Port Transformer (a) Bond-Graph Symbol; (b) Ideal Rigid Lever ; (c) Mechanical Gears; (d)Electrical Transformer; (e) Causality Assignment

Transformer

One way in which Eq. 3.18 can be satisfied is found in the 2-port known as a *transformer* and given in the bond graph symbol $TF-$. *A transformer relates flow-to-flow and effort-to-effort relationship.* The constitutive laws of the ideal 2-port transformer are

$$e_1 = me_2, mf_1 = f_2, \tag{3.19}$$

in which the parameter m is called the *transformer modulus*

The lever(figure 3.5(b)) is an ideal transformer because kinematics dictates that$(b/a)V_1 = V_2$ and moment equilibrium requires $F_1 = (b/a)F_2$.

Similarly, the gear set(figure 3.5(c)) is an ideal transformer because kinematics dictates that $(r_1/r_2)\omega_1 = \omega_2$ and moment equilibrium requires $\tau_1 = (r_1/r_2)\tau_2$

The electrical transformer from figure 3.5(d) is a transformer in the bond graph sense because the voltage is stepped up or down as the current is stepped down or up according to the turns ratio of the windings of the transformer.

The transformer, by its elemental relation, receives either flow or effort information in one bond and generates the same in its other bond. Thus, one of its port is open-ended with the other end stroked as shown in the (figure 3.5(e)).

The Gyrator

A gyrator establishes relationship between flow to effort and effort to flow, again keeping the power on the ports same. The constitutive laws of the gyrator are given below in which r is the gyrator modulus.

$$e_1 = rf_2 \tag{3.20}$$

$$rf_1 = e_2 \tag{3.21}$$

The simplest gyrator is a mechanical gyroscope, shown in the figure 3.6. In the electrical domain, an ideal DC motor is represented as an gyrator, where the output torque is pro-

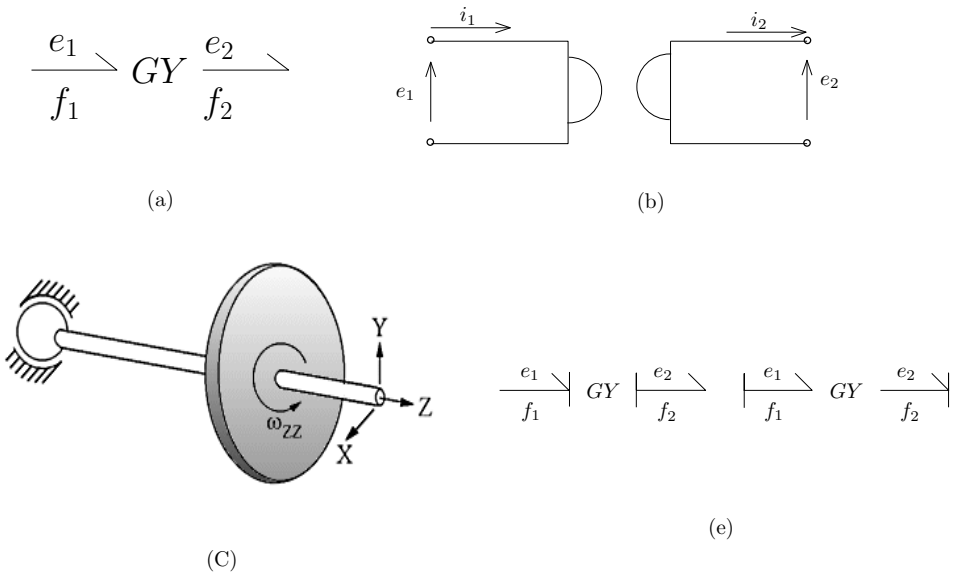

Figure 3.6: 2-port gyrator (a) Bond-Graph Symbol; (b) Electrical Gyrator ; (c) Mechanical Gyrator; (d)Causality Assignment

portional to the input current and the back emf is proportional to the motor angular speed. In general, gyrators are used in most of the cases where power from one energy domain is transferred to another, viz. electrical to rotational, electrical to magnetic, and hydraulic to rotational.

Gyrator relates flow to effort and effort to flow, therefore, both of its ports have either open-ended or stroke-ended causality as shown fig 3.6-(d).

3.3.3 3-Port Junction Elements

3-ports are called as *junctions*, since they serve to interconnect other multiport into subsystem or system models. These 3-ports represent one of the most fundamental ideas behind the bond graph formalism. The idea is to represent in multiport form the two types of connections, which,in electrical terms,are called the series and parallel connections. This kind of connections really occurs in all types of systems.

0−**Junction**

0 Junction is called as *flow junction*, or *common effort junction*. The symbol for this junction is a zero with three bonds emanating from it.

This element is ideal in that power is neither dissipated nor stored. Using the inward power sign convention shown in the last version of the junction, this implies.

$$e_1 f_1 + e_2 f_2 + e_3 f_3 = 0 \tag{3.22}$$

The 0-junction is defined such that all efforts are the same, thus,

$$e_1(t) = e_2(t) = e_3(t) \tag{3.23}$$

$$f_1(t) + f_2(t) + f_3(t) = 0 \tag{3.24}$$

In words, the efforts on all bonds of a 0-junction are always identical, and the algebraic sum of the flows always zero. In other words, if power is flowing in on two ports of the three, then it must be flowing out of the third port.

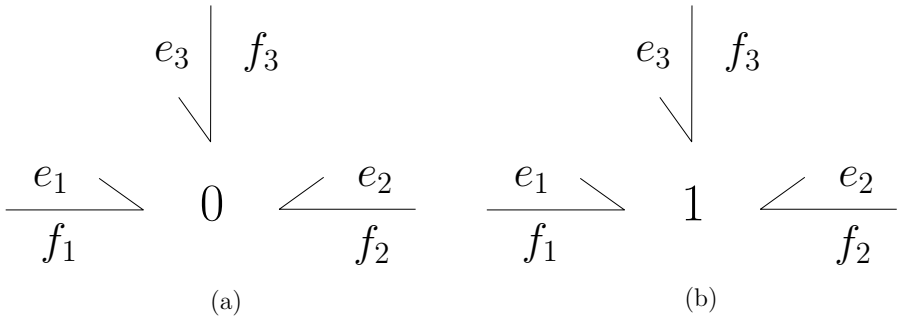

Figure 3.7: 3-Port Elements (a) 0-Junction; (b) 1-Junction

1-Junction

1-junction is called as *effort junction*, or *common flow junction*. The symbol for this multi-port is a 1 with three bonds

The 1-junction is defined such that all flows are the same, thus,

$$f_1(t) = f_2(t) = f_3(t), \tag{3.25}$$

$$e_1(t) + e_2(t) + e_3(t) = 0 \tag{3.26}$$

In words, the flows on all bonds of a 1-junction are always identical, and the algebraic sum of the effort variables is zero. In other words, if power is flowing in on two ports of the three, then it must be flowing out of the third port.

In a 0-junction, efforts are equal, in a 1-junction, flows are equal. Thus, with causal bonds, only one bond can cause the effort in a 0-junction and only one can cause the flow in a 1-junction. So, if the causality of one bond of a junction is known, the causality of the others is also known. That one bond is called the strong bond. Figure 3.8 shows causality assignment in 3 port elements.

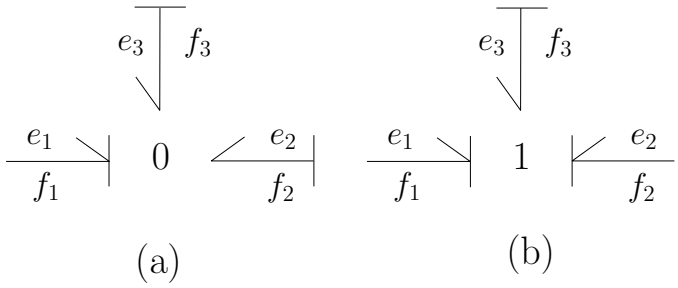

Figure 3.8: Causality in 3-Port Elements (a) 0-Junction; (b) 1-Junction

3.4 Causality Assignment Procedure (adapted from [16])

Here, in this section some causality assignment and rules are explained for basic bond graph systems.

- Choose any source (S_e, S_f), and assign its required causality.
- Extend the causal implications through the graph as far as possible, using the elements $(0, 1, GY, TF)$ which may be connected to the source. These four elements called constraint elements because only certain causal patterns are allowed.

- Repeat this procedure until all energy sources will have preferred causality.
- Choose any storage element (C or I), and assign its preferred (***integral***) causality.
- Extend the causal implications through the graph as far as possible, using the constraint elements $(0, 1, GY, TF)$.
- Repeat this procedure until all energy all storage elements have integral causality.
- Choose any unassigned R-element and assign causality to it. Extend the causal implications through the graph as far as possible, using the constraint elements $(0, 1, GY, TF)$.
- Repeat this procedure until all R-elements have been used.
- Choose any remaining unassigned bond (joined to two constraint elements), and assign a causality to it arbitrarily. Some storage elements may be forced to assign derivative causality. Repeat this procedure and try to cover all elements in the bond graph

CHAPTER IV

BICYCLE MODEL DEVELOPMENT

A detailed mathematical model of the electric bicycle is presented in this chapter. Physical principles and equations, mentioned in Chapter 2, are implemented here using the bond graph method described in Chapter 3. Figure 4.1 shows a block diagram of the electric bicycle. Modeling is done for each separate system and a combined bond graph representing the whole system is derived at the end. Equations of all states and parameters are derived at the end of the chapter for simulation purposes.

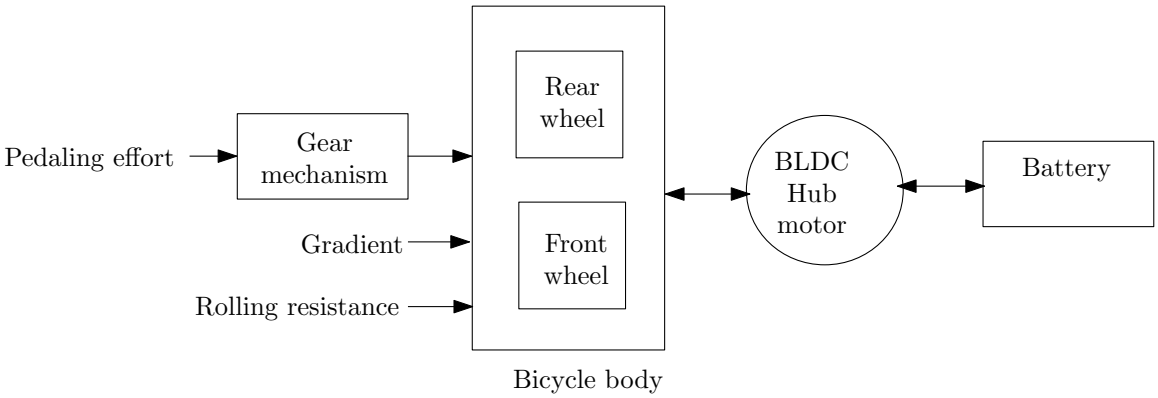

Figure 4.1: System Block Diagram of Hybrid Bicycle Mechanism

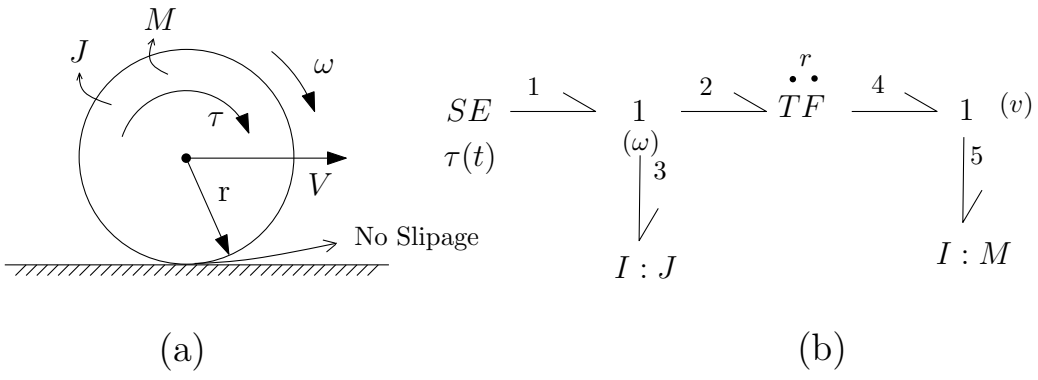

Figure 4.2: Bond Graph for Rotating Wheel System

4.1 Modeling of Bicycle Body

Modeling of bicycle wheel dynamics is done first. Figure 4.2(a) shows schematic diagram of basic mechanical system with wheel running on a flat road. Here parameters of wheel are taken as body mass M, base velocity V, wheel radius r, angular velocity ω and angular torque τ. In this model zero slip age friction is acting on a wheel.

Using the bond graph elements like R, L, C, I, TF, GY, as mentioned in Chapter 3, different systems can be modeled. The bicycle body is a mechanical system and the electric motor and battery are electrical systems. The bond graph method will help full to combine all these different kind of systems in one same terminology.

Bond graph construction procedures for mechanical systems defines the flow variable as a velocity and effort variable as a force. In this system there are two kinds of velocity *translational velocity* (V) and *rotational velocity* (ω). Both velocities will be represented by a 1-junction. System torque τ will be given by applying pedaling effort or by dc motor power. This *angular torque* is represented as *source of effort* S_e. The wheel body has two different kind of mass translational mass M and rotational mass J. They are represented as I-element with junction 1.

Now connect angular velocity ω to base velocity V. The wheel has a radius r and the

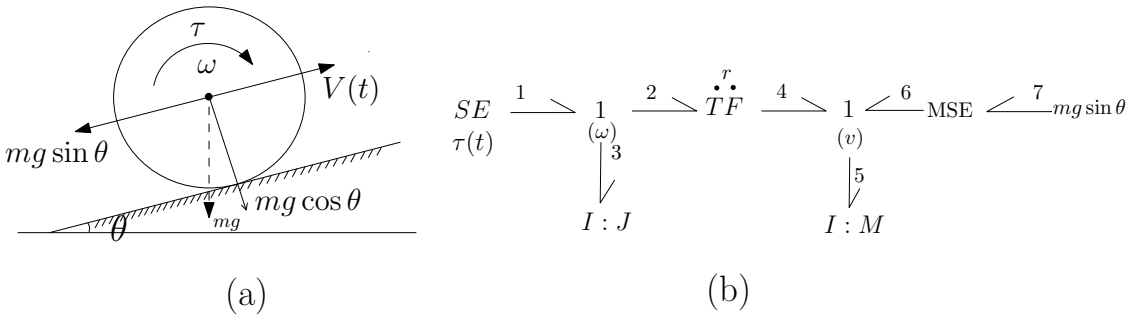

Figure 4.3: Wheel on a Slope

following formula can be used to convert angular velocity to translational velocity.

$$V = r\omega \tag{4.1}$$

A transformer element $-TF-$ can be used to represent this conversion. Figure 4.2(b) shows the complete bond graph representation of the system.

Now, consider that the wheel has rolling resistance and it is rotating on an inclined surface. In this case an extra source of effort (friction torque and rolling resistance) will be required. This friction torque and rolling resistance are acting against the motion and they will reduce the wheel speed. In bond graph it will be considered with $(-)$ negative source of effort.

Figure 4.3(a) shows the system with slope, rolling resistance ($mg\sin\theta$) and friction torque (T_f). Bond graph representation this system is shown in fig 4.3(b)

All physical parameters of the bond graph like rolling resistance, grade resistance, friction torque of bicycle, inertia of both wheel etc. are calculated using experimental setups. Following sections explain the calculation methods and the resulting parameter values.

4.1.1 Rolling Resistance

From equation 2.3 rolling resistance is Mgf_r. For inclined surface with angle θ, it is along the direction of traveling.

$$F_r = Mgf_r\cos\theta \tag{4.2}$$

Considere rider's weight is between 70 Kg to 80 Kg for calculations, F_r is rolling resistance constant. For this bicycle test we took 0.0045 value as F_r and θ is road gradient θ will be changed as per the road gradient.

4.1.2 Friction Torque Measurement

Friction torque is a minimum torque required to initiate the rotation in the wheel. This can be measured by applying known torque to the wheel till it starts to rotate. In this setup a rope was attached to the wheel circumference to hang known weights. Small calibrated weights were added until imminent motion was detected. Friction torque is simply the radius of the rope attached point multiplied by the force created by known weight as shown in the figure 4.4.

$$T_f = \text{ Static load}(F) \cdot \text{ Wheel radius}(R) \tag{4.3}$$

Front wheel weight = 225 g

Rear wheel weight = 85.5g

Wheel radius = 334.5 mm

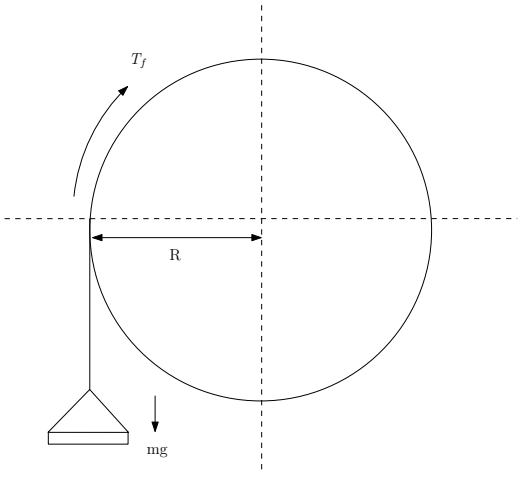

Figure 4.4: Friction Torque Setup

Friction torque value for front wheel $T_{ff} = 0.7383$ N-m

Friction torque value for second wheel $T_{rf} = 0.2806$ N-m

4.1.3 Inertia Measurement

The purpose of this test is to measure the inertia (J_w) of front and rear wheel. Moment of inertia is depends on the static friction torque (T_f) and acceleration (α_a). Friction torque is the minimum force at the distance (r) required to rotate the wheel.

I = moment of inertia

T_f= Static friction torque

α = acceleration

$$I = \frac{T_f}{\alpha_a} \tag{4.4}$$

Angular acceleration(α) of the wheel can be measured by using Spin down test. In this test, the wheel is accelerated to a constant velocity and then power is removed suddenly. The wheel decelerates to zero speed due to friction, with constant negative acceleration. The constant of the linear regression curve for time vs speed will give the acceleration (α) of the wheel.

In spindown test setup a hall-effect sensor was installed for each wheel. The sensor works by detecting the passage of a ferromagnetic bolt or a magnet in front of the sensor. The front wheel uses one magnet, while the rear wheel has 6 equally-spaced bolts. Each time the magnet or a bolt pass in front of the stationary sensor, a pulse is created. A WinCon real-time interface was prepared to record and display the incoming pulse stream. The instantaneous speed at time t is found by determining the number of pulses per second near the desired time t. The interface only records the pulses as a function of time. Using this data we calculated the speed at different time intervals and speed vs time plot was generated for both the wheels.

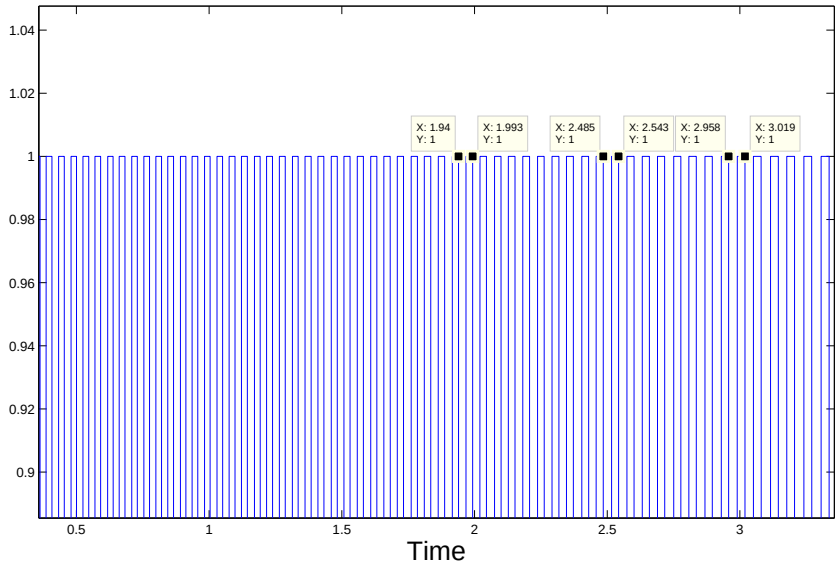

Figure 4.5: Rear Wheel Spindown Test Data

Rear wheel spindown test

Figure 4.5 shows the plot of hall effect data captured by the Win-Con interface for the rear wheel. Each pulse represent the instantaneous time.Figure 4.6 shows the speed vs time plot for rear wheel spindown test

Rear wheel friction torque (T_{fr}) = 0.2806

Linear regression coeff (α_{ar}) = -2.3501

Rear wheel Inertia J_r = 0.1194

Front wheel spindown test : method 1

Figure 4.7 shows the plot of hole effect data captured by the Win-Con interface for the front wheel. Each pulse represent the instantaneous time. Time interval between two pulses will give the instantaneous speed during that interval. For different intervals speed value can be calculated. Figure 4.8 shows the Speed Vs time plot for rear wheel spindown test

Rear wheel friction torque(T_{ff}) = 0.7383

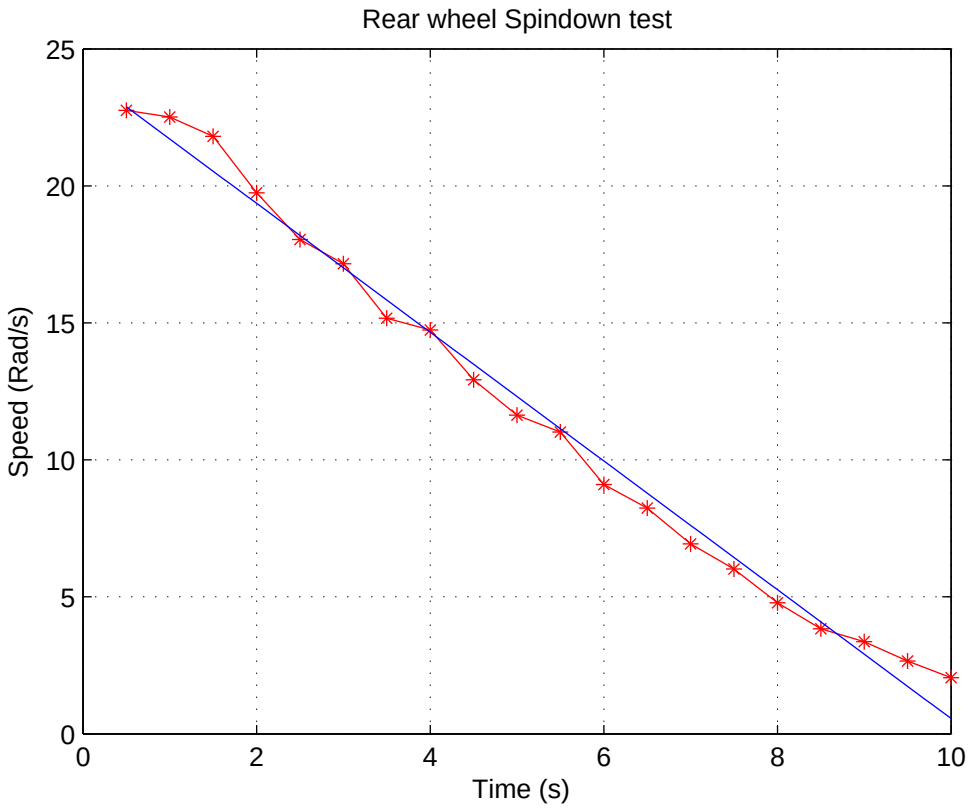

Figure 4.6: Rear wheel Spindown Test

Linear regression coeff (α_{af}) = -2.7674

Rear wheel Inertia $J_f = 0.1014$

Front wheel spindown test : method 2

In the front wheel hub motor is installed and its permanent magnets make it difficult to obtain an accurate friction torque reading using static torque method due to cogging. An alternative method is used to measure the moment of inertia of wheel. Front wheel was allowed to reach zero speed from a high initial speed and required time was measured. Two spindown tests were performed in this method. One with wheel inertia J_f and one with know, added inertia J_a. Extra inertia has been created by attaching 600g weight to the rim as shown in figure 4.9. The wheel was spun at a maximum speed of 433 rpm. Speed was

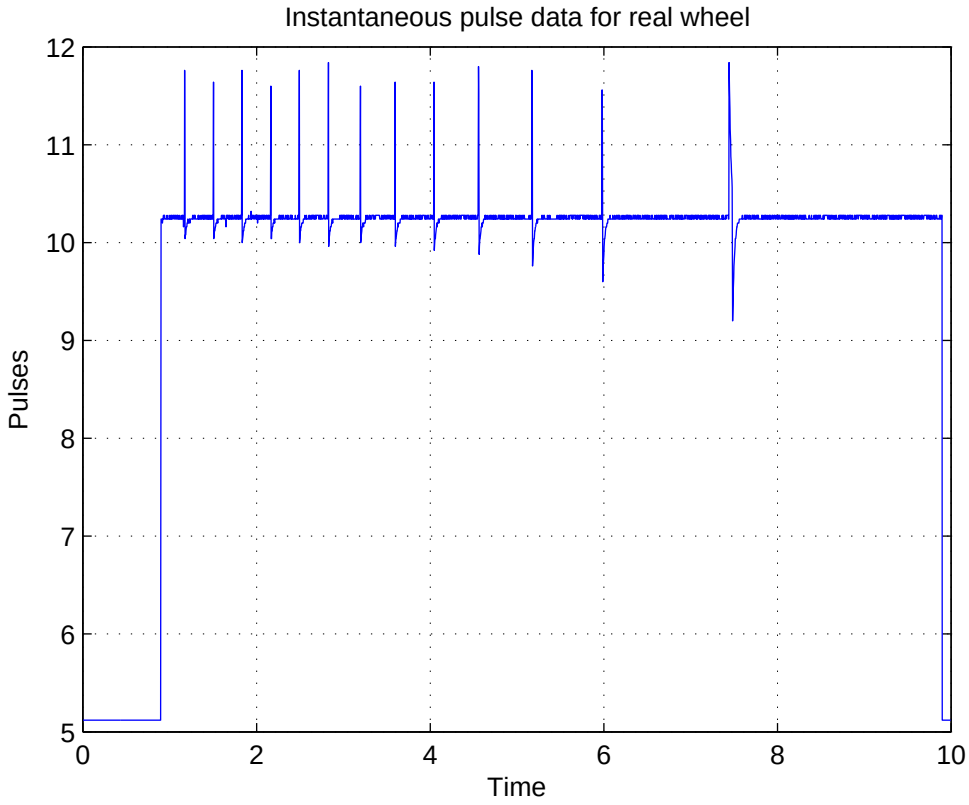

Figure 4.7: Front Wheel Spindowntest Data

measured using a tachometer and time was measured using a stop watch. Time to reach zero was 10.8 seconds without an added inertia and 12.8 with added inertia. A system of 2 equations and 2 unknowns can be formed to determine the friction torque and the moment of inertia. Comparing those equations inertia of the wheel can be calculated as shown in equation refc.

$$T_{ff} = J_w \alpha_1 \tag{4.5}$$

$$T_{ff} = (J_w + J_a)\alpha_2 \tag{4.6}$$

$$J_w = \frac{J_a \alpha_2}{(\alpha_1 - \alpha_2)} \tag{4.7}$$

$$\alpha = \frac{\omega}{T} \tag{4.8}$$

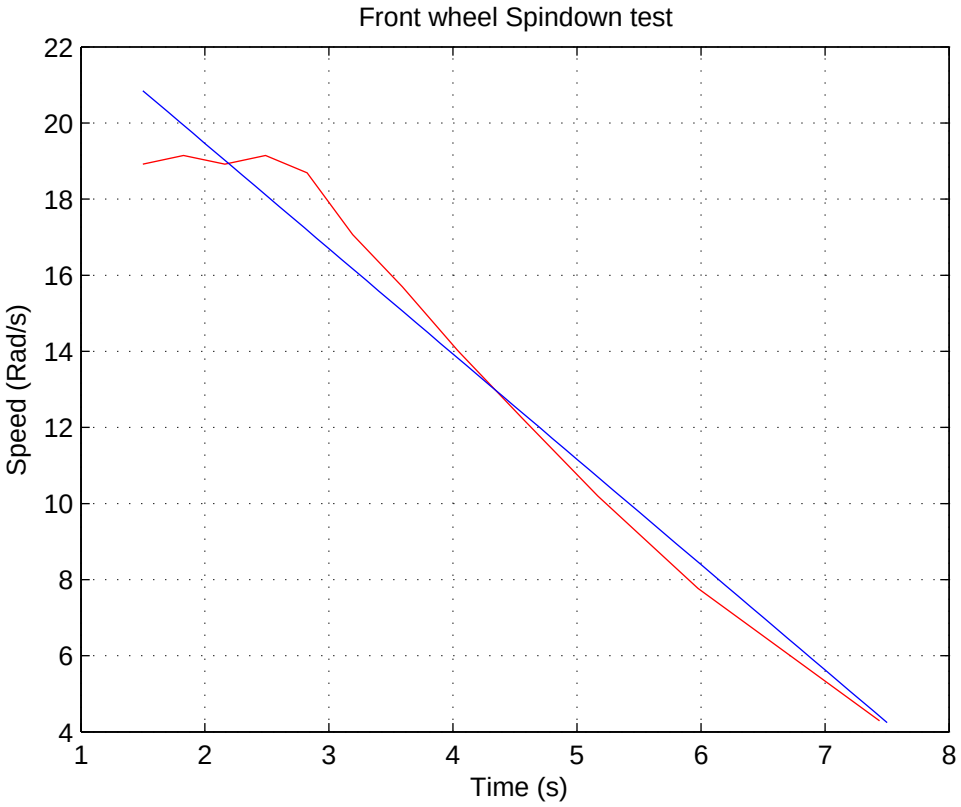

Figure 4.8: Front wheel Spindown Test

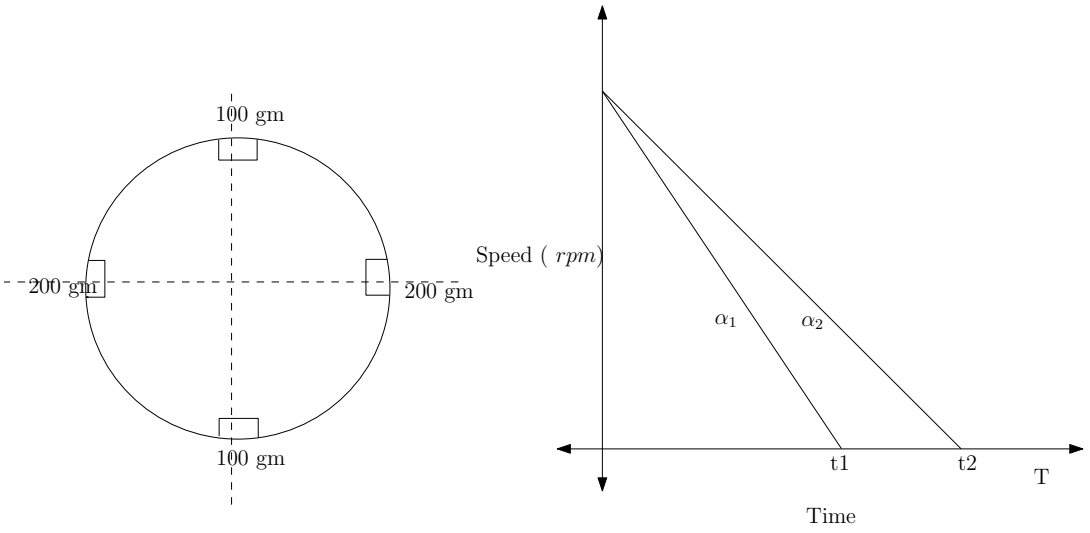

Figure 4.9: Front wheel Spindown Test

Here,

Wheel max speed = 433 rpm = 45.3437 rad/s

α_1 = Speed / Time = 4.1985

α_2 = Speed / Time = 3.5425

$J_a = 0.0187\ kg - m^2$

Rear wheel friction torque (T_{f2}) = 0.4240

Rear Wheel Inertia (J_{f2}) = 0.1010

4.1.4 Gear Ratio

The rear wheel is attached with the *Continuously Variable Transmission* or CVT system. Working mechanism and details of CVT component is explained in 2.5. This CVT mechanism is capable of adjusting the gear ratio to any value to its range. This feature is used to adjust gear ratio in electrical bicycle prototype. A potentiometer was attached with this actuator using gears to measure the position of axle. Computer controlled interface has been setup to control the rotation of ball axle shaft. Now turning the pedal for one revolution we can measure the wheel rotations. Taking different readings for different shaft positions and wheel rotations we can find the range of gear ratio.

Here the range of gear ration g is 1.2 to 4.6

$$\text{Gear ratio} = \frac{\text{Rear wheel velocity}}{\text{pedal velocity}}$$

A microcontroller base PID controller is designed in section 6.7 to control the gear ratio using position control of DC motor. With this kind of feedback controller 9 fixed value gear ratios are set from lower to higher range.

4.1.5 Weight of Bicycle

Overall weight of the bicycle was measured using the load cell. This weight is taken as constant for all ride tests.

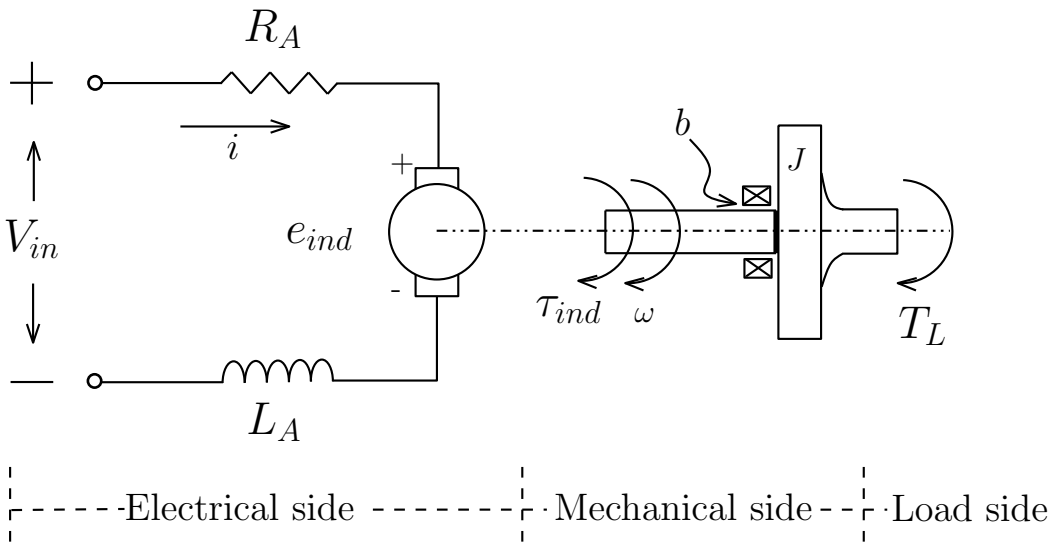

Figure 4.10: DC Motor

Bicycle weight without rider $M_b = 40.257$ kg $= 394.9212$ N

4.2 Modeling of BLDC motor

In this prototype a brushless DC motor (BLDC) is used as a main source of power. For modeling purpose, the BLDC and driving electronics are assumed to behave as a DC motor.

Figure 4.10 shows the circuit diagram of DC motor and its mechanical connections. Voltage V_{in} and current i is applied to the motor and due to this emf e_{ind} will produce in the coil. R_A is coil resistor, L_A is coil inductance. Motor is connected with the shaft using a bearing. Shaft has inertia J, bearing resistance b, torque T and angular velocity ω

When current caring conductor is placed in a magnetic field, a force is exerted on the conductor. This can be represent by following equations.

$$F = i(B \times l) \tag{4.9}$$

$$T_{ind} = \alpha i \tag{4.10}$$

Here,

B= magnetic flux,

i = armature current,

α = mechanical torque constant

According to electromagnetic induction principle when conductor moves in a magnetic field a voltage will induce. If B is the magnetic field v is a velocity of rotating coil and e_{ind} is induce emf then

$$e_{ind} = (Bl)v, \tag{4.11}$$

$$V_{in} = \alpha\omega \tag{4.12}$$

α = electrical torque constant

ω = angular speed

From equations (4.10) and (4.12) we can see that induce *emf* (*effort*) in the motor is depends on angular velocity (*flow*) and induce torque T_{ind} (*effort*) is depends on the input current i (*flow*). So this flow effort relationship can represented by a gyrator $(-GY-)$element. DC motor is perfect example of gyrator element. R_a and L_A can be placed as $R-$ element and $L-$ element both are connected in series so they have common flow (current) junction $-1-$. Same as mechanical side shaft bearing friction (R_b) represented as $R-$element and shaft inertia J represented as $I-$element.

Figure 4.11 shows the complete bond graph representation of DC motor.

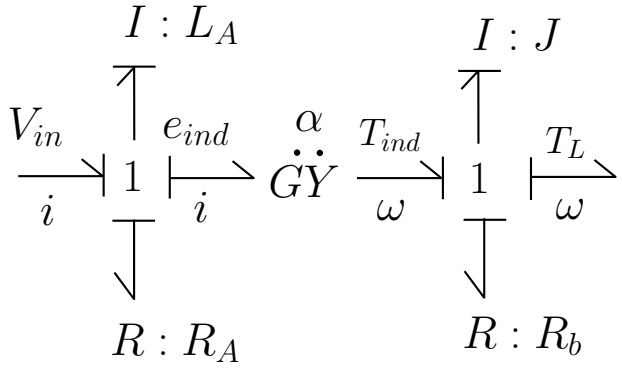

Figure 4.11: Dc Motor Bond Graph

4.2.1 Motor Torque Constant (α)

The amount of torque generated by the motor is always proportional to the current passing through the wiring. This characteristic is constant for the electric motor and it's known as torque constant (α) or K_t and expressed as Oz-in/amp or N-m/Amp.

In electric bicycle model electronic controller and brushless motor is assumed to behave as a DC motor and generates constant torque using battery current. Custom built dynamo meter setup was done to measure this torque generated by the motor. The dynamometer consists of an arm passing through the center of the wheel and a vertical bar pressing on a load cell. Current flowing from the battery is measured with multimeter.

In this setup bicycle was securely mounted on two bike trainer's supports. Custom built dynamometer setup was done to measure the torque generated by the motor. The dynamometer consists of an arm passing through the center of the wheel and a vertical bar pressing on a load cell placed on the floor. The wheel cannot rotate freely, so it will apply a force on the load cell through the vertical bar. Force will be measured in volts and can be converted in N using load cell constant. Measuring the distance between center of motor and load cell we can calculate the torque applied by motor on load cell. A multimeter was

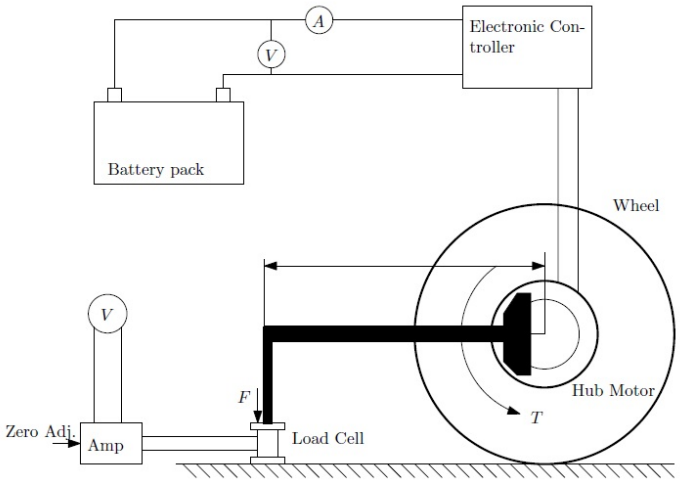

Figure 4.12: Torque Constant Setup

connected between the battery to measure the voltage and current supplied by the battery. Motor current can be changed using the throttle. As we increase the current more force will apply on load cell and voltage will decrease. Measuring different torque values at different current levels we can plot the linear relationship. Torque constant can be found by linear regression of this curve in N-m/A.

Load cell Constant(LV) = 118.21 N/V

Length of arm (L) = 24.8300 mm

Load cell voltage (LV)

$$\text{Torque} = \text{ Load cell Voltage} * \text{ Load cell Constant} * \text{ Length of arm}$$

Motor Torque constant : 4.9710

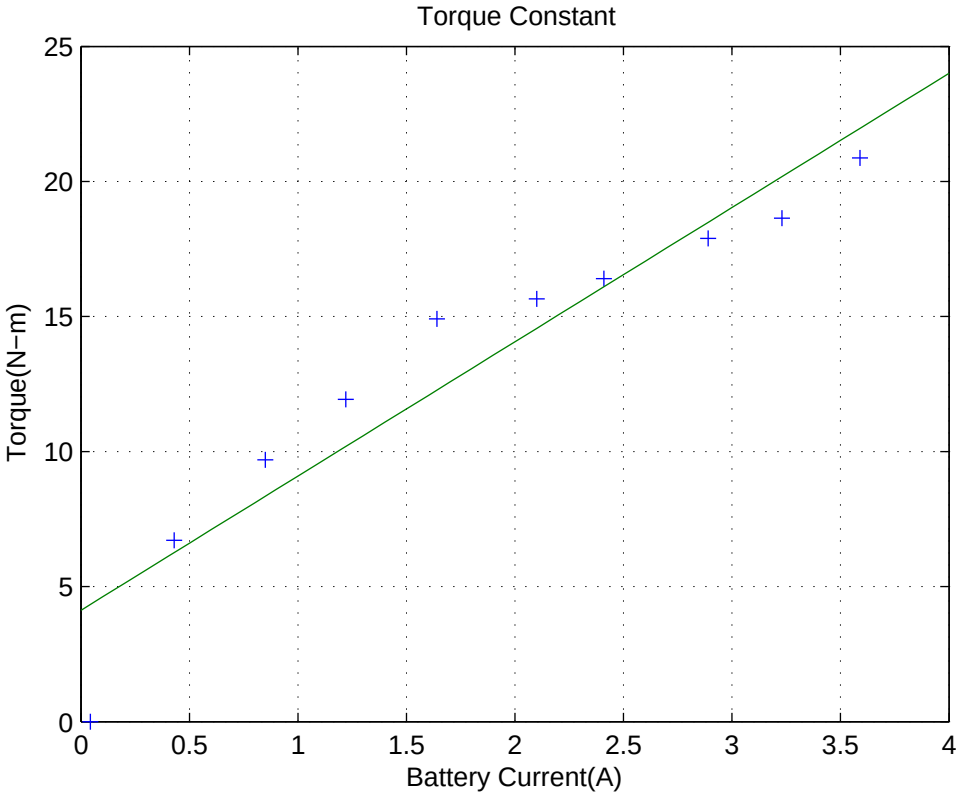

Figure 4.13: Torque Constant Curve

Table 4.1: Torque constant Experiment data

No.	Battery Voltage	Load cell current
1	0.044	0
2	0.43	0.09
3	0.85	0.13
4	1.22	0.16
5	1.64	0.2
6	2.1	0.21
7	2.41	0.22
8	2.89	0.24
9	3.23	0.25
10	3.59	0.28

4.3 Modeling of Battery

Battery is used for supplying dc power to the motor and it is also used to store the charge from regeneration. Battery is considered as a big capacitor connected with resistor in series. Figure 4.14 shows the electrical circuit of battery. C is the capacitor, R_i is internal resistance of battery, q is the charge of battery and V_t is the available voltage at the output terminal of battery.

In this circuit both capacitor and internal resistance are in series so they represented by using $R-$ and $L-$elements connected with common flow junction. When motor is in power mode battery will worker as a source of energy so here causality and power direction will change for C element. When motor will generate power, battery will store that charge and work as a capacitor. Flow direction and causality will change in both the conditions. Bond graphs for both power supply mode and charging mode are shown in figure 4.14(c)and(d) respectively.

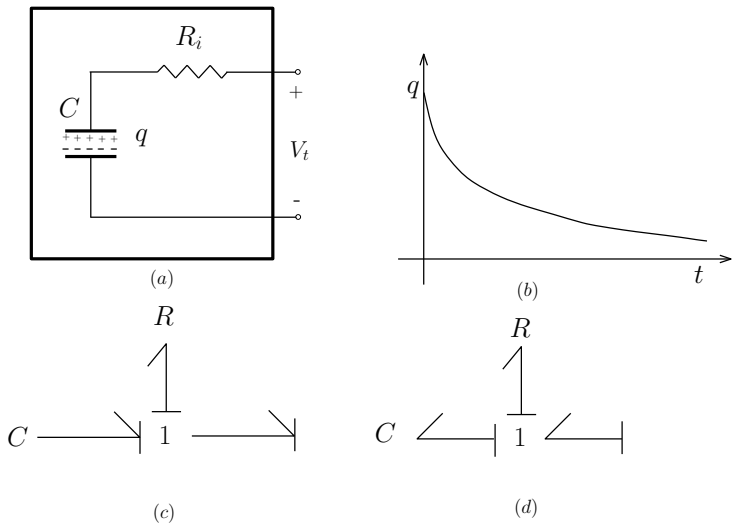

Figure 4.14: Battery

4.3.1 Battery Capacity

The batteries supplied with the bicycle motor kit are unlabeled so their charge capacity needs to be measured. The total charge drawn from the batteries is the time integral of the current. In practice batteries are regarded as discharged when current drops below the current required to overcome the friction torque and rolling resistance. A threshold voltage can also be used as a criterion to determine when a battery has become discharged. A real-time data acquisition system (wincon) was used to record the current and battery voltage simultaneously with time intervals. Throttle was fixed at maximum condition to rotate the wheel at full speed. Current and battery data was recorded until the wheel stopped rotating due to low battery power.

$$i_{batt} = \frac{dq_{batt}}{dt}$$
$$q_{batt} = \int i dt$$

4.3.2 Electric Resistance of Battery

The resistance R_e is considered that includes all electrical power losses due to the efficiency of control circuitry, motor and the copper resistance.

$$\Delta P = i^2 R_e \tag{4.13}$$

$$\Delta P = P_{ele} - P_{mech} \tag{4.14}$$

P_{mech} can be calculate by rotating wheel at constant speed. At this speed there is only friction torque acting on the wheel. The front wheel was accelerated to a constant speed of 373 rpm(39.0605 rad). T_{ff} was calculated from 4.1.2 At this condition the current flowing from the battery was 0.85A, and voltage was 51V Using this data we can also calculate P_{elec}

$$P_{ele} = VI$$

$$P_{ele} = 0.85 \cdot 51$$

$$P_{ele} = 43.3500 \text{ Watts}$$

$$P_{mech} = T_{ff}\omega$$

$$P_{mech} = 0.73830 \cdot 39.0605$$

$$P_{mech} = 28.8383 \text{ Watts}$$

Now using this data ,

$$R_e = \frac{P_{elec} - P_{mech}}{i^2}$$

$$R_e = 20.0853\Omega$$

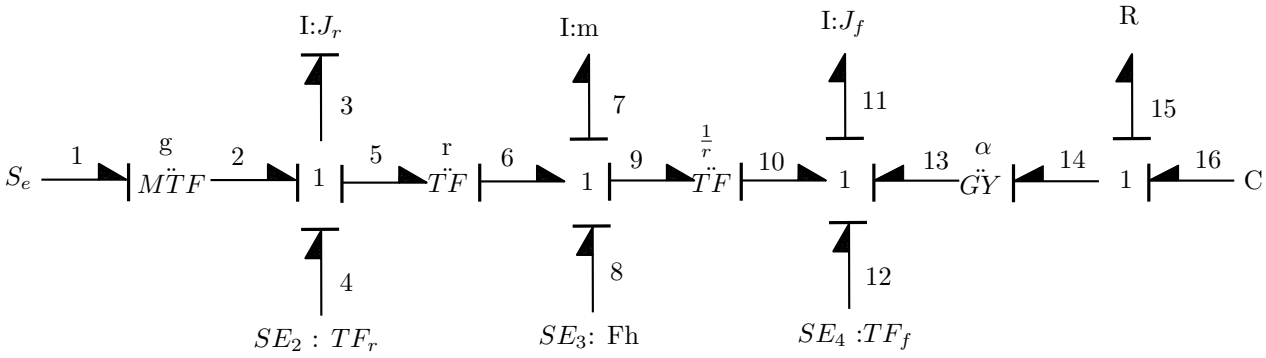

Figure 4.15: Complete Bond Graph Representation of Electric Bicycle

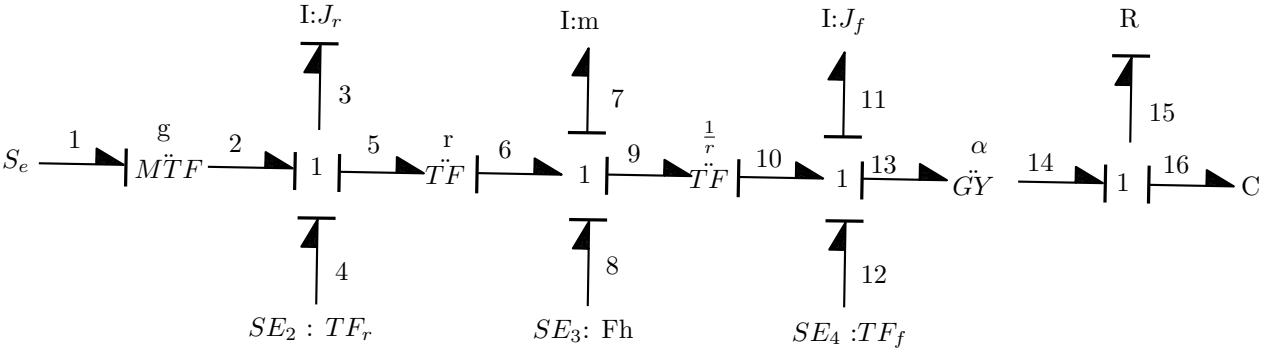

Figure 4.16: Complete Bond Graph Representation of Electric Bicycle Energy Regeneration

4.4 Bond Graph Equations

Figure 4.15 shows the complete bond graph model of electric bicycle. In this model bicycle is using manual and electric both energy sources. All different parts can be defined using bond graph method. Causality and bond numbers are assigned for all elements. We have two differential causality at I_7 and I_{11} elements. In this system there are two independent state variables p_3, q_{16} and two dependent state variables p_7, p_{11}

Here , e_1 = manual effort (S_e)

e_4 = front wheel friction torque (T_{fr})

e_8 = hub friction

e_{12} = rear wheel friction torque(T_{ff})

Outputs :

f_3 = Speed rear wheel

q_{16} = Charge of battery

Using the calculation method shown in Chapter 3 state equations can be calculated for the model.

Starting from left at -MTF- elements

$$e_1 = ge_2$$

$$f_1 = \frac{f_2}{g}$$

$$e_1 = SE_1$$

at 1-Junction

$$f_2 = f_3 = f_4 = f_5$$

$$e_2 + e_4 = e_3 + e_5$$

$$f_3 = \frac{p_3}{I} = \frac{p_3}{J_r}$$

$$e_4 = SE_4$$

at -TF- Junction

$$e_5 = re_6$$

$$f_5 = \frac{f_6}{r}$$

at 1-Junction

$$f_6 = f_7 = f_8 = f_9$$

$$e_6 + e_8 = e_7 + e_9$$

$$e_7 = \dot{p}$$

$$e_8 = SE_3$$

at -TF- element

$$e_9 = \frac{e_{10}}{r}$$

$$f_9 = r f_{10}$$

at 1-Junction

$$f_{11} = f_{10} = f_{12} = f_{13}$$

$$e_{11} = \dot{p}_{11}$$

$$e_{11} = e_{10} + e_{12} + e_{13}$$

$$e - 12 = SE_4$$

at -GY- element

$$e_{14} = \alpha f_{13}$$

$$e_{13} = \alpha f_{14}$$

at 1-Junction

$$e_{16} = \frac{q_{16}}{c_b}$$

$$e_{15} = Re f_{15}$$

$$f_{14} = f_{15} = f_{16}$$

$$e_{16} = e_{14} + e_{15}$$

Now calculate algebraic relationship for dependent states (p_7, P_{11})

- Link P_7 with P_3

$$f_7 = f_6 = r f_5 = r f_3 = r\frac{p_3}{J_r}$$

$$f_7 = r\frac{r p_3}{J_r}$$

$$\frac{p_7}{M} = \frac{r p_3}{J_r}$$

$$p_7 = \left(\frac{Mr}{J_r}\right) p_3$$

$$e_7 = \dot{p}_7 = \left(\frac{Mr}{J_r}\right) \dot{p}_3$$

- Link P_{11} with P_3

$$f_{11} = f_{10} = \frac{f_9}{r} = \frac{f_7}{r} = \frac{rp_3}{rJ_r}$$

$$f_{11} = \frac{p_3}{Jr}$$

$$e_{11} = \dot{p}_{11} = \left(\frac{J_f}{J_r}\right) \dot{p}_3$$

Sate equations for stat variables $p3$ and q_{16}

$\dot{p}_3 = e_3$

$\dot{p}_3 = \frac{e_1}{g} + e_4 - re_6$

$\dot{p}_3 = \frac{e_1}{g} + e_4 - r(e_7 + e_9 - e_8)$

$\dot{p}_3 = \frac{e_1}{g} + e_4 - r(\dot{p}_7 + \frac{e_{10}}{r} - e_8)$

$\dot{p}_3 = \frac{e_1}{g} + e_4 - r\dot{p}_7 - re_8 - e_{10}$

$\dot{p}_3 = \frac{e_1}{g} + e_4 + re_8 - r\dot{p}_7 - (e_{11} - e_{12} - e_{13})$

$\dot{p}_3 = \frac{e_1}{g} + e_4 + re_8 - r\dot{p}_7 - \dot{p}_{11} + e_{12} + \alpha f_{14}$

$\dot{p}_3 = \frac{e_1}{g} + e_4 + re_8 - r\dot{p}_7 - \dot{p}_{11} + e_{12} + \alpha f_{14}$

$\dot{p}_3 = \frac{e_1}{g} + e_4 + re_8 + e_{12} - r\dot{p}_7 - \dot{p}_{11} + \alpha f_{15}$

$\dot{p}_3 = \frac{e_1}{g} + e_4 + re_8 + e_{12} - r\dot{p}_7 - \dot{p}_{11} + \alpha \frac{e_{15}}{R_e}$

$\dot{p}_3 = \frac{e_1}{g} + e_4 + re_8 + e_{12} - r\dot{p}_7 - \dot{p}_{11} + \frac{\alpha}{R_e}(-e_{14} + e_{16})$

$\dot{p}_3 = \frac{e_1}{g} + e_4 + re_8 + e_{12} - r\dot{p}_7 - \dot{p}_{11} + \frac{\alpha}{R_e}(-\alpha f_{11} + \frac{\alpha}{R_e} e_{16})$

$\dot{p}_3 = \frac{e_1}{g} + e_4 + re_8 + e_{12} - r\dot{p}_7 - \dot{p}_{11} - \frac{\alpha^2}{R_e} f_{11} + \frac{\alpha}{R_e}(\frac{q_{16}}{C_b})$

$\dot{p}_3 = \frac{e_1}{g} + e_4 + re_8 + e_{12} - r\dot{p}_7 - \dot{p}_{11} - \frac{\alpha^2}{R_e}(\frac{p_3}{J_r}) + \frac{\alpha}{R_e C_b} q_{16}$

$\dot{p}_3 = \frac{e_1}{g} + e_4 + re_8 + e_{12} - r(\frac{Mr}{J_r})\dot{p}_3 - \frac{J_f}{J_r}\dot{p}_3 - (\frac{\alpha^2}{R_e J_r})p_3 + (\frac{\alpha}{R_e C_b})q_{16}$

$\dot{p}_3 = (\frac{e_1}{g} + e_4 + re_8 + e_{12}) - (\frac{Mr^2}{J_r})\dot{p}_3 - (\frac{J_f}{J_r})\dot{p}_3 - (\frac{\alpha^2}{R_e J_r})p_3 + (\frac{\alpha}{R_e C_b})q_{16}$

$$\dot{p_3} = \frac{(\frac{e_1}{g} + e_4 + re_8 + e_{12}) - (\frac{\alpha^2}{R_e J_r})p_3 + (\frac{\alpha}{R_e C_b})q_{16}}{(1 + \frac{Mr^2}{J_r} + \frac{J_f}{J_r})} \tag{4.15}$$

Now for $\dot{q_{16}}$

$\dot{q}_{16} = f_{16}$

$\dot{q}_{16} = f_{15}$

$\dot{q}_{16} = \frac{e_{15}}{R_e}$

$\dot{q}_{16} = \frac{1}{R_e}(e_{16} - e_{14})$

$\dot{q}_{16} = \frac{1}{R_e}(\frac{q_{16}}{C_b} - \alpha f_{13})$

$\dot{q}_{16} = \frac{q_{16}}{R_e C_b} - \frac{\alpha f_{11}}{R_e}$

$\dot{q}_{16} = \frac{q_{16}}{R_e C_b} - \frac{\alpha}{R_e}(\frac{p_3}{J_r})$

$$\dot{q}_{16} = (\frac{1}{R_e C_b})q_{16} - (\frac{\alpha}{R_e J_r})p_3 \tag{4.16}$$

Now for output parameters

- Bicycle speed

$$f_7 = (\frac{r}{J_r})p_3$$

- Pedal rpm

$$f_1 = \frac{f_2}{g} = \frac{f_3}{g} = \frac{p_3}{J_r g}$$
$$f_1 = (\frac{1}{J_r g})p_3$$

- Battery current

$$q16 = \text{charge}$$

- Battery voltage

$$\dot{q}_{16} = f_{16} = (\frac{-\alpha}{J_r R_e}) + (\frac{1}{R_e C_b})q_{16}$$

Now using state space formula

$$\dot{x} = Ax + Bu \tag{4.17}$$

$$y = Cx + Du \tag{4.18}$$

$$\begin{bmatrix} \dot{p}_3 \\ \dot{q}_{16} \end{bmatrix} = A \begin{bmatrix} p_3 \\ q_{16} \end{bmatrix} + B \begin{bmatrix} e_1 \\ e_4 \\ e_8 \\ e_{12} \end{bmatrix} \tag{4.19}$$

For output parameters

$$\begin{bmatrix} f_1 \\ f_7 \\ f_{16} \\ q_{16} \end{bmatrix} = C \begin{bmatrix} p_3 \\ q_{16} \end{bmatrix} + D \begin{bmatrix} e_1 \\ e_4 \\ e_8 \\ e_{12} \end{bmatrix} \tag{4.20}$$

Where A, B, C, D matrix are given as

$$A = \frac{1}{(1 + \frac{Mr^2}{J_r} + \frac{J_f}{J_r})} \begin{bmatrix} -\frac{\alpha^2}{R_e J_r} & \frac{\alpha}{R_e C_b} \\ -\frac{\alpha}{R_e J_r} & \frac{1}{R_e C_b} \end{bmatrix} \tag{4.21}$$

$$B = \frac{1}{(1 + \frac{Mr^2}{J_r} + \frac{J_f}{J_r})} \begin{bmatrix} \frac{1}{g} & 1 & r & 1 \\ 0 & 0 & 0 & 0 \end{bmatrix} \tag{4.22}$$

$$C = \begin{bmatrix} \frac{r}{J_r} & 0 \\ \frac{-}{RJ_r} & \frac{1}{C_b} \\ \frac{b}{J_r} & 0 \\ \frac{1}{gJ_r} & 0 \end{bmatrix} \tag{4.23}$$

$$D = 0; \tag{4.24}$$

CHAPTER V

SIMULATION STUDY

5.1 Simulation Model Development

The state space equations, derived in Chapter 4, represents the mathematical model of the electric bicycle. This bond graph-based dynamic model of the electric bicycle can be used for simulation purposes. Now we can apply a variety of test scenarios to the plant model with a variety of road profiles. This will allow us to check the system responses by measuring output parameters of the model.

Matlab/Simulink has good simulation capabilities with wide range of system libraries, which can be used to generate different scenarios for the model. Here, the bicycle model is presented as a set of state derivative equations using Matlab function blocks. From the state space system (equations 4.15 and 4.16) output parameters like vehicle velocity, battery charge, and battery current can be found. After that they can be converted into bicycle speed, velocity, battery voltage and battery current.

Figure 5.1 shows the basic simulation model for the electric bicycle generated from bond graph state space equation(4.20). Here, output parameter f_1 represents the flow of input power, which can be converted in to pedaling speed. f_7 represents the linear velocity of bicycle. These parameters are used to calculate the total distance traveled in miles and velocity in mph unit. f_{16} represents the battery current. q_{16} represents battery charge

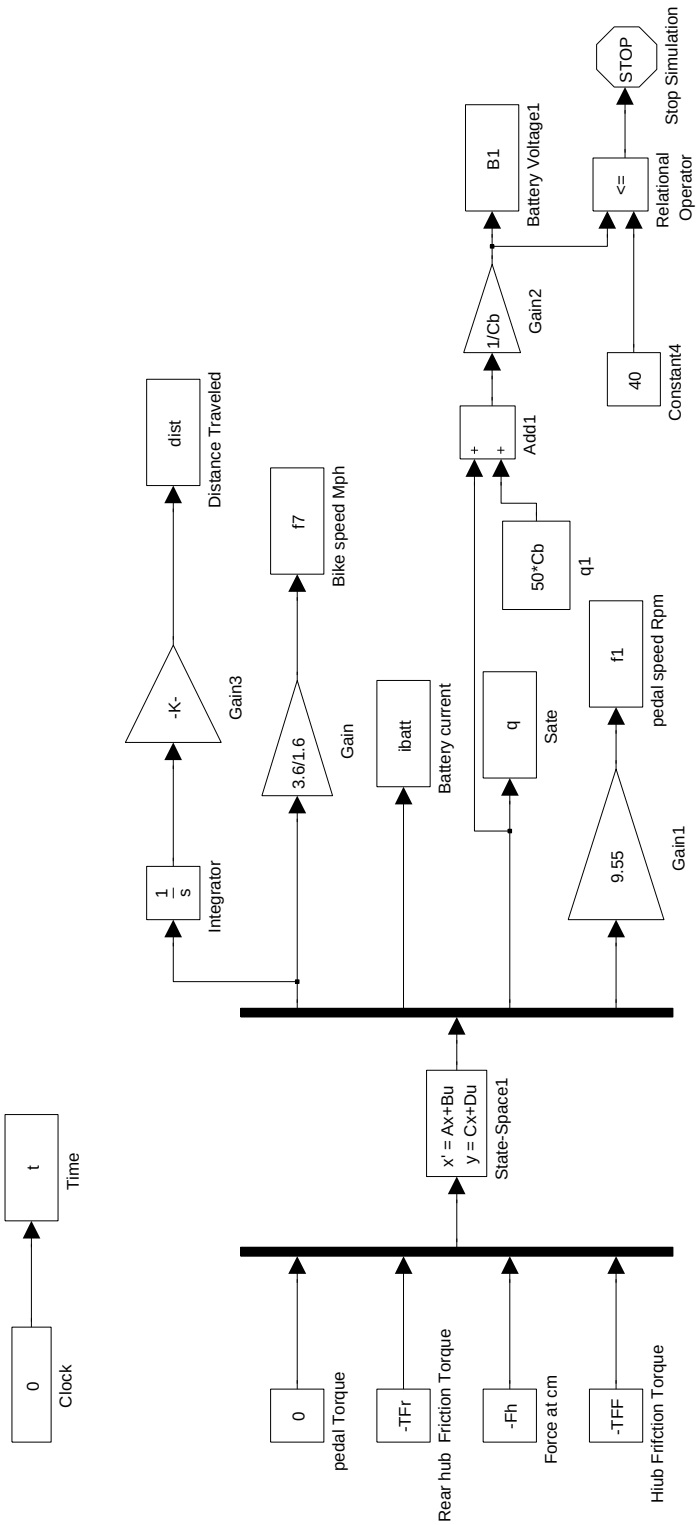

Figure 5.1: Simulation Model of Electric Bicycle with Sate Space Block

condition. The initial charge value was considered as 50 V and using q_{16} current voltage of battery can be measured. Road grade(θ), friction torque(t_f), gear ratios (g), and manual pedaling torque (S_E) are considered as input parameters of model.

For test purposes three different kind of bicycle simulation models are prepared with representing three different riding conditions as below,

5.1.1 Battery Mode

In battery mode driving condition it is assumed that the driver is using only battery power as a input source of energy to drive. Here, energy regeneration system is not enabled in the simulation. So we can calculate parameters only by using battery power. Figure 5.2 shows the simulation model representing these conditions. The state space equations and parameters of this model are shown in Matlab function file in appendix 2.2. Maximum battery voltage of this system is taken as 50 V and simulation will stop when battery voltage will drop below 40V.

5.1.2 Regeneration Mode

In this model the regeneration mode is activated. In normal conditions the rider can use battery power. The direction of energy flow may be reversed at the user's request to recharge the batteries when regenerative mode is activated. The kinetic energy of the bicycle is practically converted to electric energy. This can be used to reduce the speed of the bicycle, especially when going downhill. This model will give us the overall idea of regenerative charging theory for electric bicycle and we can compare its data with non regenerative systems. In this model user can also apply manual torque also to overcome hills or increase the driving speed. Figure 5.3 shows the simulation model representing this mode. Maximum battery voltage of this system is taken as 50 V and simulation will stop when battery voltage will drop below 40V or above 50 V.

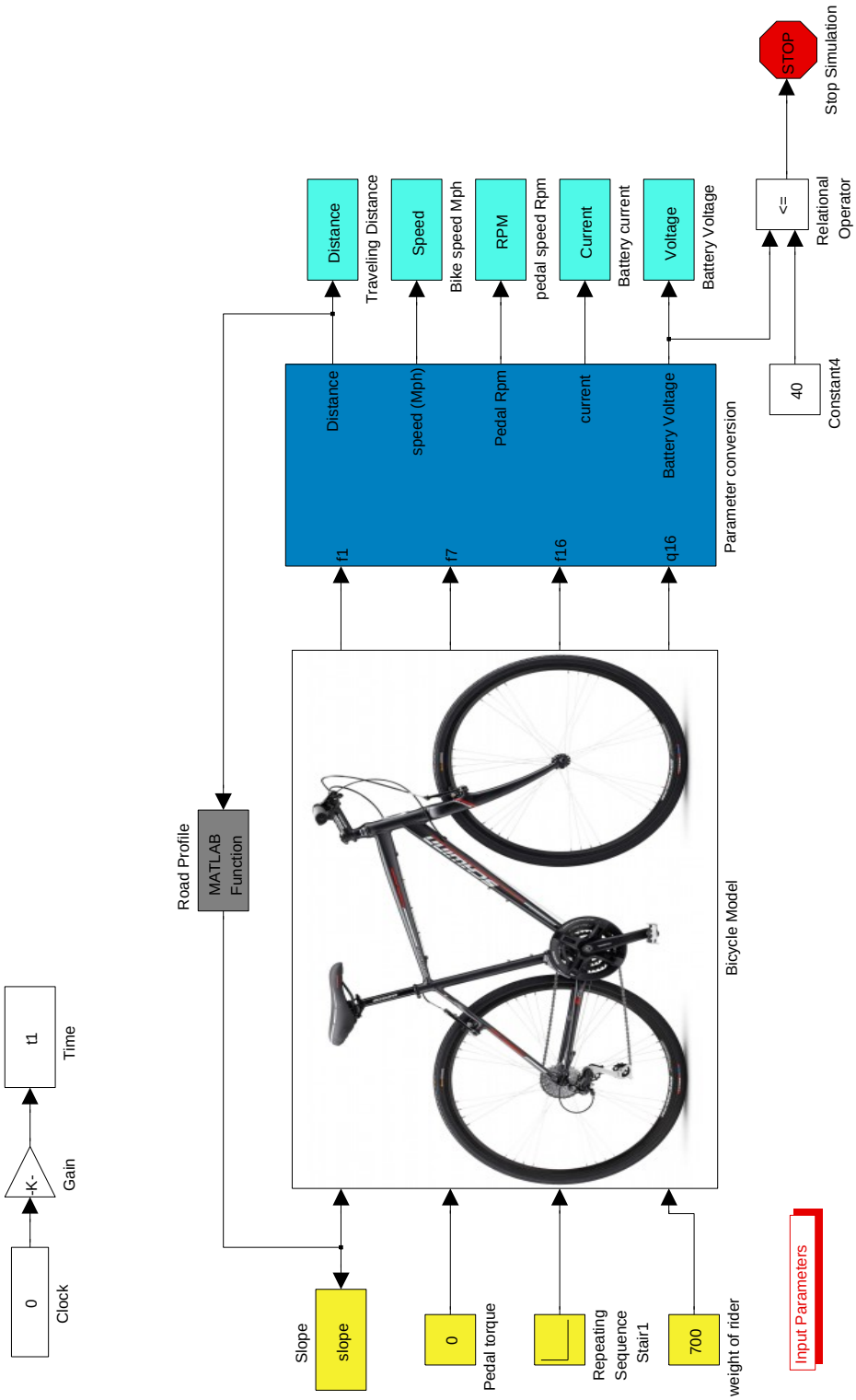

Figure 5.2: Simulink Model of Electric Bicycle System Without Regeneration System

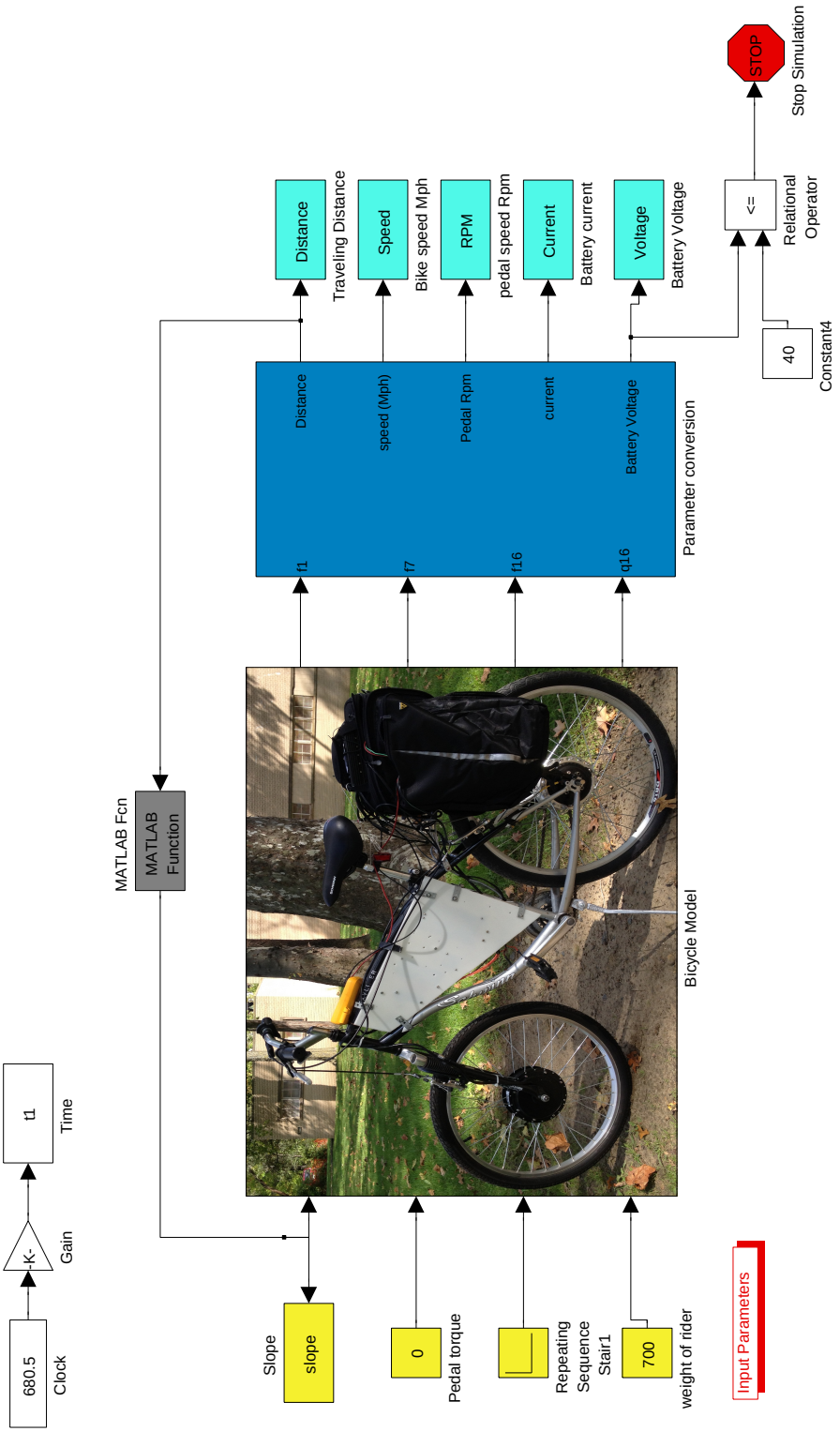

Figure 5.3: Simulink Model of Electric Bicycle System With Regeneration System

5.1.3 Charging Mode

This simulation model is created to test the recharging capacity of the prototype when the battery is below the rated voltage. Here it is assumed that user is applying only pedaling effort as source of energy, which is partially converted to charge the battery. Figure 5.4 shows the simulation model representing this mode. In this setup initial charge of battery is taken as 40V and simulation will stop when battery voltage will reach 50 V.

All this three models can be tested using different road scenarios and their results can be compared with each other.

5.2 Simulation Scenarios

Now simulation model is tested in various conditions by changing input parameters and road profiles. (appendix 2.3) shows the Matlab file to generate road profiles with respect to travel distances.

5.2.1 Scenario 1: No Slope

In this test scenario flate road profile is take with angle (θ) equals to zero. Two riders with 70kg and 80kg weight are taken. Gear ratio is taken as normal to 1.4 ratio. Battery mode and charging mode simulations are tested in this scenario. Due to the zero slope, the recharging mode will not be simulated.

The results of these simulations are shown in figures 5.5 to 5.13.

Battery Mode

Figure 5.5 shows that in ideal road conditions the bicycle can go up to 28.8 miles with 80kg rider weight. These results show that by reducing the weight of bicycle or rider we can increase the range of the electric bicycle.

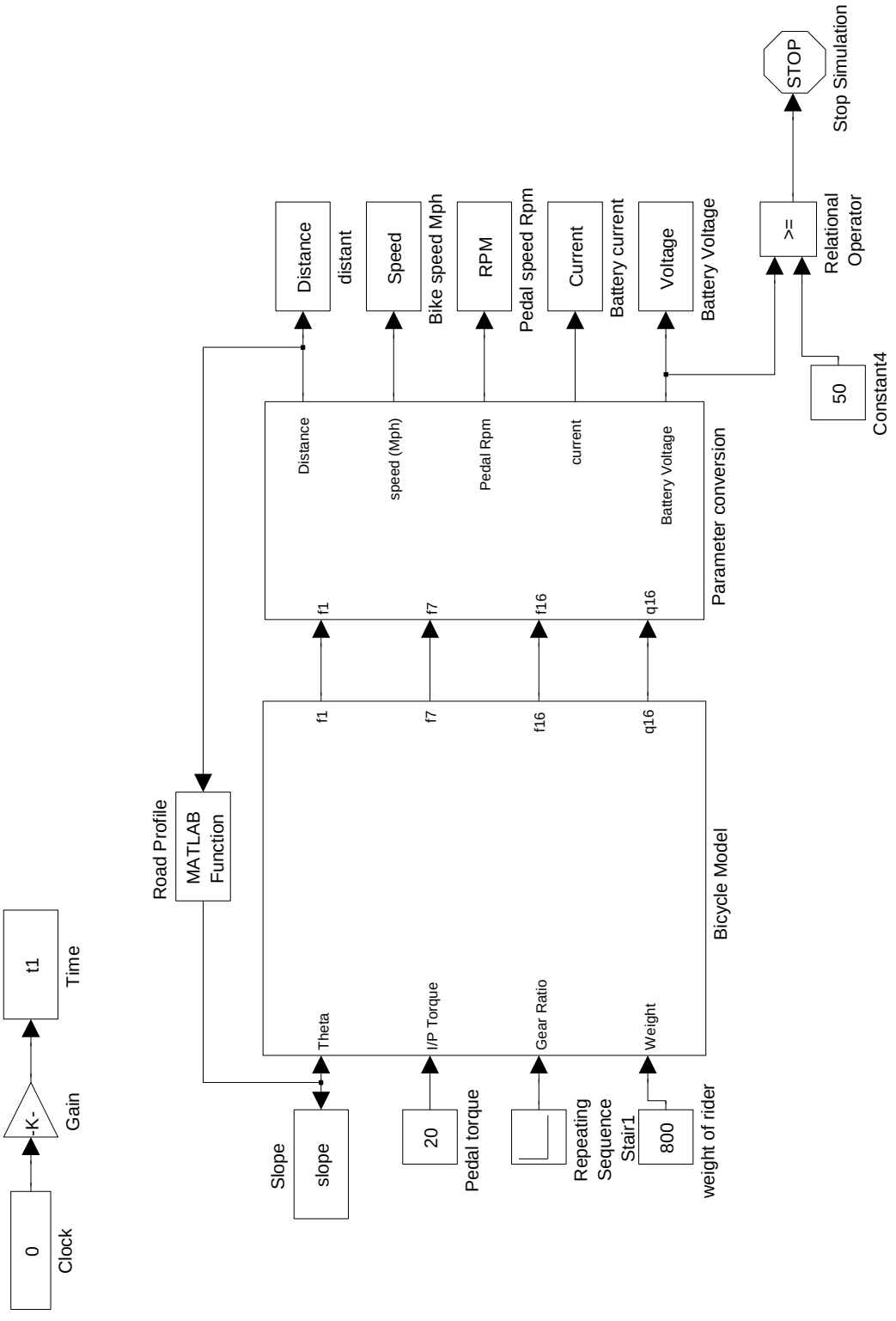

Figure 5.4: Simulink Model of Electric Bicycle With Only Manual Torque Input

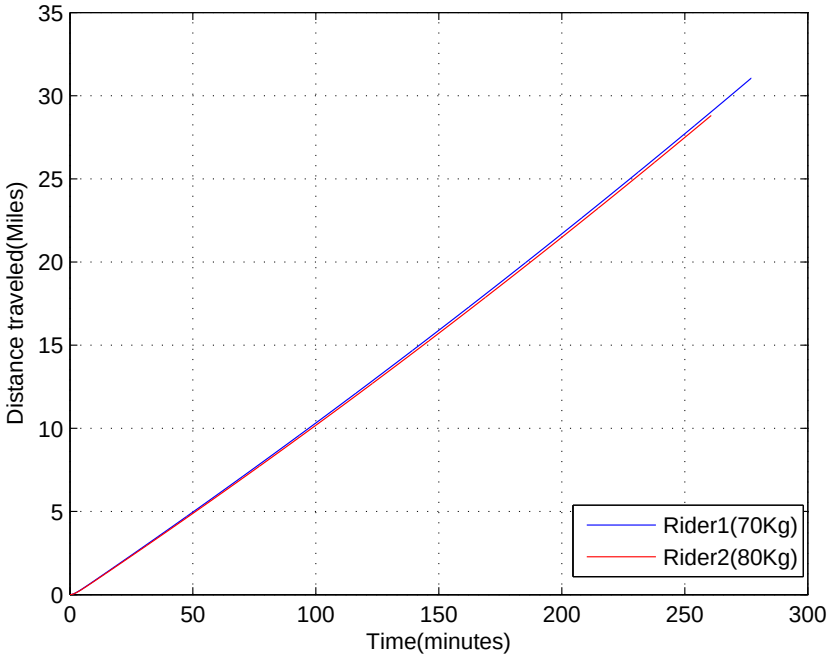

Figure 5.5: Scenario 1 Battery Mode: Total Distance Traveled

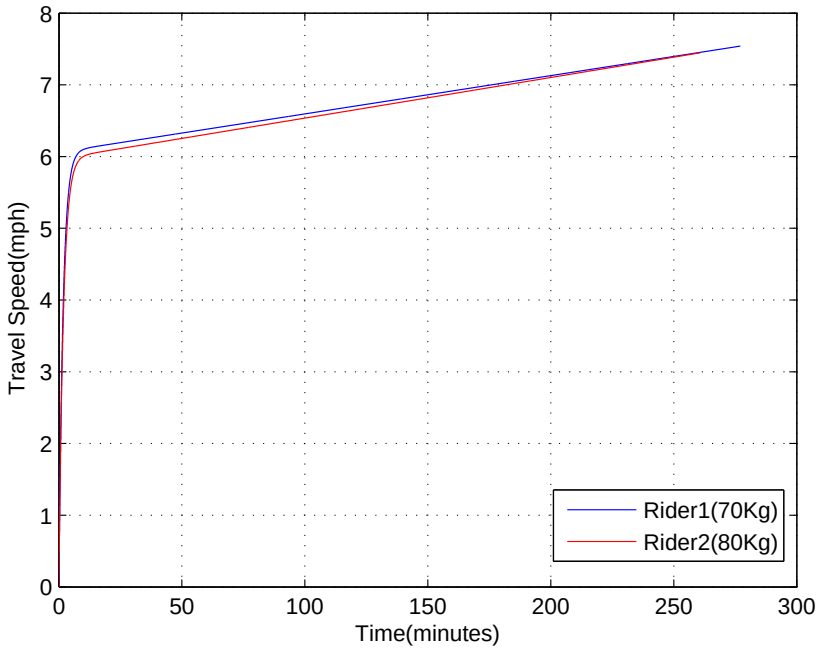

Figure 5.6: Scenario 1 Battery Mode: Bicycle Speed

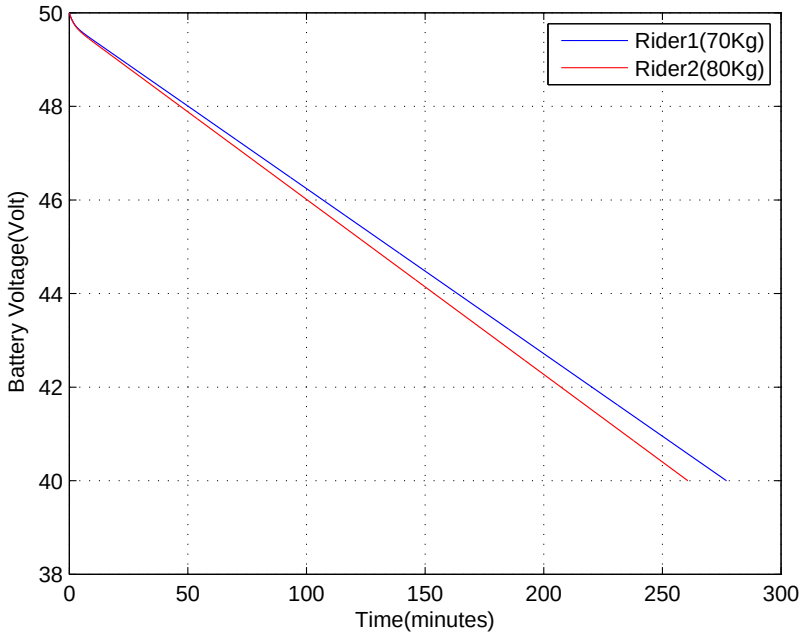

Figure 5.7: Scenario 1 Battery Mode: Battery Voltage

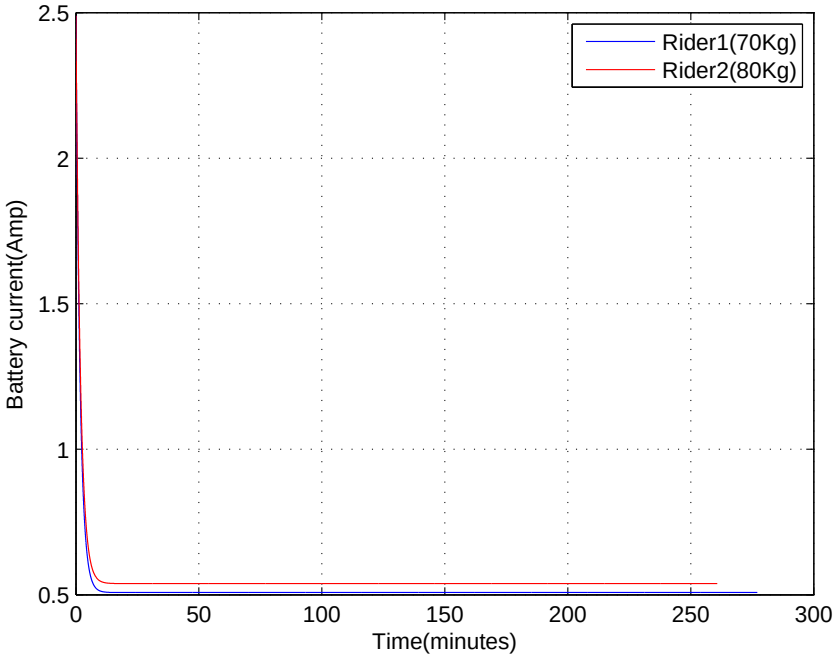

Figure 5.8: Scenario 1 Battery Mode: Battery Current

Table 5.1: Simulation results for Scenario 1

Parameters	**Rider 1 (70 Kg)**	**Rider 2 (80 Kg)**
Distance traveled (mile)	31	28.8
Time to discharge battery at 40V(min)	277	260
Battery current (A)	0.5	0.53
Average speed(mph)	6 to 7.6	6 to 7.2

These results are in ideal test conditions, air resistance is not considered in this setup. These conditions are not practically possible so real test data values may be lower compared to simulation results.

Average travel speed shown in figure 5.6 is 6 to 7.5 mph which is nearly equal to average practical speed.

Comparison of both rider tests are shown in Table 5.2.1.

Manual Mode

In this simulation is the bicycle is tested on a road profile with zero slope, 70kg rider weight and two different gear ratio values. Gear ratio 1 is taken as 1.2 value and gear ratio 2 is taken as 1.8 value. Here only pedaling torque ($20N$) was applied as a source of energy.

These simulation results show the effect of gear ratio in battery charging. On high gear ratio (1.2) (with same amount of torque) the battery was charged in only 12 miles compared to 15 miles for a lower gear ratio-2 of (1.8) as shown in figure 5.9.

Pedaling rate for a high gear ratio of 1 is 150 rpm, which is very high in comparison to typical pedaling speeds. It is difficult to drive constantly at this speed. At this high gear ratio, current generated from the motor is also high (-2.8 A), which corresponds to a very fast battery charging rate.

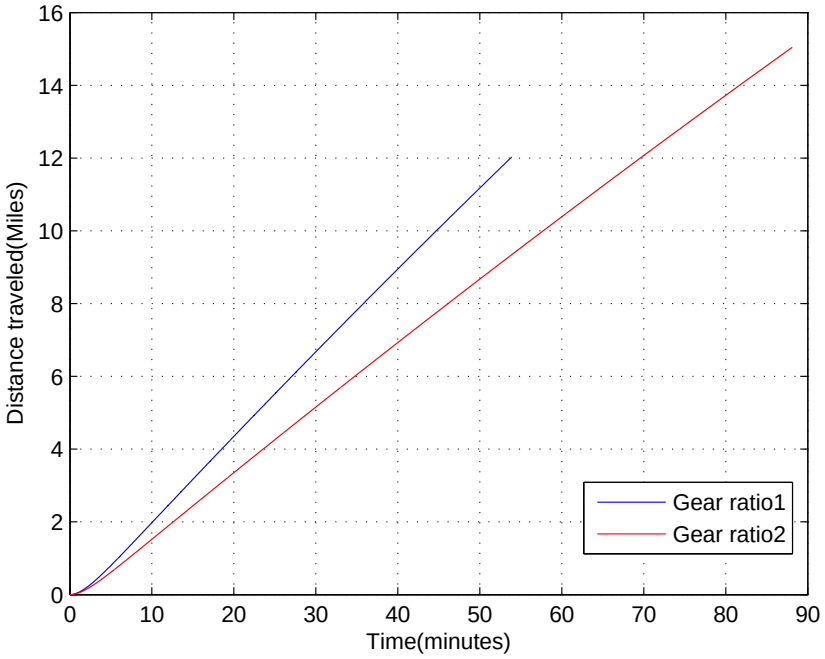

Figure 5.9: Scenario 1 Manual Mode : Total Distance Traveled

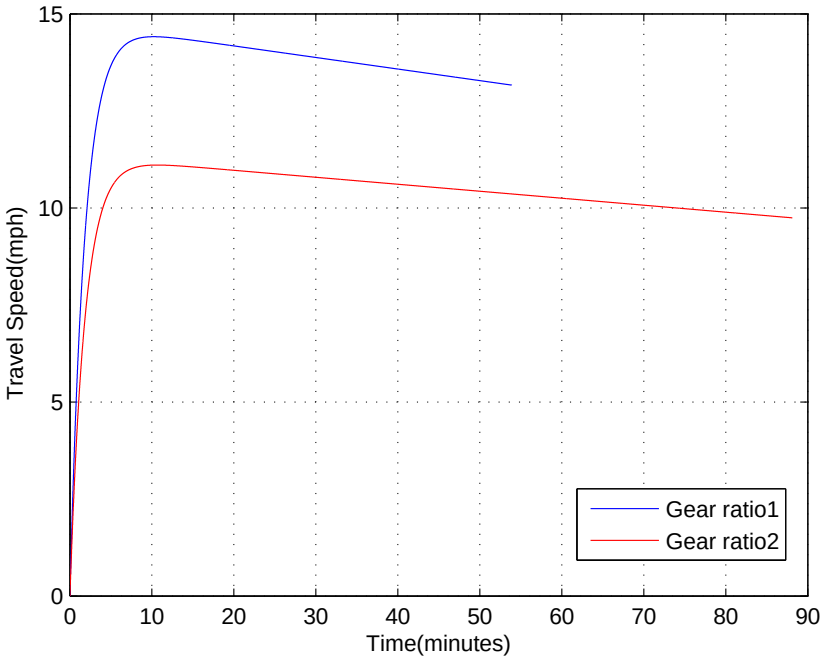

Figure 5.10: Scenario 1 Manual Mode: Bicycle Speed

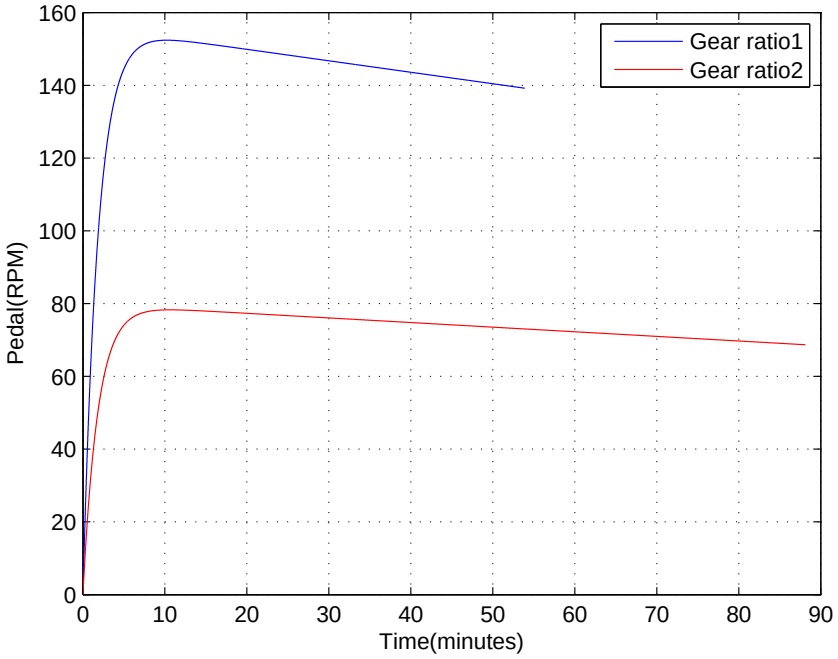

Figure 5.11: Scenario 1 Manual Mode: Pedal Speed

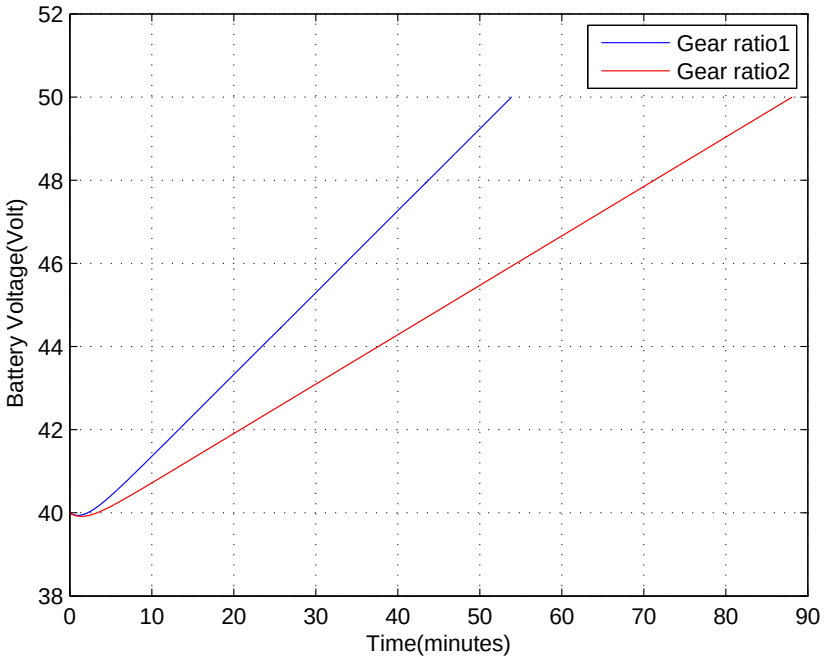

Figure 5.12: Scenario 1 Manual Mode: Battery Voltage

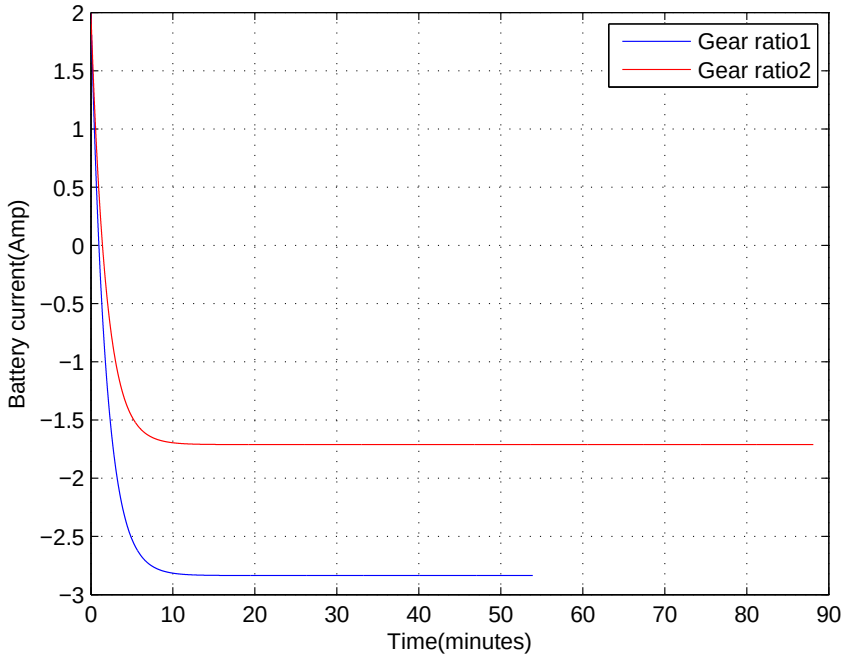

Figure 5.13: Scenario 1 Manual Mode: Battery Current

Table 5.2: Simulation Result For Scenario 1 With Manual Mode

Parameters	**Gear Ratio 1**	**Gear Ratio 2**
(at full battery charge)	**(1.2)**	**(1.8)**
Distance Traveled (miles)	12	14
Traveling Speed (mph)	14	11
Pedal RPM	150	75
Time (min)	52	88
Current	1.6	2.8

5.2.2 Scenario 2: With Slope

In this test scenarios a road profile with varying slopes was created as shown in figure 5.20. For the initial 2 miles the slope is zero, after one mile, the slope becomes 2% increasing slope, next three miles -2% decreasing slope, next 2 miles +1.5% increasing slope and after that its

flat surface for remaining ride. Both battery mode and regenerative mode simulations were tested in this profile with fixed 70Kg rider weight. This test will provide an idea about how much energy can be capture during the regeneration process on downhill motion.

Figure 5.15 shows difference between the traveling range with recharging setup (17 mile) and without recharging setup (15 mile).

Figure 5.18 and 5.19 shows the plot of battery voltage and current during the ride. Battery voltage can be compared with the road profile (figure 5.14). On a flat road the voltage is decreasing normally, during up hill portion the battery discharges rapidly with a high current (2A) rate. During downhill portions the battery is being charged and the voltage is increasing. A negative current shows that current is flowing from motor to battery.

From figure 5.17 we can see that during the uphill surface bicycle speed becomes very slow and during downhill it becomes higher.

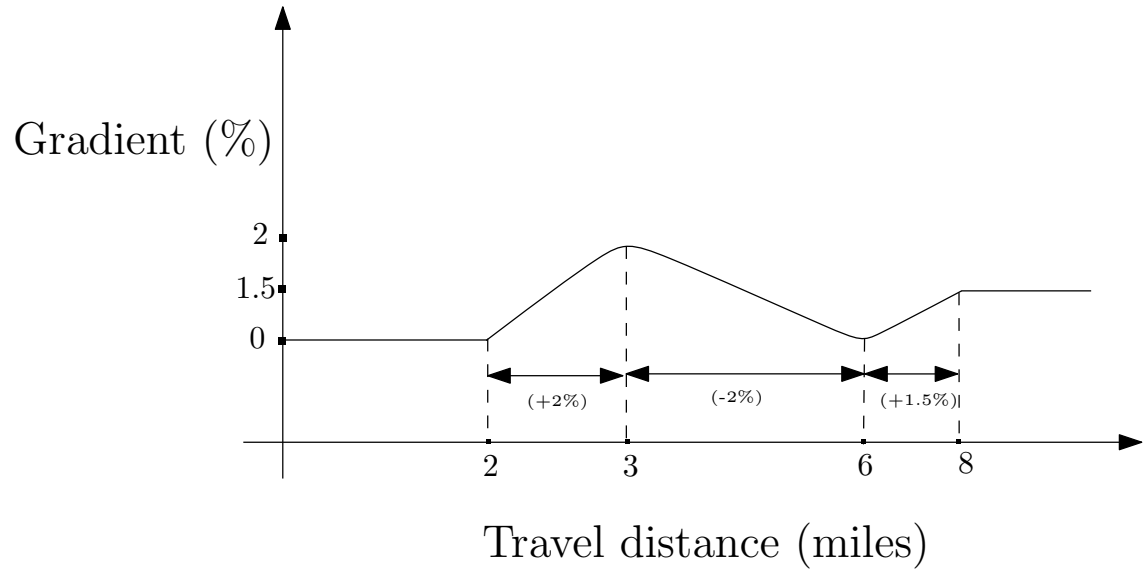

Figure 5.14: Scenario 2 Regenerative Mode : Road Profile

5.2.3 Scenario 3 : with Slope

In this scenario another road profile is crated with only one slope, as shown in figure 5.20. The slope is -2% for the first three miles and 2% for the next two miles. The rider weight,

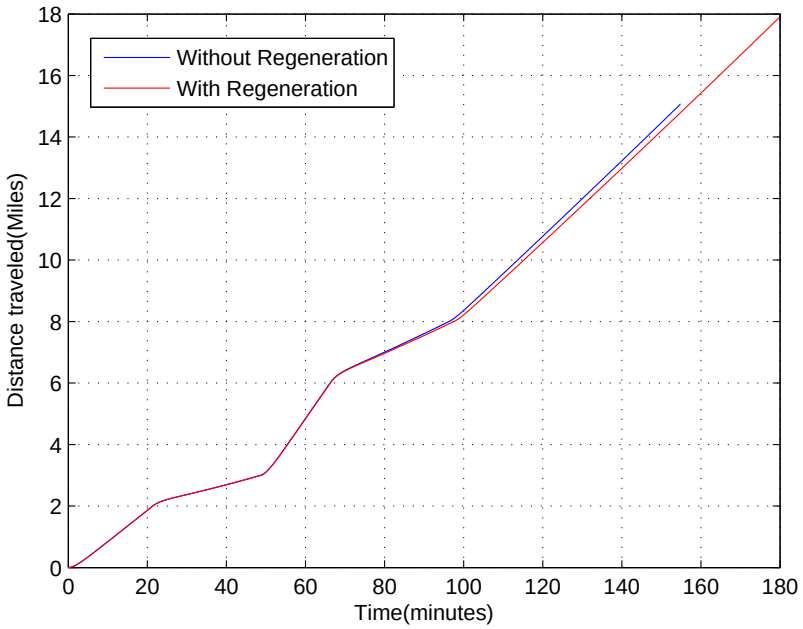

Figure 5.15: Scenario 2 Regenerative Mode: Total Distance Traveled

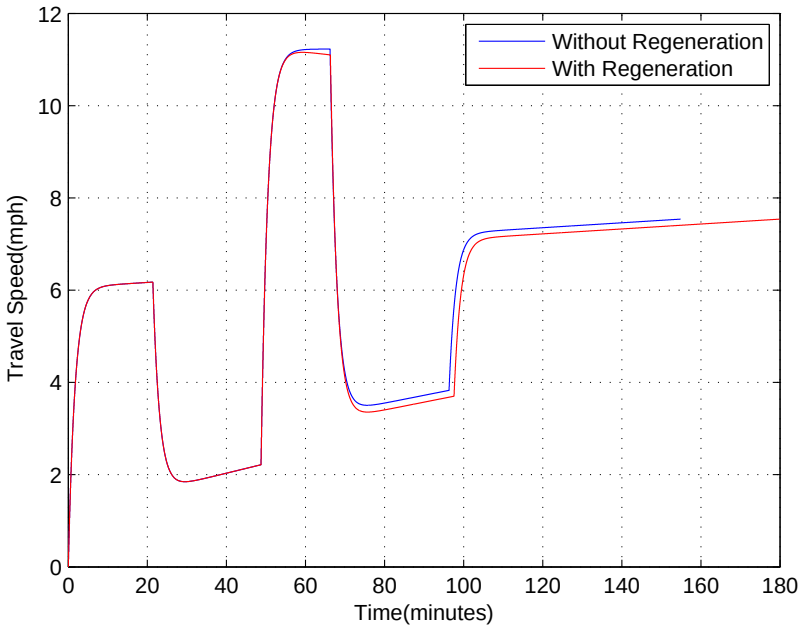

Figure 5.16: Scenario 2 Regenerative Mode: Bicycle Speed

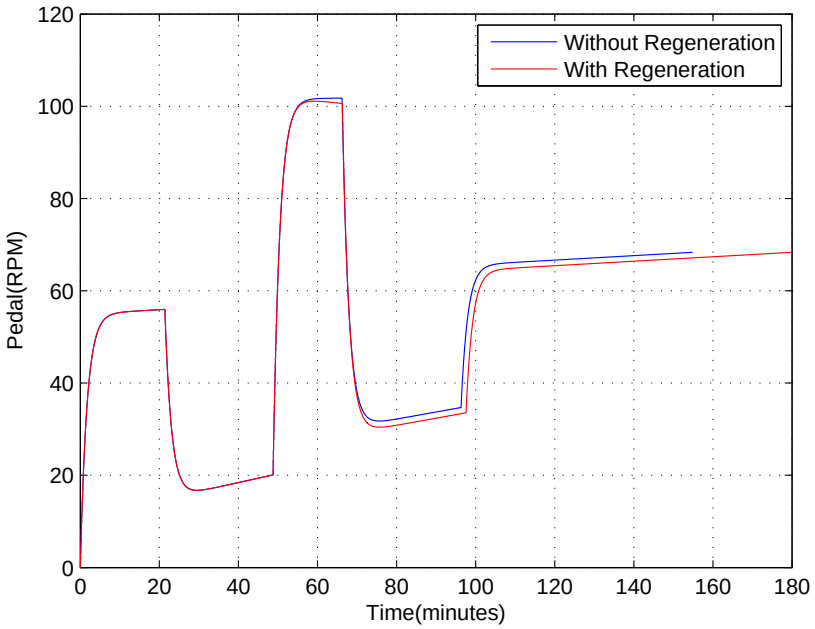

Figure 5.17: Scenario 2 Regenerative Mode: Pedal Speed

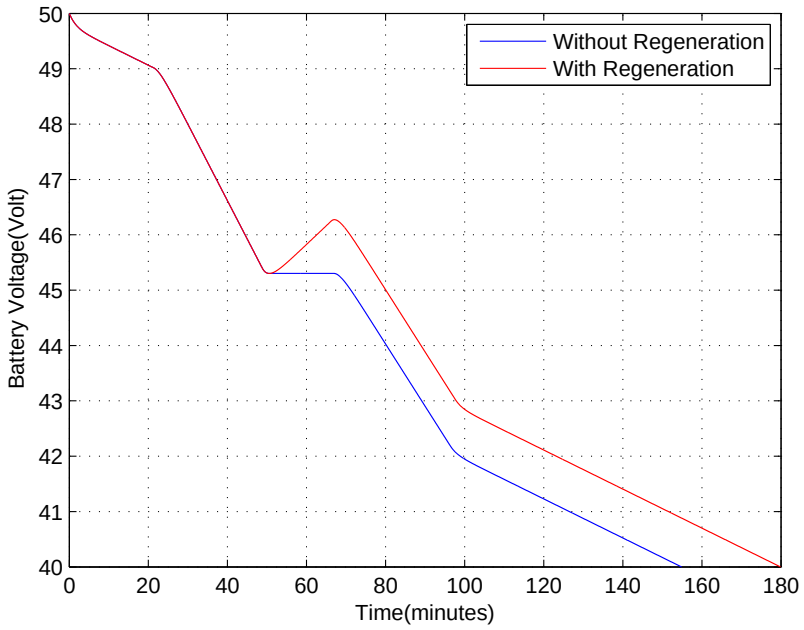

Figure 5.18: Scenario 2 Regenerative Mode: Battery Voltage

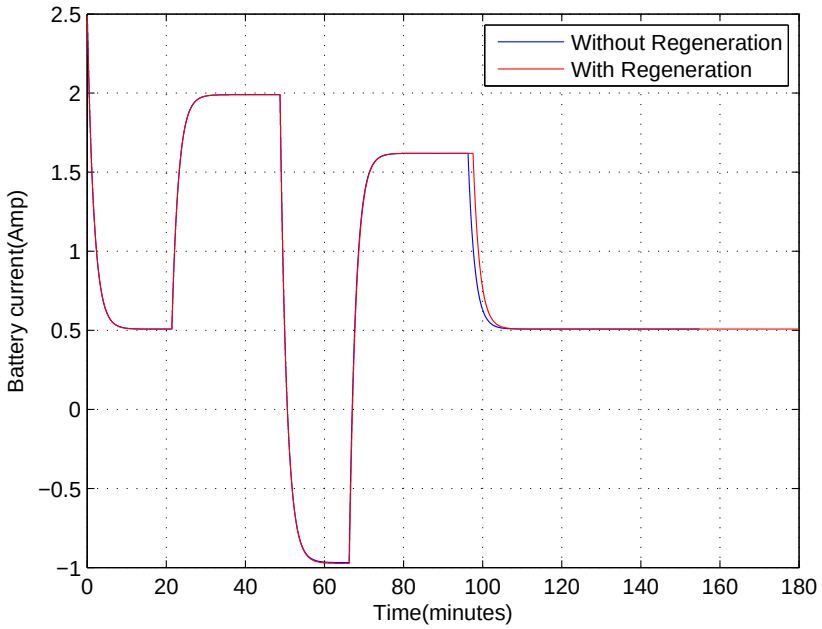

Figure 5.19: Scenario 2 Regenerative Mode: Battery Current

Table 5.3: Simulation Results for Scenario 2

Parameters	**Without Regeneration**	**With Regeneration**
Distance Traveled (miles)	15	17
Battery discharge time	150 min	180 min

gear ratio all parameters are same as scenario-2. This scenario is also tested with regenerative and without regenerative setup. Test results are shown here.

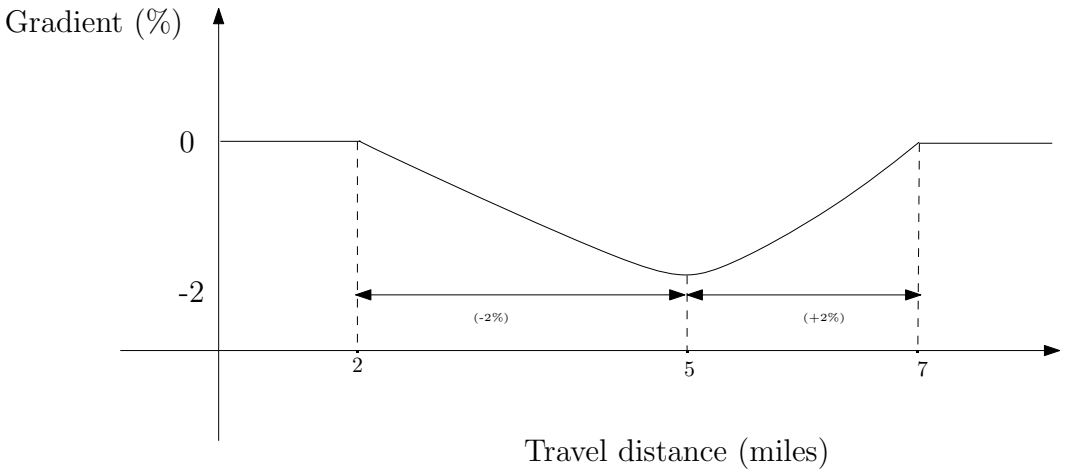

Figure 5.20: Scenario 3 Regenerative Mode: Road Profile

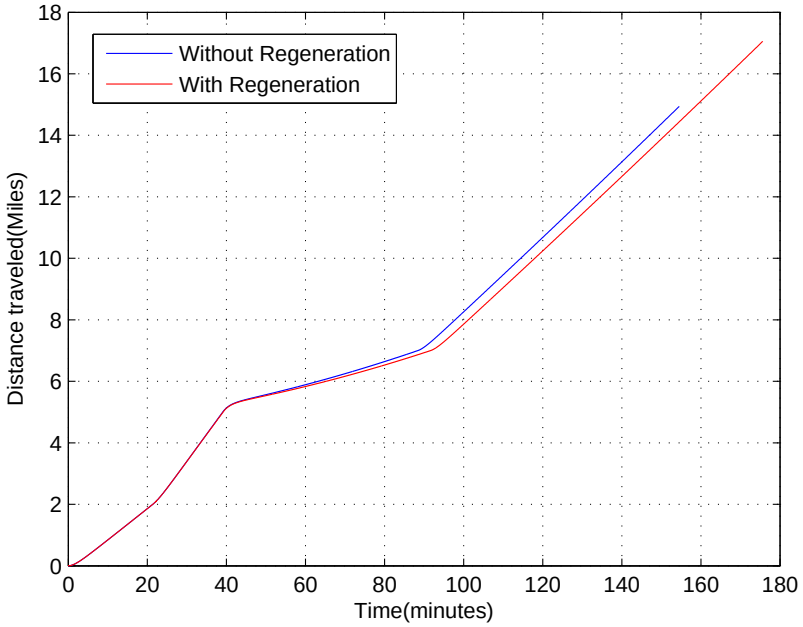

Figure 5.21: Scenario 3 Regenerative Mode: Total Distance Traveled

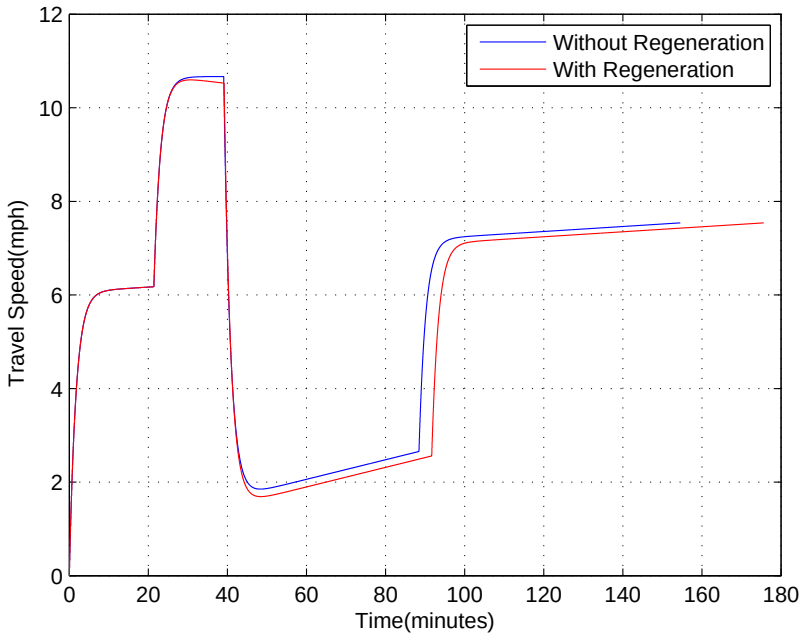

Figure 5.22: Scenario 3 Regenerative Mode: Bicycle Speed

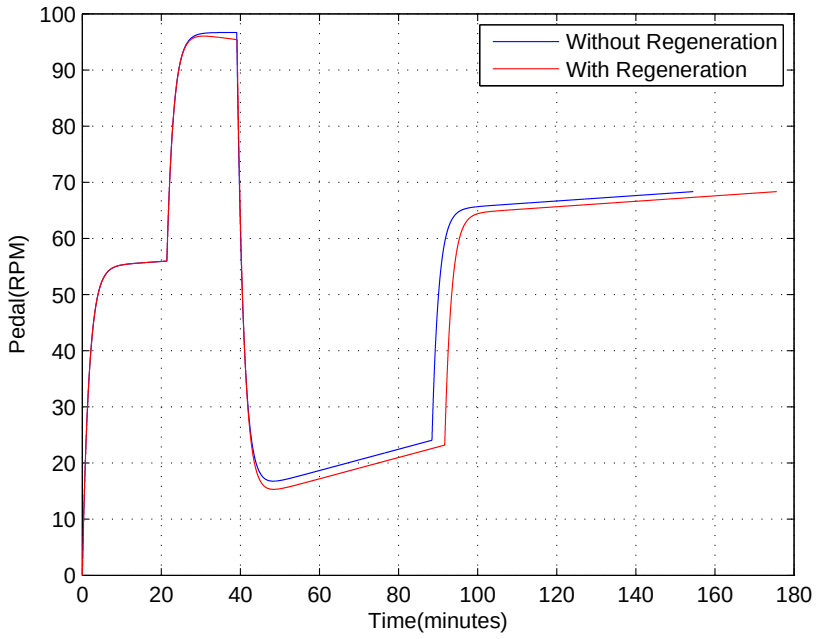

Figure 5.23: Scenario 3 Regenerative Mode: Pedal Speed

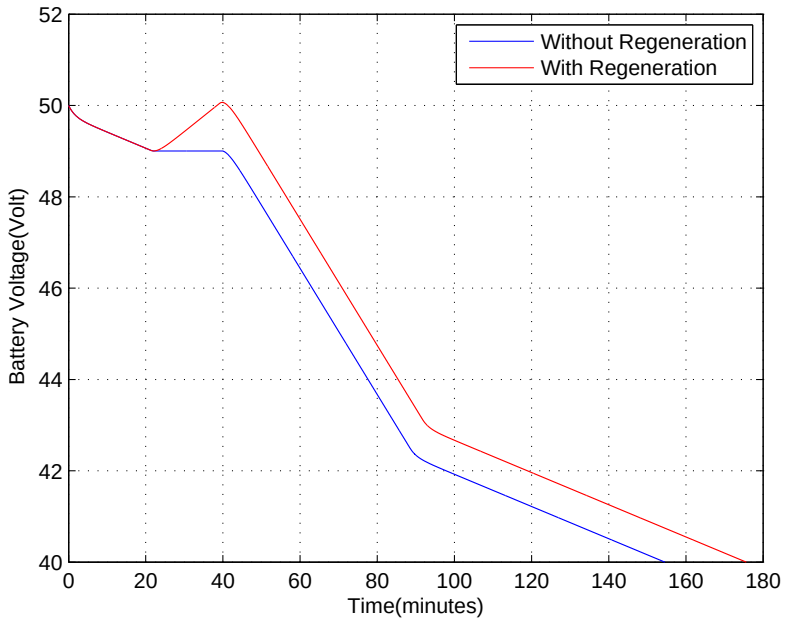

Figure 5.24: Scenario 3 Regenerative Mode: Battery Voltage

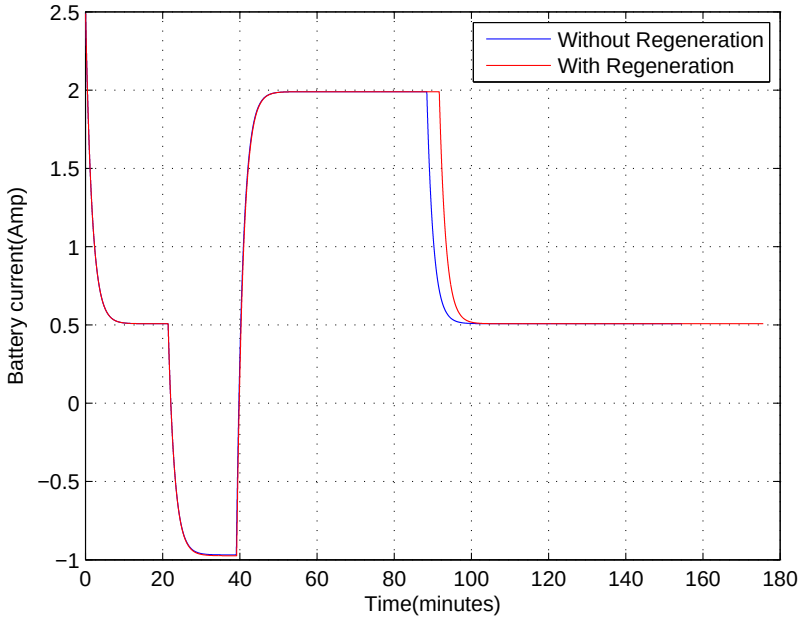

Figure 5.25: Scenario 3 Regenerative Mode: Battery Current

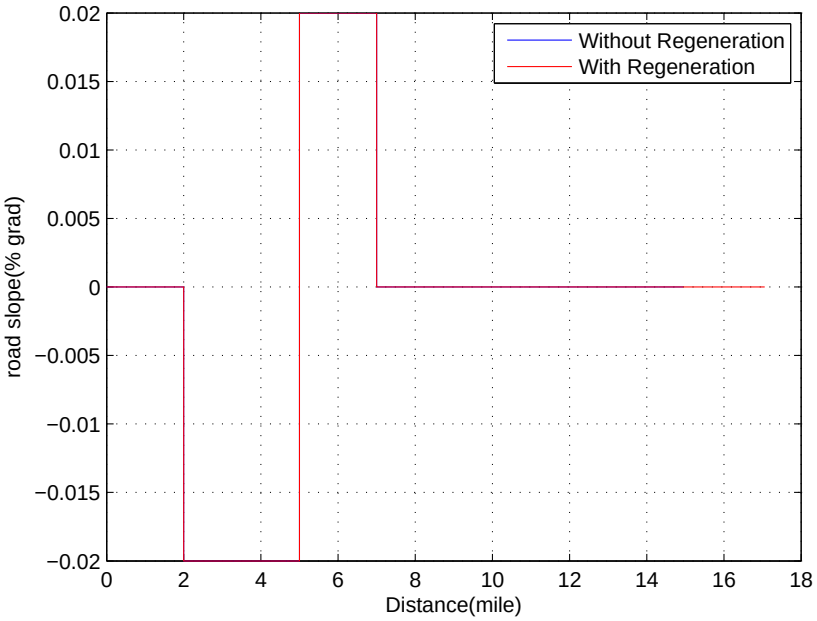

Figure 5.26: Scenario 3 Regenerative Mode: Road Slope

CHAPTER VI

EXPERIMENTAL SETUP

The experimental setup used to validate the simulation model is shown in this chapter. Block diagrams to implement regeneration circuit is explained here with all required parts and details. Position control of DC motor with PWM method using microcontroller is discussed in this chapter. This chapter also provides details about prototype development and microcontroller programming.

6.1 System Work-Flow

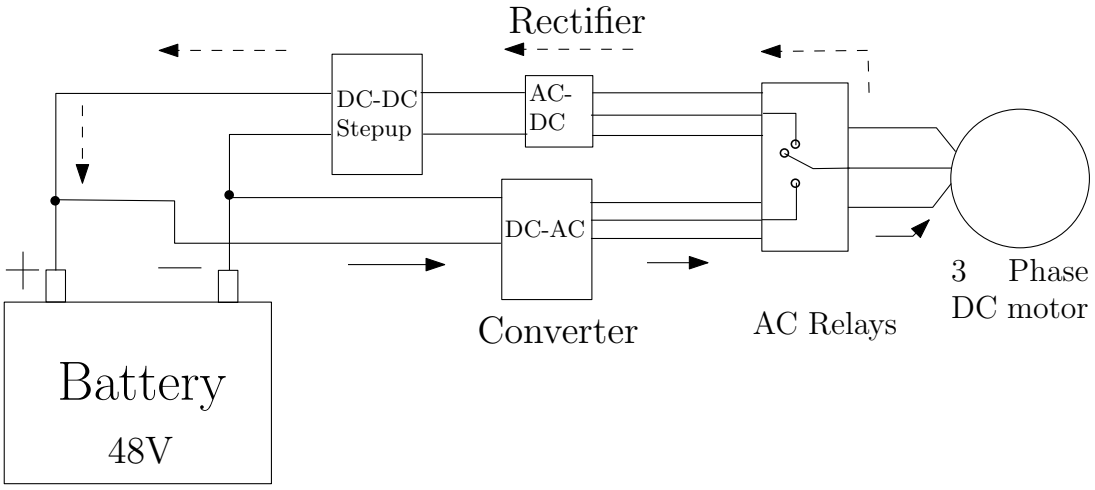

Figure 6.1: Power Flow During Driving And Regeneration Modes

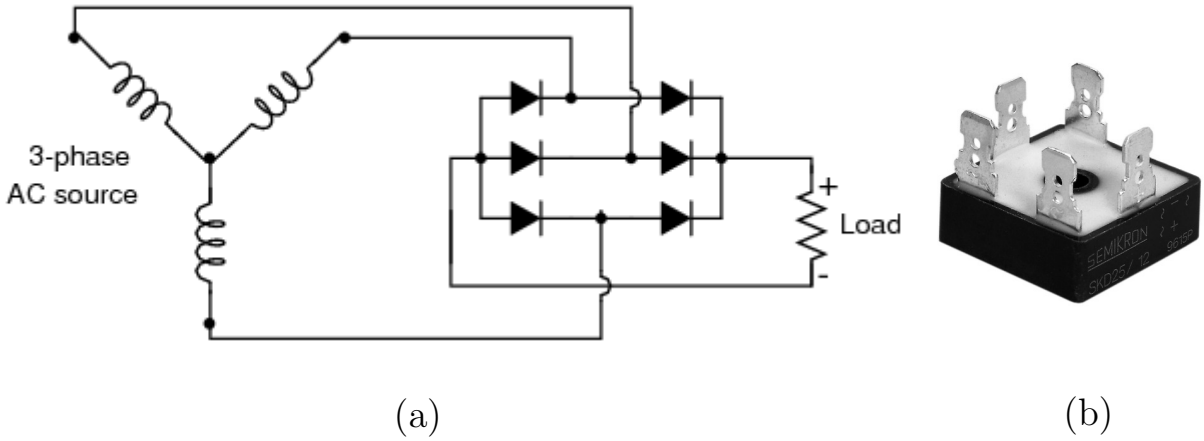

(a) (b)

Figure 6.2: Rectifiers (a) Circut Diagram (b) Semikron Power Bridge Rectifiers

Figure 6.1 shows the for electric bicycle prototype with energy regeneration setup. Battery supplies 48 V dc voltage to motor through DC-AC converter. Motor is generating 3 phase AC voltage in regeneration mode.

6.2 AC to DC Conversion

The BLDC hub motor mounted on a bicycle can also work as a generator. A 48 V Crystalyte BLDC motor was used for this prototype with 8 coils in the stator . When the bicycle wheel is rotated by external force, it will produce 3− phase AC voltage. This characteristic is used for energy regeneration setup. Figure 6.2(a) shows circuit diagram for the 3− phase full wave AC rectifier. Here, 6 diodes are used and each two diodes are in series. The anode of the first diode is connected to the cathode of the second diode.

For the three-phase full wave diode rectifier, ideal no load output voltage is

$$V_{dc} = V_{av} = \frac{3\sqrt{3}V_{peak}}{\pi} \tag{6.1}$$

A semikron (SKD - 25)(6.2(b)) three-phase power bridge rectifier is used for this prototype setup. It has three input terminals for AC input and two output terminals for DC voltage.

An experimental setup was prepared to test this rectifier. The bicycle was mounted on stand and wheel with hub motor was rotated by external force at high speed. AC voltage produced by motor was converted in to DC motor using power bridge rectifiers. This DC voltage was used to light a bulb, run DC motor. Figure 6.3 shows conversion plot of three phase AC to DC voltage .

6.3 Motor−Generator Load Test

After setting all required circuits for AC to DC voltage conversion, as shown in figure 6.3, load test of motor generator was done to check the regeneration capacity of motor on different speed and load conditions. A rheostat was used as variable input load for generator. The bicycle wheel was rotated at different speeds and different resistor values. The output voltage and the current generated from the motor were measured. The results of this setup are show in figure 6.4 and 6.5

Figure 6.4 shows a plot of voltage and current readings at different speed. Here, output readings are taken on different resistance values for same speeds. Voltage is increasing with the increase in the speed and current is increasing when input load increases with low

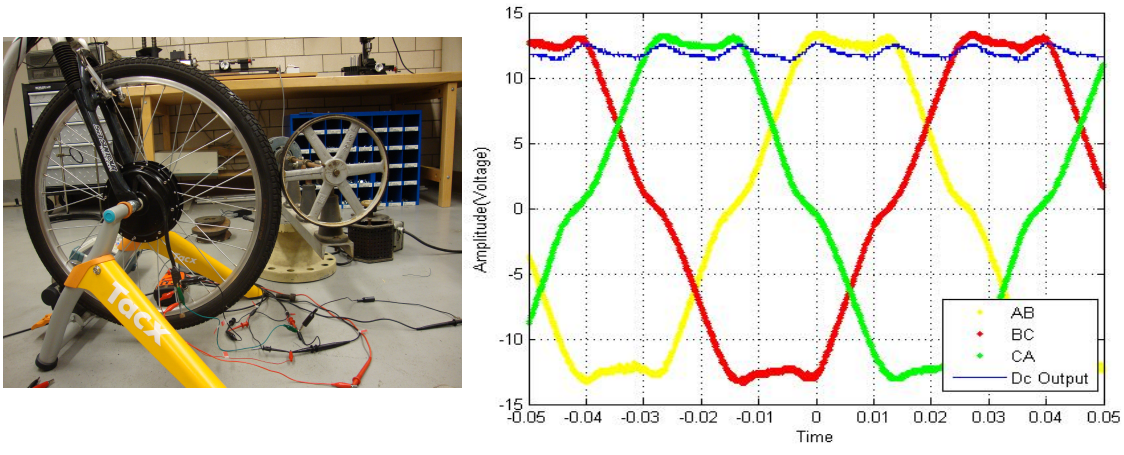

Figure 6.3: AC to DC Conversion Setup and Plots

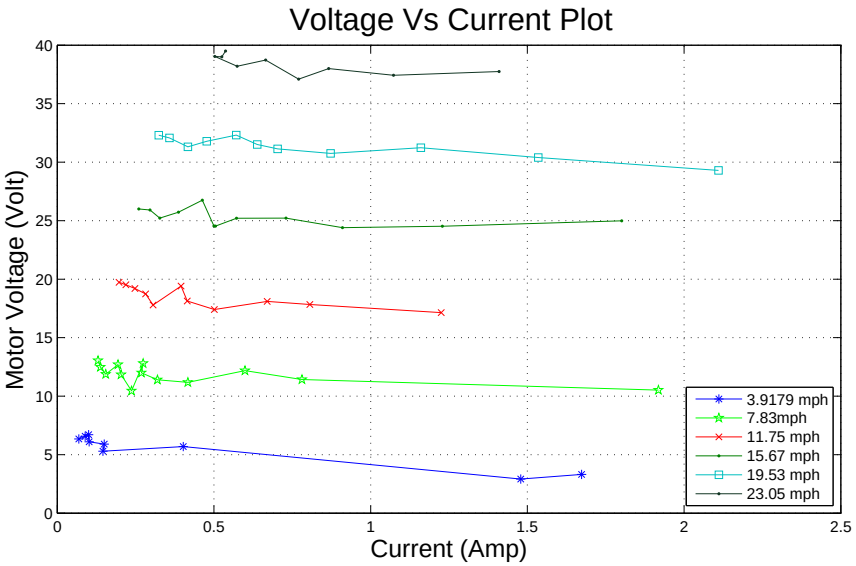

Figure 6.4: Motor−Generator Voltage-Current Curve On Different Load

resistance value.

Figure 6.5 shows a speed vs. power plot for the motor working as a generator with different input load resistance values. Total generated output power is increasing with speed and input load resistance value. Form these values we can predict the approximate power recovery in regenerative braking at different speed and load values.

6.4 Switching Mechanism

From above description, this designed prototype setup can work as a power mode for driving and in regeneration mode to recharge the battery. The switching logic is done by using opto isolated high current AC relays. These relays are AC 250 V, 10 A rating capacities and they can be turned on/off by only 5 V DC supply. Using microcontroller's 5 V logic signals we can control the relay switching.

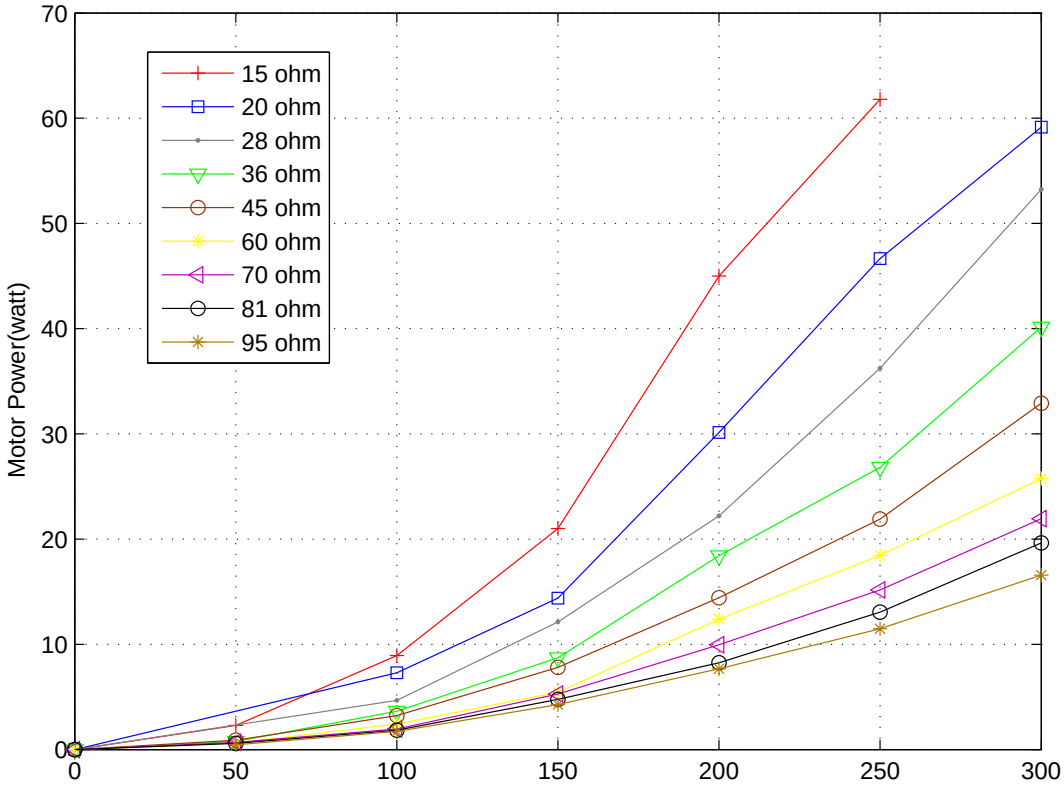

Figure 6.5: Motor−Generator Speed-Power Curve On Different Load

Figure 6.6(a) show the circuit board with 8 relays. 6 relays are used to control the flow of power in motor in both directions.

This relay switching is controlled by PIC microcontroller. Here, six port of microcontroller PIC16F877A (B2 to B7) are configured as output port and connected with six relays. On low voltage signal relay will turn ON and on high voltage signal relays will turn OFF. Now using programming method direction of voltage in motor can be controlled.

6.5 Charging System

The load test results show that the voltage generated from the hub at different speeds is smaller then the battery power. A minimum voltage higher than the battery voltage is required to charge it. It may be difficult to obtain the required minimum voltage under

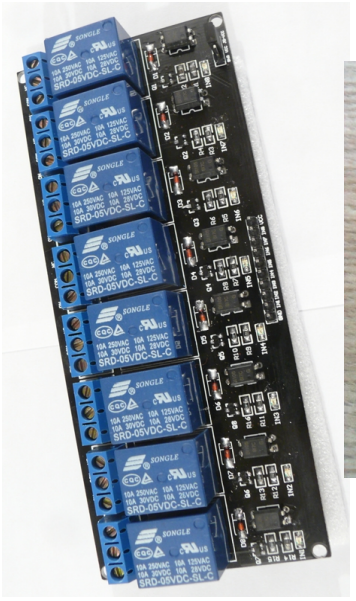

(a)

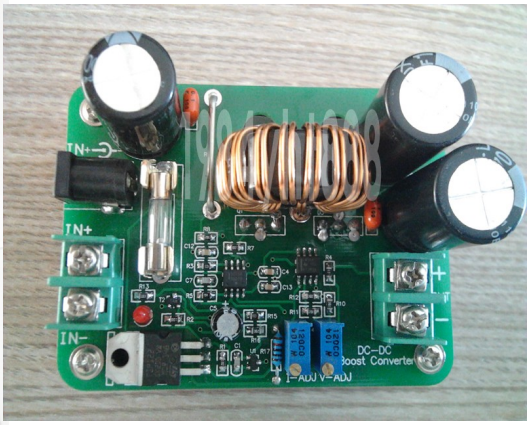

(b)

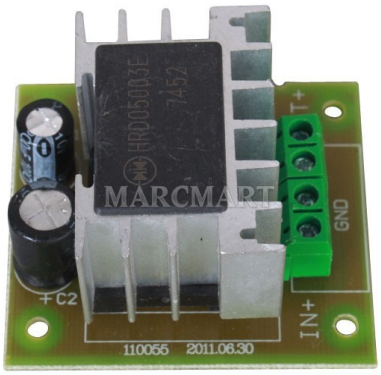

(c)

Figure 6.6: Parts (a) Relay Board, (b) DC-DC Step-Up Converter, (c) 24-9V Converter

normal riding condition. This is the main limitation of the regeneration system. A DC-DC boost up converter is used to amplify this voltage to a level higher then battery voltage.

Figure 6.6 (b) shows the circuit board of the DC-DC step-up boost converter. It has an input range of $10 - 60V$ and an output range of $12 - 80V$ with a power rating of 600W. This is a key element in this prototype setup. Form figure 6.5 we can say that with 7mph driving speed we can produce 10 V output for boost converter and it will amplify it up to 52V set value to charge the battery. In this setup we need minimum 7 mph speed to charge the battery.

6.6 Energy Storage and Supply

Main energy supply and storage element is rechargeable battery. Battery basic details are discussed in chapter-2 and 4. In this setup four valve regulated lead Acid batteries (VRLA) with 12V, 10A-h rating from B.B Battery Inc. Figure 2.7(b) shows the battery used in prototype. Four batteries are placed in parallel so total available output voltage at the

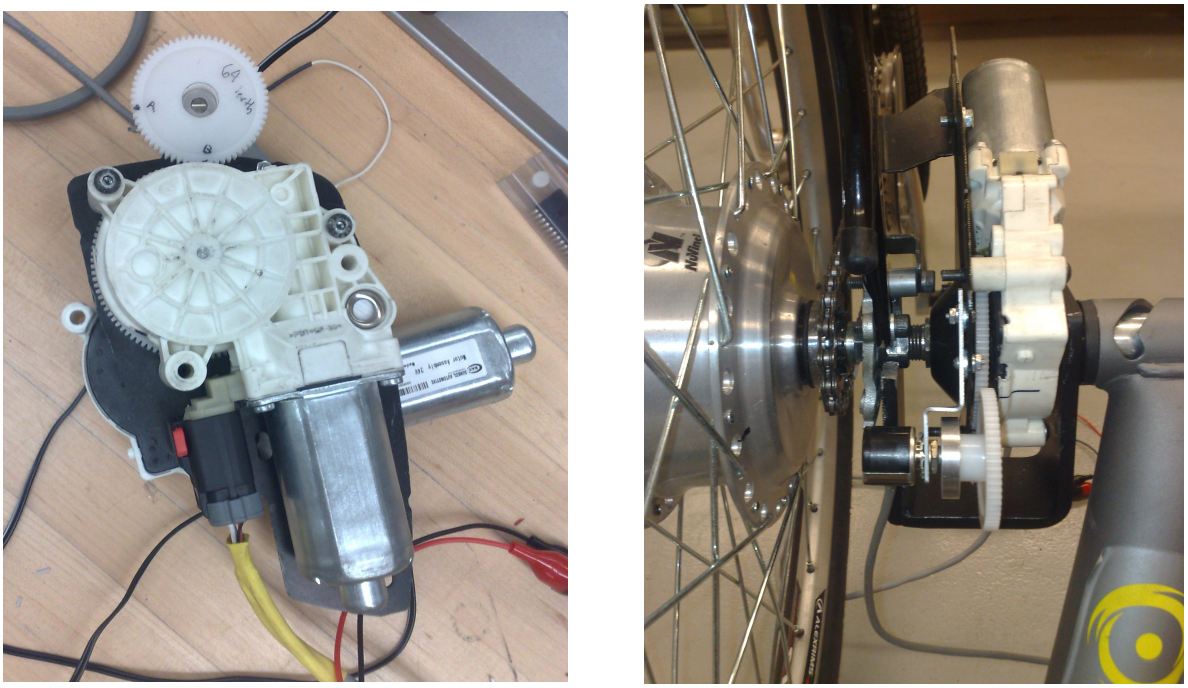

Figure 6.7: (a) Actuator with Potentiometer (b) CVT Unit With Actuator

terminals is 48 V. This voltage will use to drive different parts and circuits of the electric bicycle prototype. 48 V will use to drive hub motor. 24 V will used to drive CVT actuator dc motor. The microcontroller used in this setup also requires 9V constant DC power supply. A 24 to 9 V step down converter is used to supply power to MCU board from the battery. Figure 6.6 (c) shows the circuit board of the 24-9V step down converter.

6.7 Position Control of CVT Actuator Motor

As mentioned in Chapter II, A *Nu Vinci* CVT system is used in this project as a transmission unit. A mechanism with 24 V DC motor is used in to adjust the gear ratio in CVT using gear shaft (figure 6.7). Gear shaft is attached with this mechanism and it will rotate in clockwise or anticlockwise direction and desired gear ratio can be adjusted in CVT. The objective of this setup is to achieve a desired angular position control of output shaft according to requirements input. It is accomplished by feedback control loop with PID control

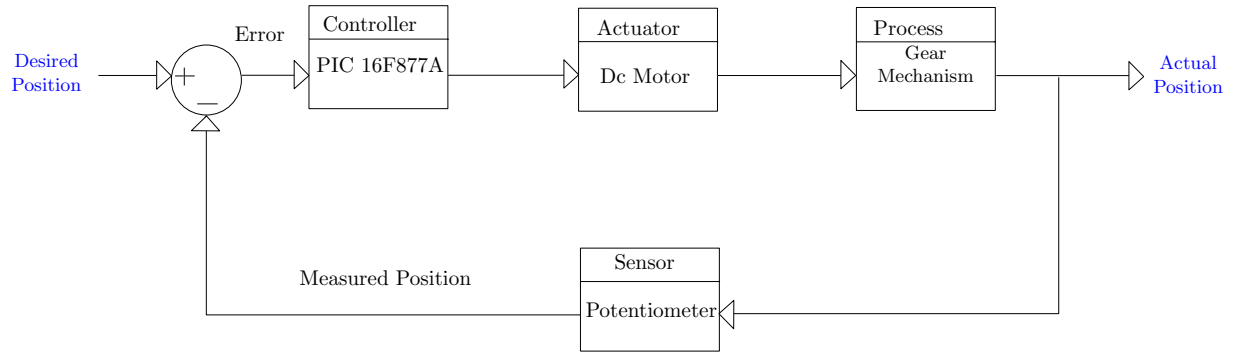

Figure 6.8: Feedback Loop System

logic using a PIC 16F877A Microcontroller.

The PID controller has been in use for over a century in various forms. It has enjoyed popularity as a purely mechanical device, as a pneumatic device, and as an electronic device [20]. The digital PID controller using a microprocessor has recently become of widespread use in industry. PID stands for proportional, integral, derivative. Each of these elements performs a different task and has a different effect on a system response.

Figure 6.8 shows typical block diagram of feedback loop system. Potentiometer is used as a sensor feedback device and the DC motor works as an plant actuator. PIC 16F877A is a controller used for all PID calculation, feedback, reference input and error calculations. It also controls the DC motor driver circuit.

6.7.1 Modeling of Actuator's DC Motor

DC Motor shaft angular speed ω depends upon the induced emf in the winding

$$E_g = K_E \omega \tag{6.2}$$

where K_E = Voltage constant

$$K_E = \frac{Z_p}{60\eta'}\phi \tag{6.3}$$

where ,

P= number of poles

Z= No of conductors moving through the field

ϕ= Radial magnetic flux

Now motor generated torque is

$$T_g = K_T I_a \tag{6.4}$$

where,

$$K_T = \frac{Z_p}{2\pi\eta'}\phi \tag{6.5}$$

K_T= Torque Constant

$K_T(N-m/A)$= 9.5493×10^{-3} K_E(V/k rpm)

$$\omega_0 = \frac{K_T V_a}{R_a K_M^2} \tag{6.6}$$

From equation 6.6 we can say that, speed of DC motor is proportional to applied voltage. So, DC motor speed can be changed by changing the applied voltages. Voltage variation can be done by Pulse width modulation method (PWM).

6.7.2 DC Motor Speed Control Using PWM Method

PWM is a simple form of analog to digital conversion used to obtained a high resolution control of slowly changing variables like voltage, temperature. A PWM signal is a wave of fixed frequency and varying duty cycle(Pulse width).

The *Duty cycle* in the PWM context is refer to the percentage of time that the signal is in the active state. It is a ratio of the time the signal high (T_{on}) to the period of one cycle.

PWM can be used in the application that requires fast switching control, such as speed and position control of DC and stepper motor, exciting speakers to generate a variety of

sound effects, and controlling light intensity. If the supply voltage to DC motor is vs, the average DC Value of the output voltage is proportional to the PWM duty cycle.

$$\text{Duty cycle} = \frac{T_{on}}{T} \times 100\% \tag{6.7}$$

So, the net output DC Voltage is ,

$$Vdc = Vs \times (\text{duty cycle}) = Vs \times \frac{T_{on}}{T} \tag{6.8}$$

The PWM period depends on the MCU clock frequency.

6.7.3 DC Motor Driver : LMD18200

Power amplifiers are used to control the speed and direction of DC motors. They are coming in two types, linear amplifiers and PWM switching amplifiers. These amplifiers are arranged in two types of basic design ,"T" type and "H" Type. "T" type (Half bridge) requires bipolar power supply and two transistors. The "H" type (full bridge) type configuration requires unipolar power supply and four transistor. Bridge configuration is arranged such a way that only two transistors are on at a time.

The h-bridge configuration is used to achieve bipolar operation using unipolar supply. Figure 6.9 shows simple H bridge circuit driving a load [18]. H bridge circuit consist four transistors, connected in a wheatstone bridge configuration. When transistor T1 and T4 conduct and T2 and T3 are off, the current will flow from A to B and the motor will rotate in one direction. If transistor T2 and T3 conduct T1 and T4 are turned off then current will flow from B to A and the motor will rotate in reverse direction. If terminals are floating then motor will run in freewheel. If terminals are short then motor will brake if it is PM motor.

A switching amplifiers uses power transistors that can be switched at Megahertz rates. The amplifiers generate the voltage that switches between the high level and low levels of the DC supply voltage. These type of switching amplifiers are more suitable with digital control. The most common method of switching amplifier is PWM. Here the transistors are

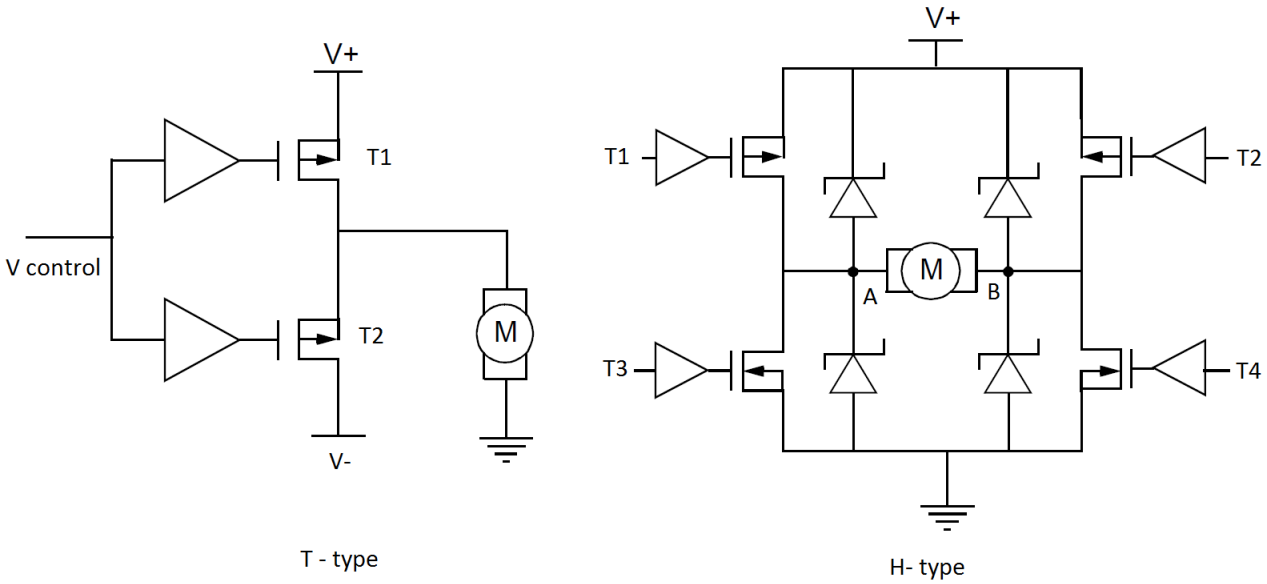

Figure 6.9: (a)Actuator with Potentiometer (b) CVT Unit With Actuator

switched at a constant frequencies and resulting output voltage varies between two extreme values. By varying the pulse width of PWM called duty cycle the output voltage can be changed. The practical range of switching frequency is 1KHz to 15 KHz [18]. Frequencies higher then the 15 KHz causes the transistors to operate in the active region for significant portion of the overall switching period which results in high power loss.

Instead of using discrete component full bridge driver ICs are commercially available in the market. LMD18200, L298 are most commonly used H-bridge driver ICs. They can be selected according to power speed and direction requirements.

In this project we use DC motor with a rating of 48 V, 3A. The LMD18200 is rated as 55 V, 4A rating. A functional block diagram is shown in figure 6.10

The LMD18200 readily interfaces with different forms of PWM signals. Popular forms of Sign/magnitude PWM method is shown in the figure 6.11. Sign/magnitude PWM consists of separate direction (sign) and amplitude (magnitude) signals. PWM signal is applied on the pin 5 and direction signal is applied on pin 3.

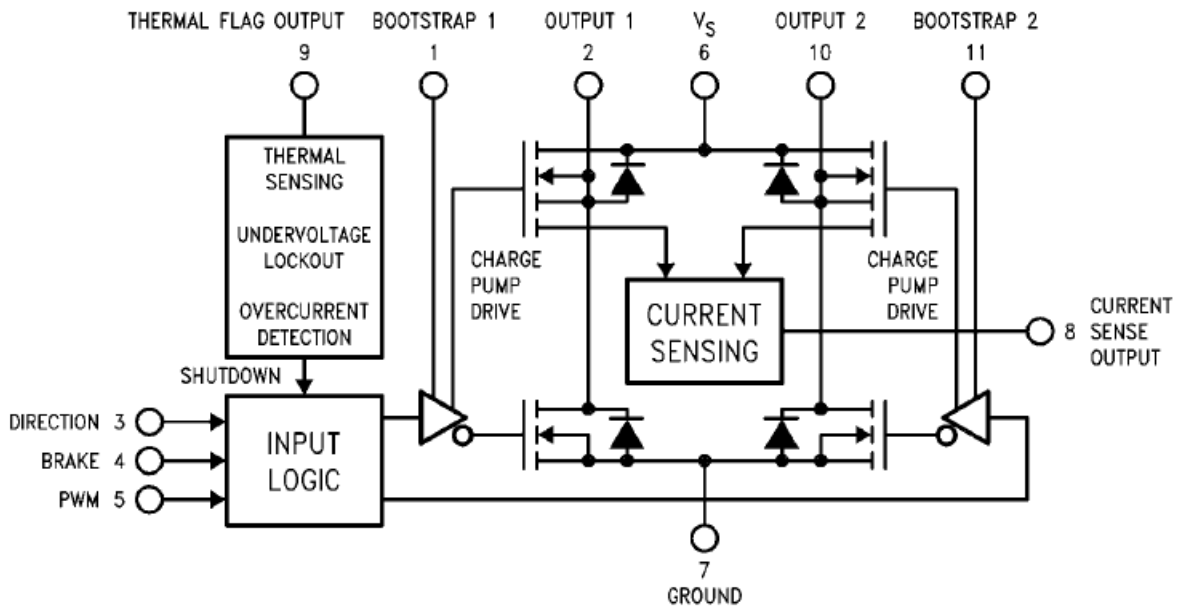

Figure 6.10: Functional Block Diagram of LMD18200 [17]

As shown in figure 6.11 by changing the duty cycle or PWM signal output voltage is also changing in this way motor speed can be changed. Voltage delivered to the load is proportional to pulse width of the PWM signal. Now as the value of direction signal is changed on pin 3 polarity of output voltage will be reversed and motor will rotate in reverse direction. Micro controller PIC16F877A can control both PWM and direction signals.

Position Sensor : Potentiometer

In this setup a potentiometer is used as sensor to measure the angular position of the motor. It is a resistive type transducer which consists of a single wire resistive element and a sliding contact known as the wiper or brush. The resistance per unit length of the resistive element is constant along the element. The wiper connects mechanically to the object whose position is to be measured.

When an excitation voltage is applied across the resistive element , an output voltage V0

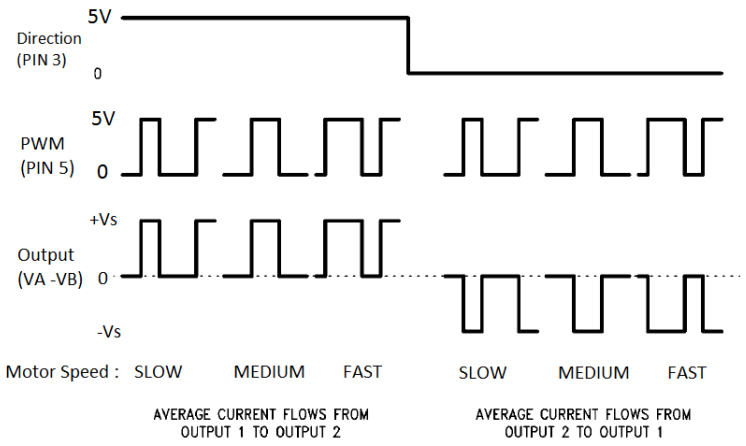

Figure 6.11: PWM signal [17]

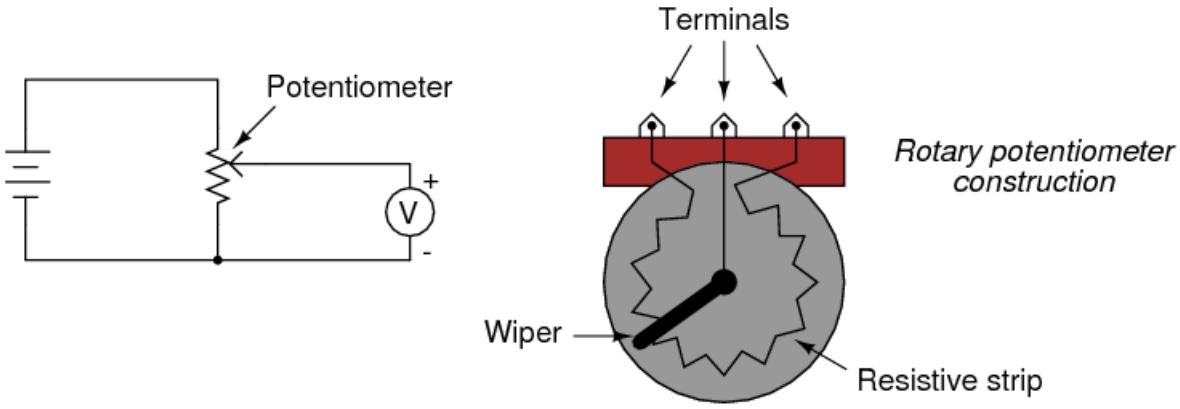

Figure 6.12: Potentiometer circuit

is proportional to the wiper that slides along the resistive elements .

$$\frac{V_o}{V_r} = \frac{x}{x_m} \tag{6.9}$$

$$\frac{V_o}{V_r} = \frac{\theta_a}{\theta m} \tag{6.10}$$

In this project setup the range of the potentiometer is 0-5K. The rotating system of the potentiometer is attached to the gear train attached to the motor output shaft.

Output from the potentiometer sensor is in voltage and microprocessor requires digital

signals for processing. Analog to digital converter is used to convert analog voltage in to digital signal. Analog signals are sampled at discrete time interval to convert it in to digital signal. The rate at which analog signal is sampled is called as a sampling frequency Fs (Hz) which effects the accuracy of ADC representation.

MCU 16F877A has A/D converter module which has eight inputs. The conversion of analog input signal results in to 8 bit or 10 bit digital values. The range of digital values generated by n bit ADC signals can be represented by $2^n - 1$. 8 bit signal will generate 0-255 values and 10 bit will generate 0-1023 values. Smallest voltage value (V_r) that can be measured by digital signal is called resolution of ADC. It can be measured by using following formula.

$$V_r = \frac{V_{max}}{2^n - 1} \tag{6.11}$$

For 8 bit signal with 0 to 5 V range, ADC resolution is 0.0196 V.

6.8 Embedded programming Using Microcontroller

A controller device is required to perform all functions and control algorithms mentioned in above sections. The 8 bit microcontroller PIC 16F877A from Microchip is widely used in developing projects and industries to control devices. This PIC controller is used in this setup. Some features of this controller are mentioned below:

- Operating speed : 20MHz, 200ns instructions
- 15 Interrupt sources
- Flash memory : 14.3KB(8192 words)
- Data SRAM:368 bytes
- Data EEPROM:256 bytes

- 33 I/O pins and 5 I/O ports
- Timer0:8-bit timer/counter with 8-bit prescaler
- Timer1:16-bit timer/counter with prescaler
- Timer2:8-bit timer/counter with 8-bit period register, prescaler and postscaler
- Two capture, compare, PWM modules
- 10-bit, 8-channel A/D converter

A software prototyping board from CCS,inc is used to program and interface PIC16F16f877A. This prototyping board includes a PIC16F877A with connectors and expanders to develop a variety of applications before the final target platform is designed.

Figure1 6.13 show the prototyping board for PIC16F877A.

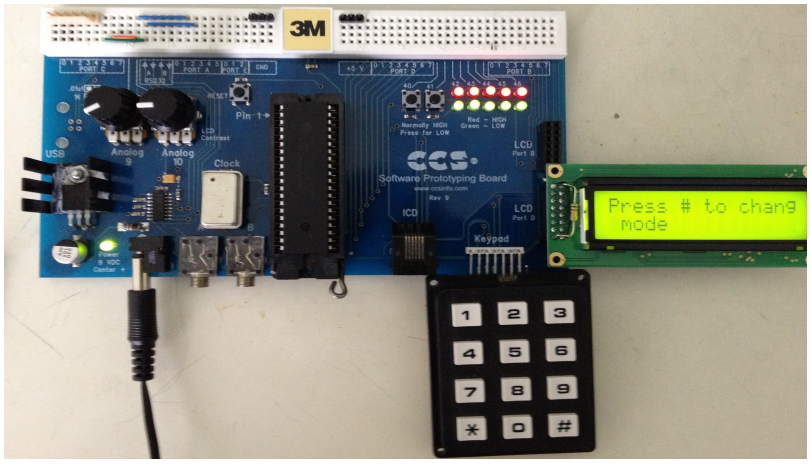

Figure 6.13: CCS Prototying Board

6.8.1 PWM Signal Generation

PWM signal can be produce by Capture/Compare/PWM (CCP) module in MCU 16F877A. Both CCP module pin ,CCP1 and CCP2, produce 10 bit resolution pwm output. Timer 2

is used as a time base for generating PWM signals. Some features of Timer 2 are mentioned below

- Timer-2 is 8-bit timer with a prescaler and a post scaler.
- TMR2 register is readable and writable and is cleared on any device Reset.
- Timer2 module has an 8-bit readable and writable period register, PR2.
- PR2 register can be initialize before starting the Timer2.

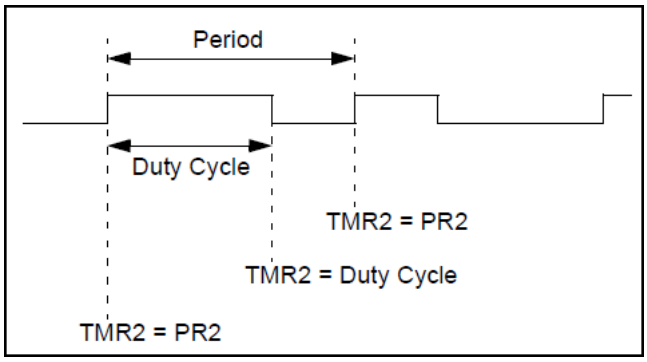

Figure 6.14: PWM Period and Dutcycle For Timer2 [11]

PWM Period:

PWM period is specified by writing in to the PR2 register. The PWM period can be calculated using the following formula

$$\text{PWM Period } = [(PR2) + 1] \cdot 4 \cdot TOSC \cdot (\text{TMR2 PrescaleValue}) \tag{6.12}$$

$$\text{PWM frequency} = \left[\frac{1}{\text{PWM period}}\right] \tag{6.13}$$

PWM dutycycle:

PWM dutycycle is specified by writing to the CCPR1L register and to the $CCP1CON < 5:4 >$ bits. Up to 10-bit resolution is available in this . This 10-bit value is represented by

$CCPR1L : CCP1CON < 5 : 4 >$. The following equation is used to calculate the PWM duty cycle in time:

$$\text{PWM DutyCycle} = (CCPR1L : CCP1CON < 5 : 4 >) \cdot TOSC \cdot (\text{TMR2 PrescaleValue}) \tag{6.14}$$

CCPR1L and CCP1CON<5:4> can be written to at any time during program execution.

Figure 6.15 shows steps of configuring PWM signal as below.

- When we initialize Timer 2 in in the program it starts and increments as input clock from 00h and compare with PR2 register value.
- When it matches with PR2 value it resets to 00h on the next increment cycle. Here input clock (FOSC/4) has a prescale option of 1:1, 1:4 or 1:16

The PWM period is specified by writing to the PR2 register. The PWM period can be calculated using the following formula:

$$\text{PWM Period } = [(PR2) + 1]$$

Using PIC C compiler PWM can be setup by following codes:

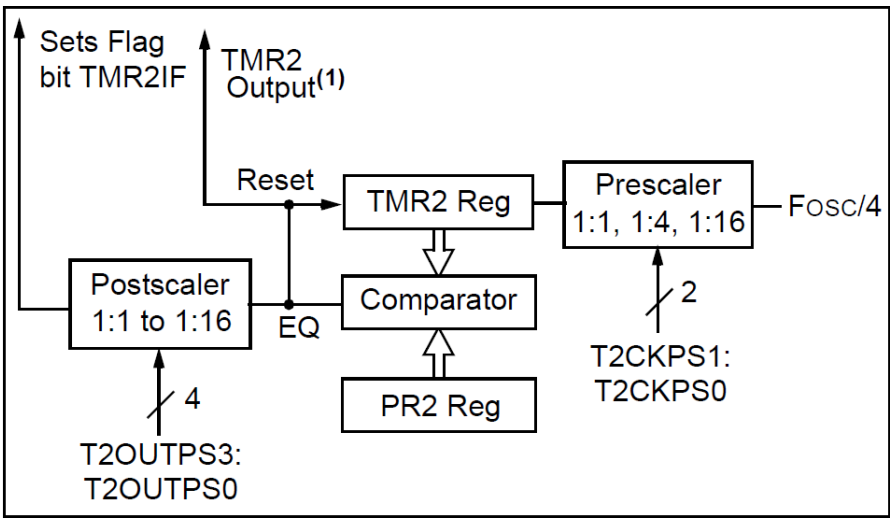

Figure 6.15: Timer-2 Functional Block Diagram [11]

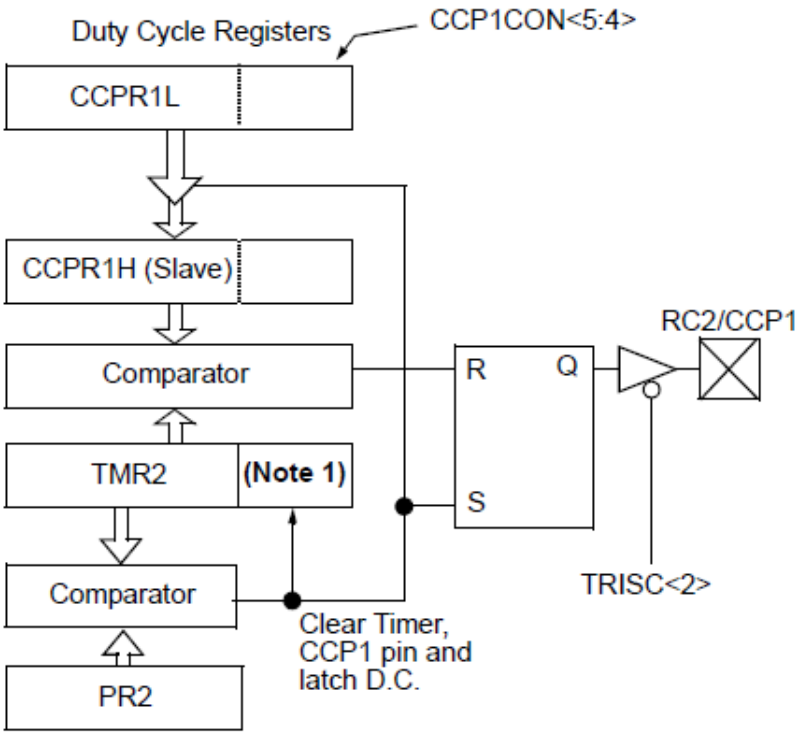

Figure 6.16: CCPR Register [11]

```
setup_ccp2(CCP_PWM);

setup_timer_2(T2_DIV_BY_4,155,1);
```

Here, from above formulas,

PWM freq = 16MHz / (4*1*(256+1))

PWM freq ≅ 15.6kHz

6.8.2 ADC Setup

IN MCU 16F877A Analog-to-Digital (A/D) Converter module has eight input ports. The conversion of an analog input signal results in a corresponding 8-bit and 10-bit digital number.

The A/D module has four registers as below:

- A/D Result High Register (ADRESH)

- A/D Result Low Register (ADRESL)
- A/D Control Register 0 (ADCON0)
- A/D Control Register 1 (ADCON1)

The ADCON 0 register controls the operation of the A/D module. The ADCON 1 register configures the functions of the port pins. The port pins can be configured as analog inputs or as digital I/O.

A/D Conversion can be done using follow these steps:

1. Configure the A/D module:
    - Configure analog pins/voltage reference and digital I/O (ADCON1)
    - Select A/D input channel (ADCON0)
    - Select A/D conversion clock (ADCON0)
    - Turn on A/D module (ADCON0)
2. Configure A/D interrupt (if desired):
    - Clear ADIF bit
    - Set ADIE bit
    - Set PEIE bit
    - Set GIE bit
3. Wait the required acquisition time.
4. Start conversion:

    Set GO/DONE bit (ADCON0)
5. Wait for A/D conversion to complete by either:
    - Polling for the GO/DONE bit to be cleared (interrupts disabled); OR

- Waiting for the A/D interrupt

6. Read A/D Result register pair (ADRESH:ADRESL), clear bit ADIF if required.

7. For the next conversion, go to step 1 or step 2 as required. The A/D conversion time per bit is defined as TAD.

Following codes shows the ADC setup in CCS c compiler

```
setup_adc_ports(AN0);
setup_adc( ADC_CLOCK_INTERNAL );
set_adc_channel( 0 );
```

6.8.3 Programming Algorithm

Figure 6.17 shows the program flow of PID based position control of CVT actuator DC motor. ADC port and pwm signals will be setup initially. Set point positions values will be entered using key pad interface. PID function will be called to set the position value. Figure 6.18 shows the flow chart for PID function detailed program is shown in appendix 3.1

6.9 User Interface

A user LDC- keypad interface is created to perform all operations during the riding. Instructions will appear on LCD screen for users and guide for different driving mode. Three basic function modes are created in this setup. This program will ask user to choose one of the following modes and enter the value on keypad.

- Gear changing mode
- Power mode
- Regeneration mode.

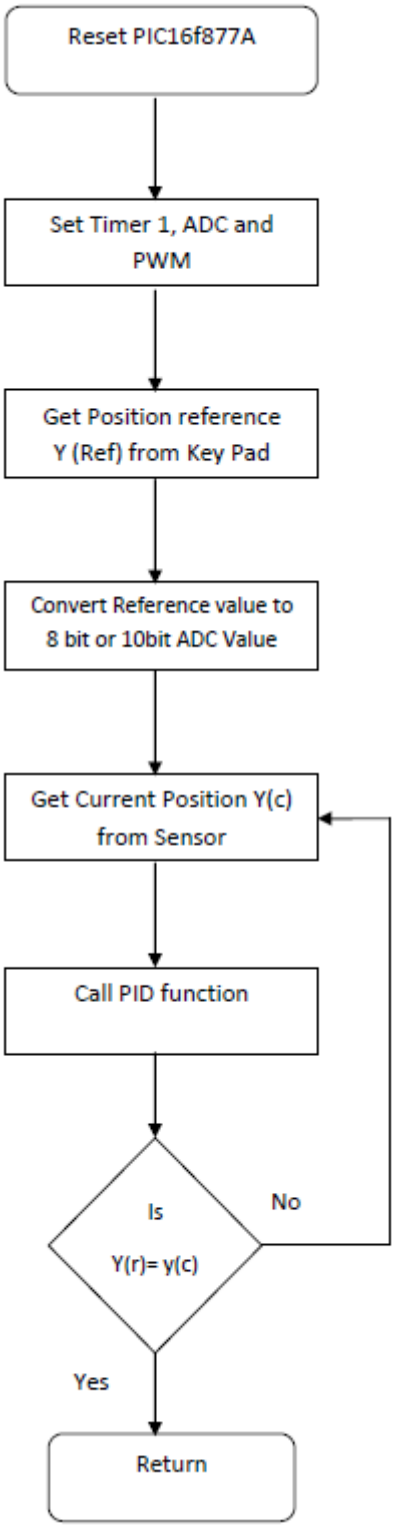

Figure 6.17: Program flow chart

In Gear changing mode user can set different gear ratios using CVT as per driving conditions. For simplicity and testing purpose nine different values are set from low gear ratio to high gear ratios. User can select 1-9 value from the key pad and actuator's servo control mechanism will set CVT on that gear ratio.

In power mode bicycle will set on driving mode. Relays will turn ON/OFF in a way so that power will flow from battery to motor. Power mode is a basic function of electric bicycle in which user doesn't have to apply external pedaling force to drive the bicycle. It will run on battery power.

In Regeneration mode relays will turn ON/OFF such a way that power will flow from motor to battery. This mode is used to charge the battery. Whenever user wants to stop bicycle or take an advantage of downhill shop to charge the battery, just enter this choice form keypad and bicycle will set on charging mode. During both power and regenerative mode we can also change the gear ratio to get the full advantage of battery of pedaling torque.

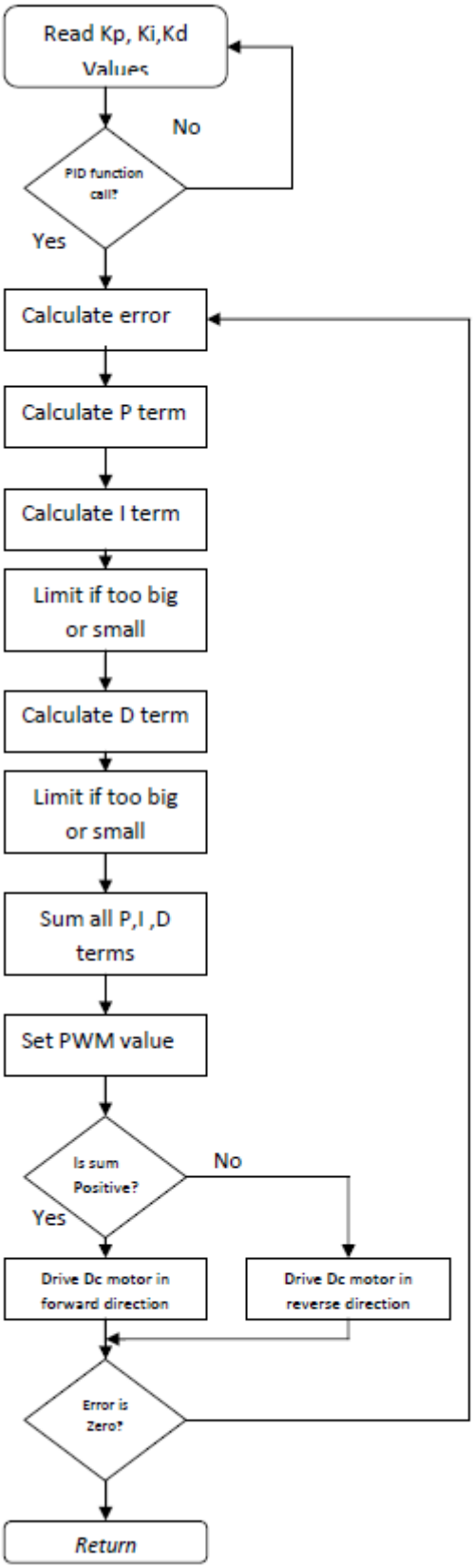

Figure 6.18: PID Flow Chart

CHAPTER VII

EXPERIMENTAL RESULTS

This chapter details the test results for the PID controller and the bicycle model, designed in Chapter VI. CVT Actuator PID controller tuning method is explained here with the step response of system. The bicycle prototype was tested on road and driving parameters were measured on different road profiles. This chapter will help readers to understand effectiveness of regenerative braking in bicycle by comparing real parameters data.

7.1 PID Controller Results

A microcontroller-based PID algorithm is designed for CVT actuator position control. PID flow chart for this system is shown in section 6.8.3. PID controller can be tuned by setting different values of K_p,K_d, and K_i [4]. Potentiometer values are measured as a feedback sensor in 0 to 5 V range. The microcontroller will read these positions in 8bit ADC signal from 0 to 255 range values. Desired position values can be set using ADC signal.

Now for tuning the controller we are applying desired ADC set point values to the system and system will change the position and stop on set point. Here initial position was set at 100 ADC value (1.920V) and applying set point position 150 ADC value (2.889V) to system. System responses for different gain values are shown in the following figures.

Figure 7.1 show the step response of system without PID controller. This open loop type

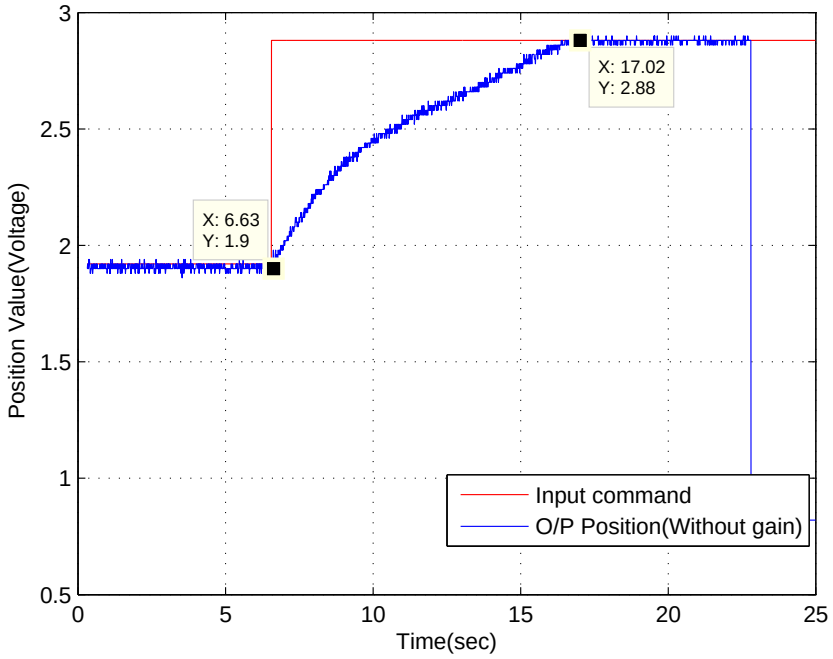

Figure 7.1: Step Response of Open Loop System

system takes approximately 10 second to reach at set point position which shows requirement of closed loop feedback control in the system. Using some simple closed loop controller we can make the system response faster.

7.1.1 Proportional (P) control

Proportional control is the easiest feedback control to implement. A proportional controller is just the error signal multiplied by a constant and fed out to the drive. If simple proportional control is applied using gain $K_p = 10$ in the system, it takes 2.4sec to settle. Figure 7.2 shows the step response of system. System response is underdamp.

By increasing K_p gain value we can still make the system faster. Step response of system with $K_p = 20$ is shown in Figure 7.3 Now there is small overshoot appear in the step response so gain value should not be increase more.

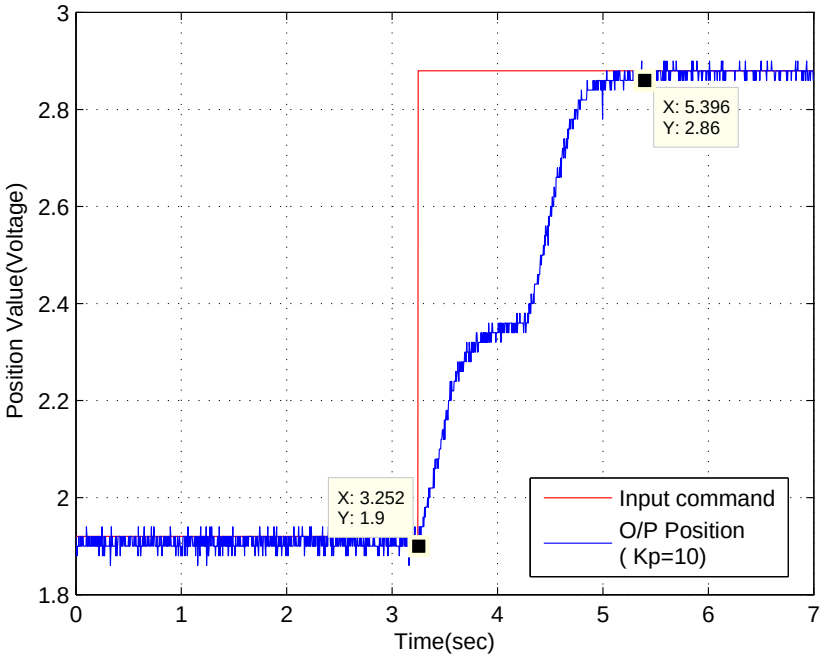

Figure 7.2: Step Response of P Control system ($K_P = 10$)

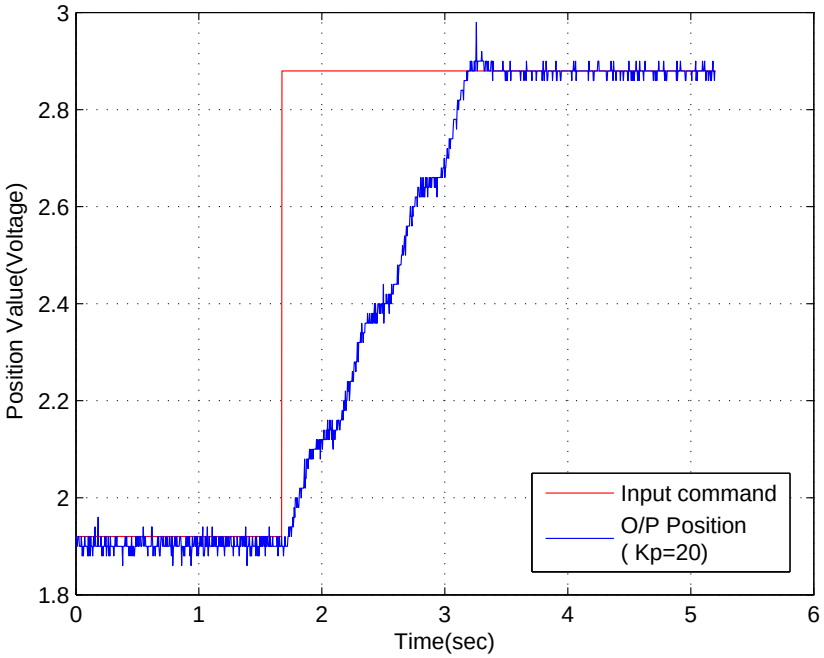

Figure 7.3: Step Response of PI Control system ($K_p = 20$)

7.1.2 Proportional and Integral (PI) control

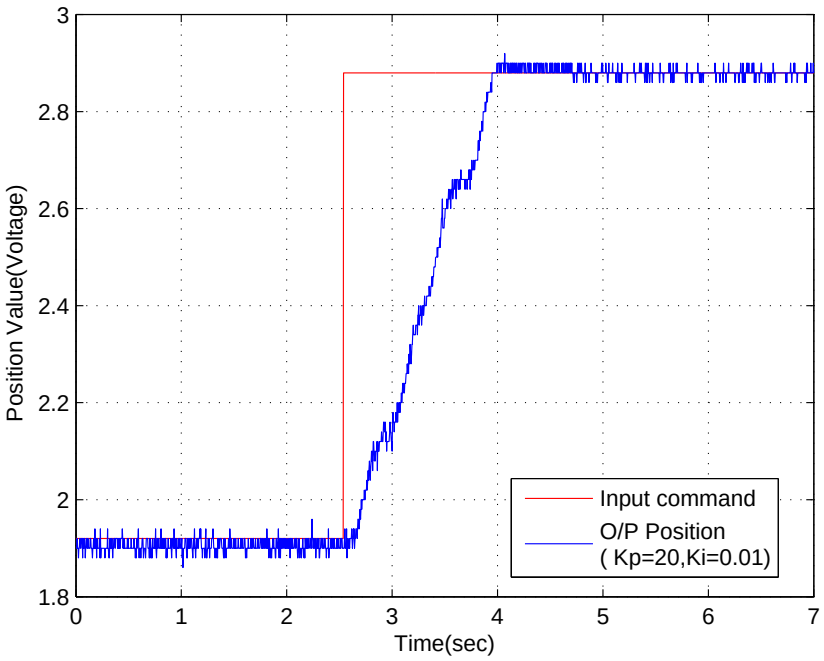

Figure 7.4: Step Response of PI Control system ($K_p = 20, K_i = 0.1$)

Integral control is used to add long-term precision to a control loop. It is almost always used in conjunction with proportional control.

With $K_p = 10, K_i = 0.1$ gain values system's setting time is 1.5 seconds.(Figure 7.4) and with ($K_P = 20, K_i = 0.01$) it takes 1.56 second to reach steady-state. (Figure 7.5).

7.1.3 Proportional, Integral and Derivative controller (PID)

Proportional control deals with the present behavior of the plant, and that integral control deals with the past behavior of the plant. If some element can predicts the plant behavior then this might be used to stabilize the plant. A differentiator is used for stability of the system.

Figure 7.6 shows the PID controller step response with $K_p = 20, K_i = 0.001, K_d = 10$ gain values. System's setting time is 1.9 second. At this gain value system is not fast and

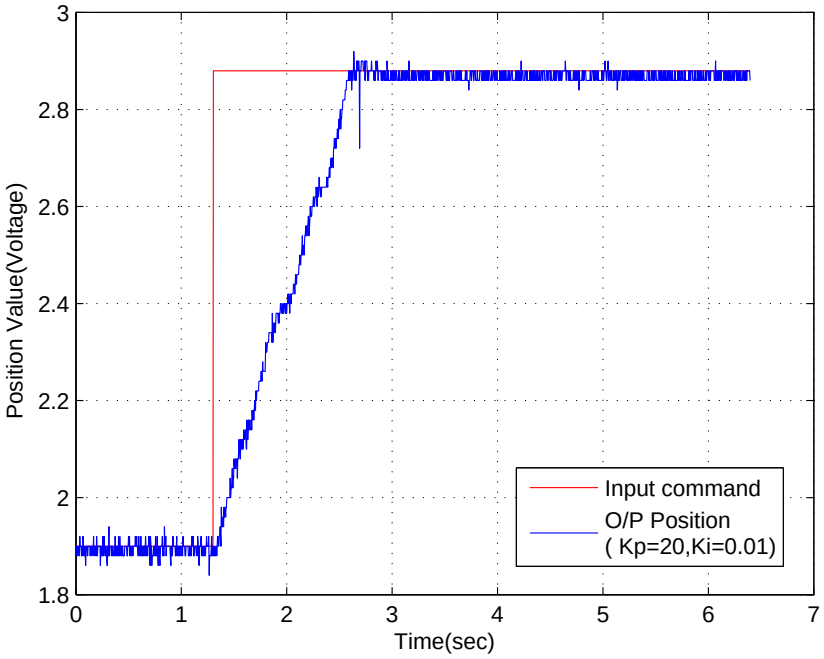

Figure 7.5: Step Response of PI Control system ($K_p = 20, K_i = 0.01$)

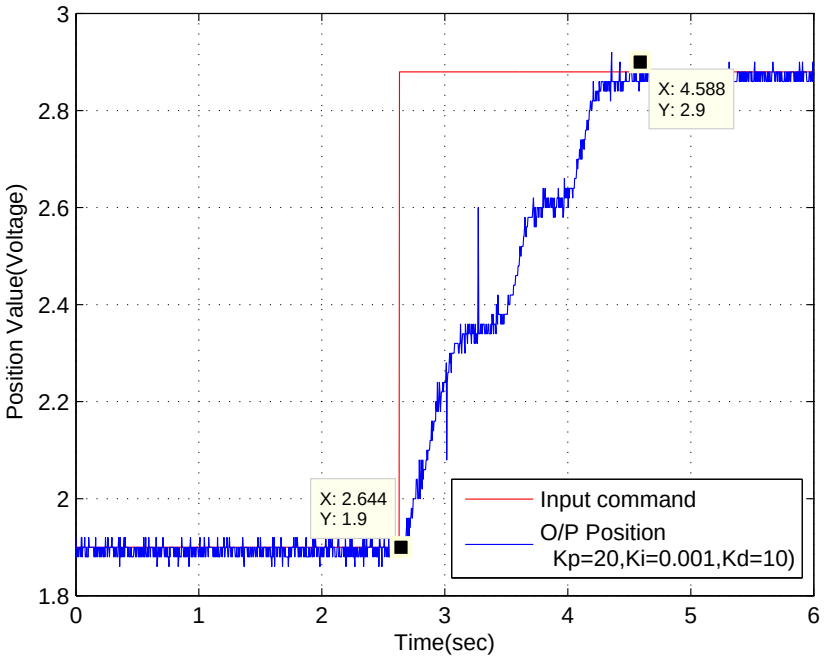

Figure 7.6: Step Response of PID Control system ($K_p = 20, K_i = 0.001, K_d = 10$)

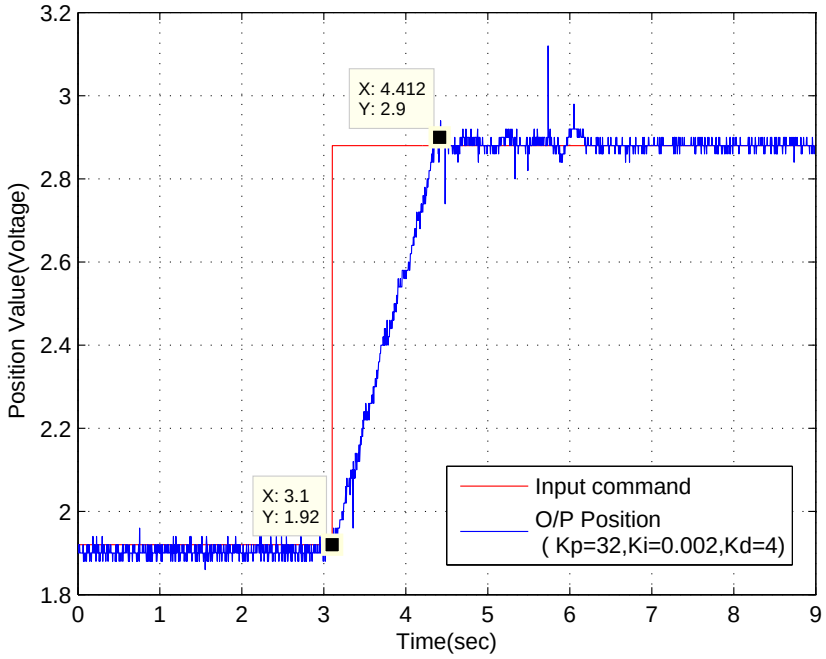

Figure 7.7: Step Response of PID Control system ($K_p = 32, K_i = 0.002, K_d = 4$)

stable so some more tuning required.

Figure 7.7shows the PID response of system at ($K_p = 32, K_i = 0.002, K_d = 4$) . It takes 1.21 sec to stable. These gain values are used for initial controller design.

7.1.4 10bit ADC Proportional Control

PIC16F877A has one more ADC port with 10bit precision. We also used 10bit ADC signal for controller design. Initial position was set at 600(1.92V) and final set point position at 800 (2.88V) values. Figure 7.8 shows the step response of open loop and closed loop system with 10 bit ADC precision. We used only $K_p = 20$ gain here and get the faster and smooth response of system .

Finally $K_p = 20$ gain value with 10bit ADC precision is used for final controller gains.

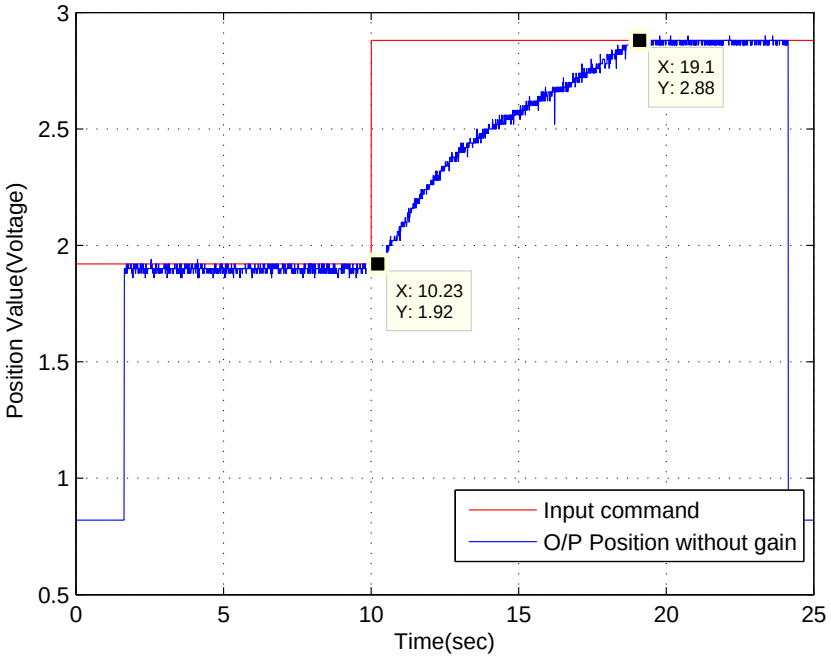

Figure 7.8: Step Response of 10bit Open Loop Control System

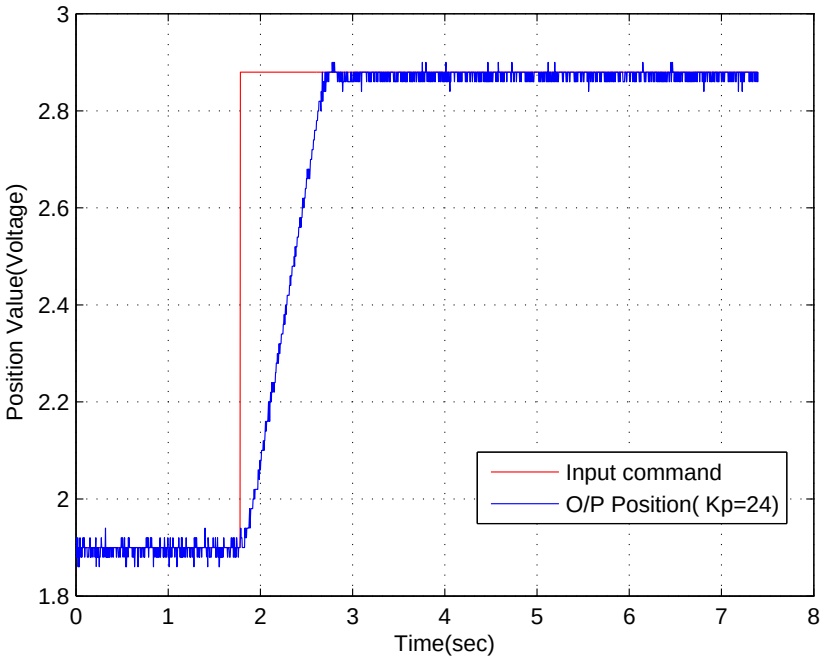

Figure 7.9: Step Response of 10bit P Control system ($K_p = 20$)

7.2 Bicycle Test Drive Results

The complete working prototype with all parts designed in Chapter VI was tested on different road profiles in the Cleveland area. These test drives were conducted to check all functions of prototype and its efficiency. Cleveland downtown, Euclid Avenue has a separate bike lane which connects commercial offices, universities, hospitals. This offers a good opportunity to check urban commuting conditions. The response of hill is also convenient to test the regenerative functions. All test drive maps and speed data are measured with mobile GPS enabled applications like Endomondo and Mapmyride. These results can be used for further calculations.

7.2.1 Test 1 : Battery Mode

Table 7.1: Test drive-1 Data

Test drive Parameters	***Reading***
Total Distance Traveled	12 miles
Duration	1h:18m
Avg. Speed	10.1 mph
Max. Speed	21.7 mph
Max Altitude	963ft
Min Altitude	633ft
Total Ascent	361 ft
Total Descent	561 ft

The purpose of this test drive is to check the efficiency of bicycle battery and measure the total range of electric bicycle. In this full charged battery with terminal voltage 51.5

V was connected to motor. Bicycle was using only battery power for driving. No manual power or regenerative braking was used in this ride. Test was stopped when bicycle get low power signal at 43.6V battery voltage. Figure 7.10 shows the route of test drive, elevation profile, speed graph and lap times during the drive.

This test drive parameters(Table 7.1) shows that full charged electric bicycle traveled 12 miles distance with average of 10.1 mph and maximum speed was 21.7 mph. Here, from elevation data we can calculate the percent grade value.

$$\text{vertical inclination} = (968f - 682f) = 286ft$$

$$\text{horizontal traveling distance} = (7.01mile - 2.47mile) = 4.5mile$$

$$\%\ \text{Grade} = +1.203$$

$$\text{vertical descent} = (680ft - 968ft) = 286ft$$

$$\text{horizontal traveling distance} = (10.5mile - 7.01mile) = 3.1mile$$

$$\%\ \text{Grade} = \text{-}1.7$$

During this ride there are many stop signals in urban area, where regenerative braking can be applied to stop the bicycle. Downhill slope of -1.7 % can also help to capture the free kinetic energy of the bicycle to charge the battery using regenerative setup. All this features can use to recharge the battery and increase the total range of bicycle travel.

7.2.2 Test 2 : Regenerative Mode

In this test drive we want to measure the range of the bicycle using the regenerative braking feature. During the ride regenerative braking was applied at stop signals using keypad interface. Sometimes, pedaling effort was applied to recharge the battery. In downhill areas bicycle was put on charging mode to capture the kinetic energy.

Table 7.2: Test Drive-2 Data

Test Drive Parameters	***Reading***
Total Distance Traveled	14.19 miles
Duration	2h:18m
Avg. Speed	8.2 mph
Max. Speed	16.9 mph
Max Altitude	902ft
Min Altitude	144ft
Total Ascent	1232 ft
Total Desent	1424 ft

This ride was started with 51.5 V and after all driving conditions as mentioned above 14.19 miles were completed and battery voltage was 46V. Battery condition was good and still able to travel few more miles. Test drive map, speed and elevation profile data are shown in figure 7.11 and table 7.2.

7.2.3 Test 3 : Manual Mode

This test drive is done to test only recharging capacity of this bicycle prototype when batter is discharged. In this test bicycle was set on charging mode. Only manual power was applied to drive the bicycle. Figure 7.12 shows the map and elevation profile of the route.

This drive was stared with initial battery voltage 36.5 V. At this low voltage battery was not able to drive the motor. As shown in elevation profile during the initial flat drive surface and downhill slope average driving speed was 10 mph and maximum speed was 18 mph. At this average speed battery was charged successfully. Even the motor-generator test data shows that at this speed minimum will voltage generate to boost it at 52 V using DC-DC charge boost up converter. During uphill sections bicycle speed was too low to generate the minimum voltage required for the converter.

After completing 12 miles of ride battery was charged up to 50 V. At this point, battery was not fully charged with its 10 A-hr rating. It required more charge to reach full battery capacity.

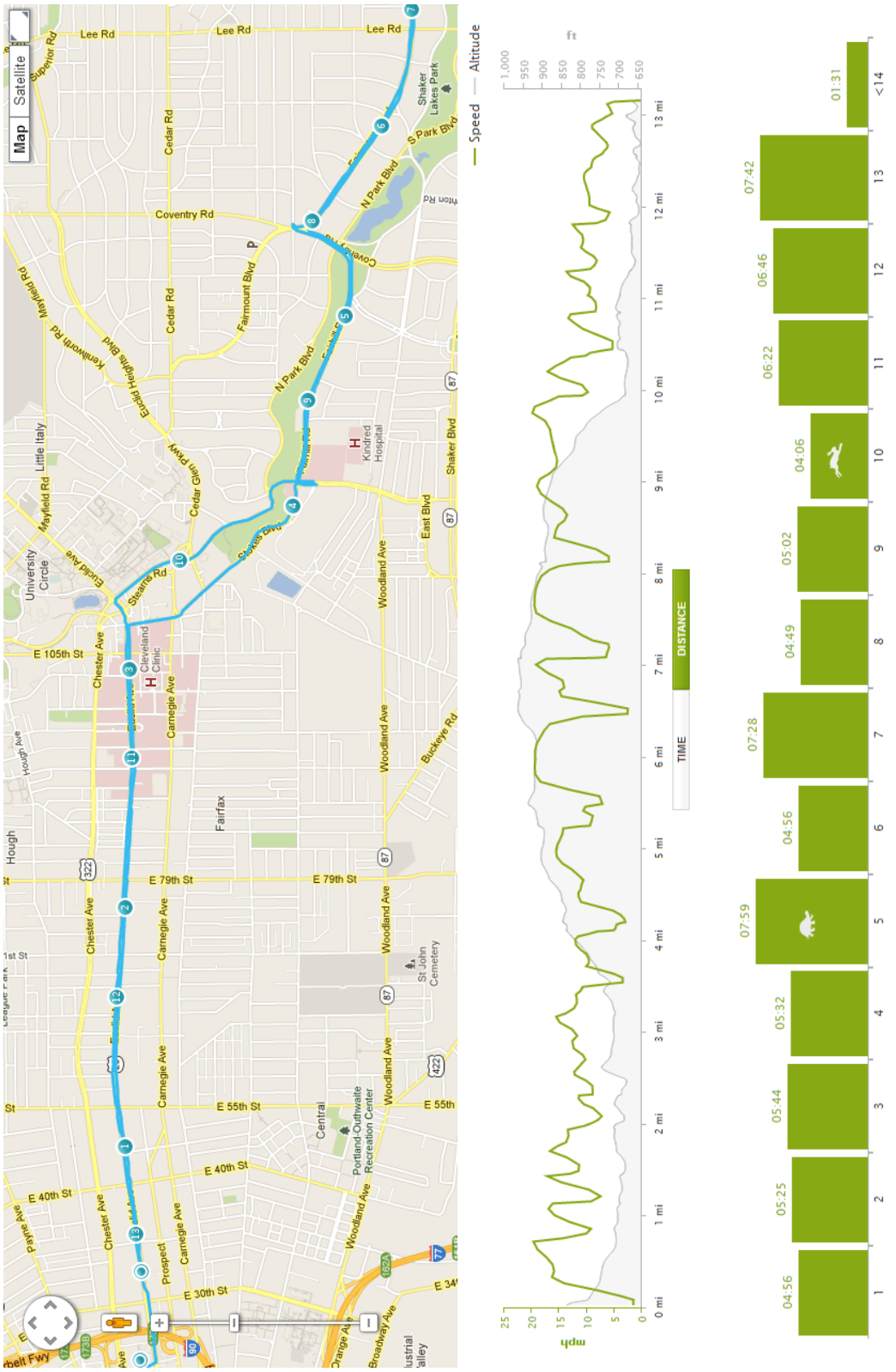

Figure 7.10: Bicycle Speed And Elevation Profile Of Test Drive 1 Route

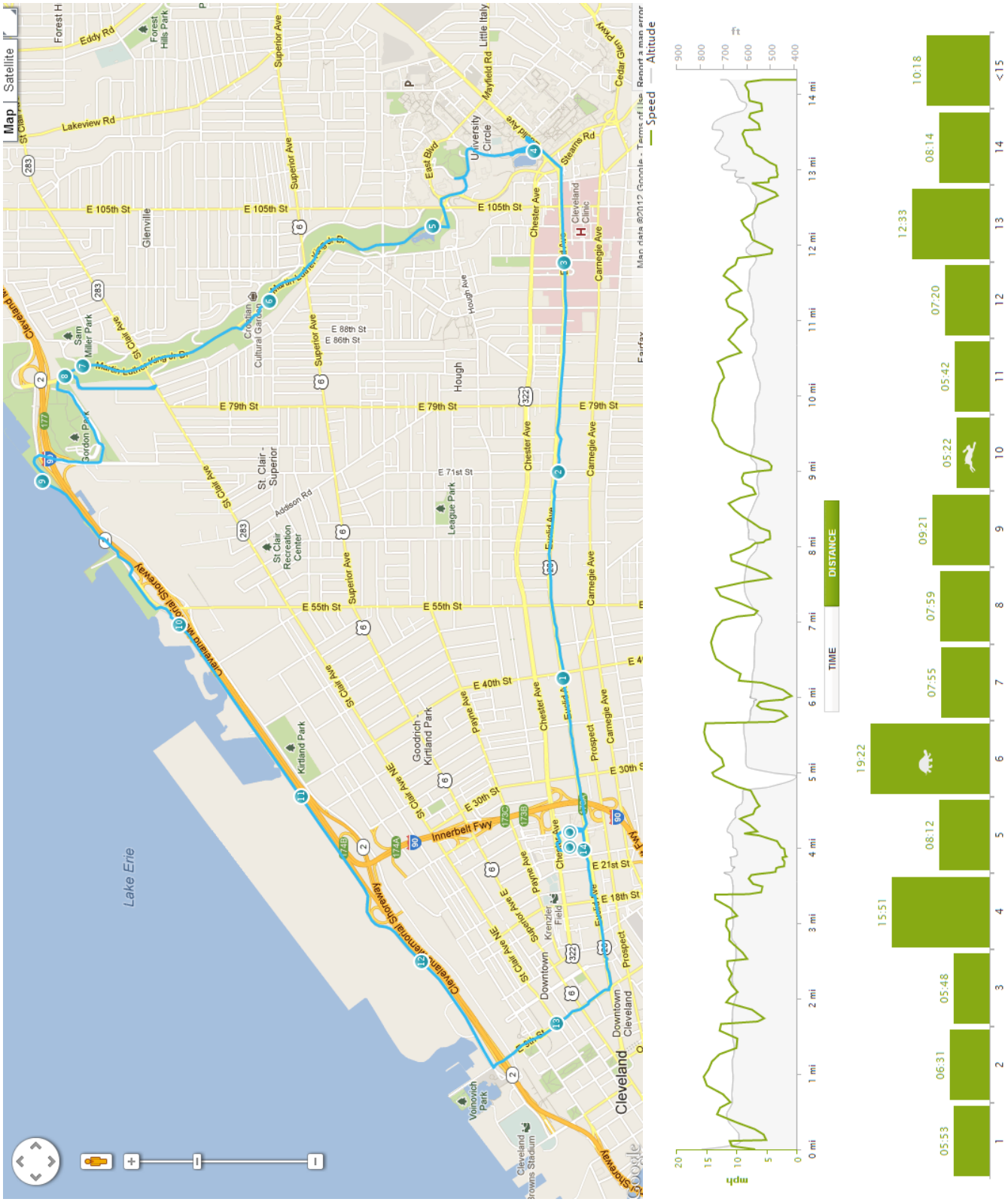

Figure 7.11: Bicycle Speed And Elevation Profile Of Test Drive 2 Route

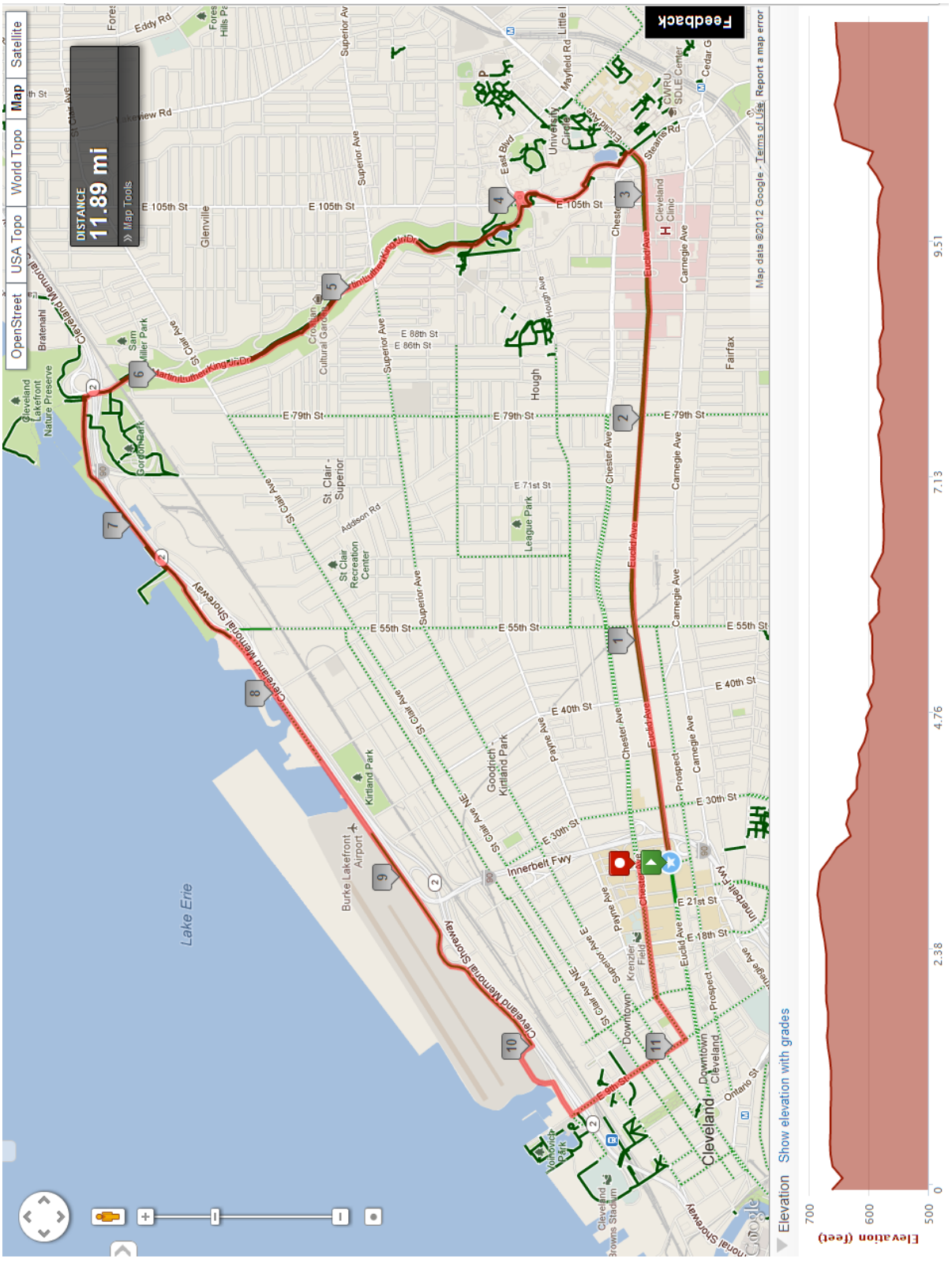

Figure 7.12: Bicycle Speed And Elevation Profile Of Test Drive 3 Route

CHAPTER VIII

CONCLUSION

The purpose of this thesis was to design and simulate the mathematical model of electric bicycle with regenerative braking setup. Simulation model based on mathematical equations was derived from bond graph method. This thesis shows the ability to design and simulate mechatronics systems using the bond graph method. The bond graph method allows us to estimate the both electrical and mechanical systems variables like voltage and velocity.

To develop a bond graph system model, some basic physical parameters were measured using different tests. All equations and parameters were used in the simulation model. Simulation based model developed in this thesis was used to estimate key bicycle parameters like battery range and bicycle velocity at different loads and conditions. Simulations conducted with various riding scenarios indicate that energy regeneration produces a useful increase in traveling range between battery recharging.

To confirm regenerative braking theory and simulations, a practical prototype model was designed. Details of electronic parts required to setup electric bicycle model with battery recharging setup is shown in this thesis. This thesis will help to develop commercial models based on theory and work flow explained here. The bicycle prototype model was tested on different road profiles and shows excellent results.

The advantage of using a CVT mechanism are also tested in this thesis. A microcontroller based PID control is designed for CVT actuator to set different gear ratios. This PID

algorithm can use to control any DC motor position.

Based on simulation results and test drive, the following conclusions are drawn:

- Amount of regenerative braking power is relatively small but still it can be used to charge the battery using a prototype shown here.
- Regenerative braking will slow down the vehicle due to motor torque but still we need to apply physical brake for instant stopping in emergency conditions or to reduce the stopping distance.
- The DC-DC boost converter required a minimum of 10 V input for amplification to 52 V. A bicycle speed of 6mph is required to generate 10 V , so recharging system will not work in slow riding conditions.
- Simulation results show by reducing the bicycle weight we can increase its range. If we use low weight bodyframe or reduce weight of some component we can increase bicycle range. This is mainly due to rolling resistance and the influenc of weight during uphill segments.
- The batteries used in this setup are 10A-h of lead-acid type rated at and the bicycle can travel up to 12 miles with them. If high rating batteries are used, like 20A-h or some light weight more efficient batteries they will help to increase the bicycle range.
- Simulation and practical results shows the effectiveness of gears while driving in up hills or recharging the battery. We can also use high torque ratio to maintain the bicycle speed above 6 mph for battery recharging.
- CVT is a good mechanism with infinite gear ratio range but it adds extra weight and cost to the bicycle. It adds more complexity to the circuit and requires 24 V DC supply for actuator motor with driver circuit. It is used for high initial torque and climbing up hills slops. A high initial torque is available from the motor while using battery

power. A conventional gear sets also would also serve the same purpose with less cost and weight. The use of CVT is not economical in cost and weight wise.

8.1 Future Work

This thesis gives an idea about bond graph methods use for system modeling and its parameters calculation. This methodology can be used for modeling and simulation different kind of mechatronics systems.

Here, the bicycle model is designed with basic vehicle dynamics and friction parameters more sophisticated models can be created in future to simulate real time system.

This is an initial prototype with only three basic mode of user interface. More features like driving speed based regeneration, pedal assistance for exercises purpose, etc. can be done by using more complex embedded programming.

Basic hardware and simulation work flow for the electric bicycles with regenerative braking is established in this thesis for future research. In the future, anyone can test their regenerative algorithms for optimizing cost and power with different parameters like speed, rider weight, gear ratio, regeneration timing. The simulation model will help to estimate the parameters for research studies. These algorithms can be further evaluated on hardware prototype. The prototype setup will be helpfull for advanced research studies on optimizing cost and power for electric vehicles.

BIBLIOGRAPHY

[1] *Bondgraph*, `http://www.bondgraph.org`, Accessed March,2011.

[2] Carter, Jeremy, McDaniel, Loren, Vasiliotis, and Christopher, *Use of a continuously variable transmission to optimize performance and efficiency of two-wheeled light electric vehicles (lev)*, EET-2007 European Ele-Drive Conference Brussels (2007).

[3] J. Dill and T. Carr, *Bicycle commuting and facilities in major u.s. cities: If you build them,commuters will use them*, Transportation Research Record (2003), 116–123.

[4] Richard C. Dorf and Bishop Robert H., *Modern control systems*, fifth ed., Prentice Hall, 2012.

[5] Z. Dunl, D. Yin-zhou, and L. Yang, *Rising of electric bicycle in china*, InternationalWorkshop on Rare Earth PermanentMagnets& Their Applications, Proceedings of 19th.

[6] M. Ehsani, Y. Gao, and A. Emadi, *Modern electric , hybrid electric and fuel cell vehicles fundamentals, theory, and design*, second ed., CRC Press, 2010.

[7] Peter J. Gawthrop and Geraint P. Bevan, *Bond-graph modeling*, Control Systems, *IEEE* (2007).

[8] Iqbal Husain, *Electric and hybrid vehicles design fundamentals*, first ed., CRC Press, 2003.

[9] J. Hwang, D. Wang, N. Shih, D. Lai, and C. Chen, *Development of fuel-cell-powered electric bicycle*, Journal of Power Sources (2004), no. 133, 223–228.

[10] Fallbrook Technologies Inc, `http://www.fallbrooktech.com/nuvinci-technology`, Accessed June 2011.

[11] Microchip Technology Inc., *Pic16f870/871 data sheet*, `http://www.microchip.com/`, February 2003.

[12] D. Karnoop, D. Margolis, and R. Rosenberg, *System dynamics modeling, simulation, and control of mechatronic systems*, 5th ed., Jhon Wiley, 2012.

[13] T. Morse, *Rolling resistance of bike tires*, `http://www.terrymorse.com/bike/imgs/rolres.gif`, Accessed August 2012.

[14] Pieter J. Mosterman, *Hybrid dynamic systems: A hybrid bond graph modeling paradigm and its application in diagnosis.*, Diss. Vanderbilt University (1997).

[15] City planning comission, *Cleveland bike way master plan*, `http://planning.city.cleveland.oh.us/bike`, Accessed June 2012.

[16] Hanz Richter, *Class note*, `http://academic.csuohio.edu/richter_h/courses/mce503/`, Accessed January 2011.

[17] National Semiconductor, *Lmd 18200 -data sheet*, `http://www.national.com`, February 2011.

[18] A. Smaili and F. Mrad, *Mechatronics*, first ed., Oxford, 2009.

[19] K. Ulrich, *Estimating the technology frontier for personal electric vehicles*, Transportation Research (2005), Part C,448–462.

[20] T. Wescott, *Pid without a phd*, Embedded Systems Programming (2000).

APPENDICES

APPENDIX A

BICYCLE PARAMETERS

Following table shows the experimental values of different parameters used for bicycle simulation model.

Parameter	$Value$	**Units**
Torque Constant (alpha)	4.97100	N-m/A
Rear Deceleration	-5.26180	rad/s^2
Rear Inertia (Jr)	0.05330	$Kg - m^2$
Rear Friction Torque (Tfr)	-0.28060	N-m
Front Deceleration 1	-3.19900	rad/s^2
Front Inertia 1	0.23080	$Kg - m^2$
Front Friction Torque 1	0.73830	N-m
Front Inertia 2	0.10000	$Kg - m^2$
Front Friction Torque 2		0.50340 N-m
Equivalent Resistance (Re)	20.08500	Ohms
Efficiency	66.50000	
Front Wheel Inertia (Jf)	0.16540	$Kg - m^2$
Front Hub Friction Torque (Tff)	-0.62085	N-m
Rider weight	700.00000	N
Gear Ratio (gear)	1.20000	
Tire Radius (r)	0.33450	m
Gravity (g)	9.81000	m/s^2
Bike Mass	40.25700	kg
Bike Force	394.92120	N
Total Weight (M)	1094.92117	N
Total Weight (m)	111.61280	kg
Theta	0.00000	rad
Battery Capacitance (Cb)	864.00000	F

Table 1.1: Experiment Values

APPENDIX B

MATLAB PROGRAMS FOR SIMULATION MODELS

2.1 Bicycle Model Parameters Calculation

```
% Program to calculate parameters for bond graph calculation
%  Prepared by - Maulik Kalolia
%% Part 1: Parameters and constants
% Parameters and constant usedfor the Calculaitos are given here.
%
LC=118.21;                %% smallload cell sensitivity(N/V)
Rd=0.3345;                %% Wheel radius (M)
Mb=40.257;                %% Bike mass (Kg)
Cb=864;                   %% Battery capacitance (f)
L=24.83;                  %% Moment arm of torque measuring device(in)
Ca=0.044;                 %% idle current(A)
RRC=0.0045;               %% Mean rolling resistance coefficient(N)
G=1.2;                     %% gear ration

%% Part 2 : Inertia Measurement : Spindowntest
```

```
%% Part 2.1: Rear wheel Spindown Test
time=[.5:.5:10];
speed=[22.75362319 22.50896057 21.80555556 19.74842767 18.04597701
    17.15846995 15.16908213 14.74178404 12.9218107 11.62962963 11.01754386
    9.101449275 8.241469816 6.931567329 6.01532567 4.779299848 3.833943834
    3.365487674 2.656514382 2.048271363 ] ;
coeff=polyfit(time,speed,1)
x2=0.5:.1:10;
value=polyval(coeff,x2);
figure(2)
plot(time,speed,'r-*',x2,value)
title('Rear wheel Spindown test');
ylabel('Speed (Rad/s)');
xlabel(' Time (s)');
grid on
%  Linear Regression coeff (Alpha_f)= -2.3501
Tfr= 0.8388*Rd ;
Jr= Tfr/2.3501;
%   Rear wheel friction torque(Tfr) = 0.2806
%   Rear Wheel Inertia        (Jr)  = 0.1194

%% Part 2.2: Front Wheel spindown test (Method-1)
Time= [1.5 1.828 2.16 2.488 2.824 3.192 3.592 4.04 4.552 5.168 5.976 7.44];
Speed=[18.91566265 19.14634146 18.91566265 19.14634146 18.69047619
17.06521739 15.7 14.01785714 12.265625 10.19480519 7.772277228
4.289617486 ];
coeff=polyfit(Time,Speed,1)
x3=1.5:.1:7.5;
value=polyval(coeff,x3);
```

```
figure(3)
plot(Time,Speed,'r-',x3,value)
title('Front wheel Spindown test');
ylabel('Speed (Rad/s)');
xlabel(' Time (s)');
grid on
% Linear Regression coeff = -2.7674
Tfr= 2.2073*Rd ;
Jf1= Tfr/2.7674;
%   Front wheel friction torque (Tff1) = 0.7383
%   Front Wheel Inertia(Jf1)           = 0.1014

%% Part2.3 : Front Wheel spindown test (Method-2)
%
Fr=433;                          % Front wheel Rpm
FR=433*pi/30;                    % RPM to Rad/s
FT1=10.8;                        % Time required to rech zero
FT2=12.8;                        % Time required to rech zero with inertia
SL1=(FR/FT1);                    % Slpoe (alpha 1)
SL2=(FR/FT2);                    % Slpoe (alpha 2)
Ja=0.0187;                       % Kg.M^2
Jf2=Ja*SL2/(SL1-SL2);
Tff2=SL1*Ja;
%   Rear wheel friction torque(Tff2) = 0.4240
%   Rear Wheel Inertia(Jf2)          = 0.1010
%% Part 3: Torque Constant Measurement
% Load test result shown in chapter-4 are stored in 'torquetest120110.mat'
% file. This file is used for matlab calculation
st='torquetest120110.mat';
```

```
open(st);
LV=T;                          % load cell voltage
LV(:,1)=[];
LV(:,2)=[];
BC=T;                          % Battery Current
BC(:,2)=[];
BC(:,2)=[];
l= convlength(L,'in','m');
torque=LC*l*LV;
coeff=polyfit(BC,torque,1);
x1=0:.1:4;
value=polyval(coeff,x1);
figure(1)
plot(BC,torque,'+',x1,value)
grid on;
title('Torque Constant');
ylabel('Torque(N-m)');
xlabel('Battery Current(A)');
% Motor Torque constant :  4.9710

%% Part 4:  Equivqlent electrical Resistance
%
BI=0.85;
BV=51;
Tff=0.73830;
Pmech=Tff*(373/60)*2*pi;           %Mechanical power
Pele=BV*BI;                        %Electrical power
Re=(Pele-Pmech)/BI^2;
Peff= Pmech/Pele;
```

```
%% Part 5: Final Parameters from calcuation part
%
Al=4.97100;          % Motor torque constant
Cb=864;
g=1.2;               % geat ratio
w=700;               % rider weight(N)
Mb=40.257*9.81;      % Bicycle weight(N)
TFr = Tfr;            % rear wheel friction torque
Jr;                   % Rear wheel inertia
Tff1 ;                % Front wheel torque (Method-1)
Jf1;                  % Front wheel inertia (Method-1)
Tff2;                 % Front wheel torque (Method-2)
Jf2;                  % Front wheel inertia (Method-2)
Jf=(Jf1+Jf2)/2;
TFF=(Tff1+Tff2)/2;
M=(Mb+w);             % Total weight
Fh=(M*0.0045);        % Friction Coeff
```

2.2 Bicycle model State Derivative Function

```
% This matlab function calculates the state derivative equations using input
% values
%
function [xdot]= Bicycle_Statederivative_manual(p1,theta,torque,g,w,q1)
LC=118.21;                %% smallload cell sensitivity(N/V)
Rd=0.3345;                %% Wheel radius (M)
Mb=40.257*9.807;          %% Bike mass (Kg)
```

```
Cb=864;                    %% Battery capacitance (f)
L=24.83;                   %% Moment arm of torque measuring device(in)
Ca=0.044;                  %% idle current(A)
RRC=0.0045;                %% Mean rolling resistance coefficient(N)
Al=4.97100;                % Motor torque constant
Re= 20.0853  ;             % Equivalent rasistance
Cb=864;
Mb=40.257*9.81;            % Bicycle weight
TFr = 0.2806;              % rear wheel friction torque
Jr = 0.1194 ;              % Rear wheel inertia
Tff1 = 0.7383;             % Front wheel torque (Method-1)
Jf1 = 0.1014  ;            % Front wheel inertia (Method-1)
Tff2 = 0.4240;             % Front wheel torque (Method-2)
Jf2  = 0.1010  ;           % Front wheel inertia (Method-2)
Jf=(Jf1+Jf2)/2;
TFF=(Tff1+Tff2)/2;
M=(Mb+w);
Fh=M*0.0045*cos(theta)+M*sin(theta);
bt=(1+(M*Rd^2)/Jr+(Jf/Jr));
A=[-(Al^2/Re/Jr/bt) (Al/Cb/Re/bt);-(Al/Re/Jr) (1/Cb/Re)];
B=[(1/(g*bt)) 1/bt Rd/bt 1/bt;0 0 0 0];
C=[(Rd/Jr) 0;(-Al/Re/Jr) (1/Re/Cb);0 1;(1/g/Jr) 0];
D=[0 0 0 0 ;0 0 0 0;0 0 0 0;0 0 0 0];
p=0+p1;
q=40*Cb+q1;
pdot=(-Al^2/Re/Jr/bt)*p+(Al/Cb/Re/bt)*q+(1/(g*bt))*(torque)
      +(1/bt)*(-TFr)+(Rd/bt)*(-Fh)+(1/bt)*(-TFF);
qdot=(-Al/Re/Jr)*p+(1/Cb/Re)*q;
f7=(Rd/Jr)*p;
```

```
f16=(-Al/Re/Jr)*p+(1/Re/Cb)*q;

q16=q;

f1=(1/g/Jr)*p;

xdot=[pdot;f1;f7;f16;q16;qdot];
```

2.3 Road Profile Function

```
% This function will generate different road porofile functions

 function [theta] = roadprofile(dist)

%UNTITLED2 Summary of this function goes here

%   Detailed explanation goes here

theta = 0;

if (dist<2)

    theta = 0;

else if (dist<=5)

        theta =-0.02;

    else if (dist<7)

            theta = +0.02;

        else if (dist>7)

             theta =0 ;

            end

        end

    end

end

end
```

APPENDIX C

MICROCONTROLLER PROGRAM

3.1 PID function

PID logic as shown in figure 6.18 can be done in MCU PIC 16F877A using following C codes.

```
void PID()
{ error = ((signed int16)yref-(signed int16)y);
  SumE = SumE + (error/16);          // SumE is the summation of the error terms
  if(SumE > SumE_Max)                // Test if the summation is too big
   { SumE = SumE_Max;}
   if(SumE < SumE_Min)    // Test if the summation is too small
   { SumE = SumE_Min;}
  proportional_term = error*kp;
  integral_term=SumE*ki;
  derivative_term =(error-errorold)*kd;
  temp =( proportional_term + derivative_term+integral_term);
if (error == 0) //motor should stope
        {
             output_low(pin_C0);   // direction pin
             set_pwm2_duty(1023);  // PWM pin
```

```
            output_high(pin_C2);  // brake pin
            brake;
        }
  if (temp> 0) // If error is +ve then  motor should run forword
     {
        value=(unsigned int16)temp;
       if (value<40)                 // lower PWM speed limit
            {   value1=40; }
      else if(value>900)            // higher PWM speed limit
            {value1 =900;}
      else
            { value1 = value;}
        output_high(pin_C0);           // direction pin
        output_low(pin_C2);           // brake pin
        set_pwm2_duty(value1);      // pwm pin c1
      }
if (temp<0) // If error is -ve then  motor should run forword
     {
      value=(unsigned int16)abs(temp);
       if (value<40)                  // lower PWM speed limit
            {   value1=40; }
      else if(value>900)            // Higher PWM speed limit
            {value1 =900;}
      else
            { value1 = value;}
       output_low(pin_C0);         // direction pin
       output_low(pin_C2);        // brake pin
       set_pwm2_duty(value1);    // pwm pin
     }
```

```
 output_low(PIN_B6);
  return;
}
```